(20) B.S.

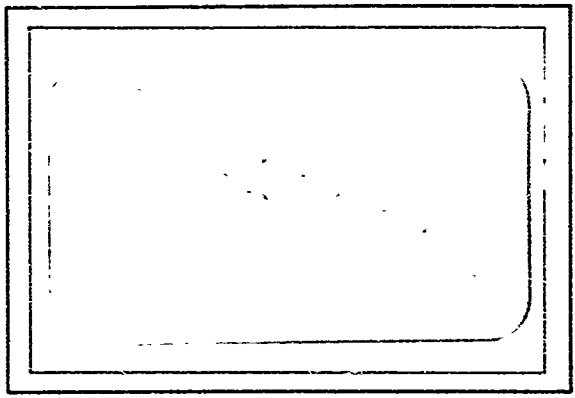

UNITED STATES NAVAL ACADEMY
DIVISION OF
ENGINEERING AND WEAPONS
ANNAPOLIS, MARYLAND

20

THE KINETICS OF EVOLUTION OF WATER VAPOR CLUSTERS IN AIR

A. A. Pouring*

December 1975

Report E.W. #3-74

*Naval Air Systems Command Research Professor
United States Naval Academy
Annapolis, Maryland 21402

Work Supported by: Power Branch and Atmospheric Sciences Program, Office of Naval Research and Naval Air Systems Command (Air 03)

*Now Chairman, Aerospace Engineering Department

UNCLASSIFIED

SECURITY CLASSIFICATION OF THIS PAGE (When Data Entered)

REPORT DOCUMENTATION PAGE

READ INSTRUCTIONS BEFORE COMPLETING FORM

1 REPORT NUMBER: USNA-E&W #3-74

2. GOVT ACCESSION NO.

3. RECIPIENT'S CATALOG NUMBER

4 TITLE (and Subtitle): The Kinetics of Evolution of Water Vapor Clusters in Air.

5. TYPE OF REPORT & PERIOD COVERED: Final Report, 1964-1975

6 PERFORMING ORG. REPORT NUMBER

7 AUTHOR(s): A. A. POURING

8. CONTRACT OR GRANT NUMBER(s)

9 PERFORMING ORGANIZATION NAME AND ADDRESS
United States Naval Academy
Aerospace Engineering Department
Annapolis, Maryland 21402

10. PROGRAM ELEMENT, PROJECT, TASK AREA & WORK UNIT NUMBERS
140 p.

11. CONTROLLING OFFICE NAME AND ADDRESS
United States Naval Academy
Annapolis, Maryland 21402

12. REPORT DATE
December 1975

13. NUMBER OF PAGES
134

14. MONITORING AGENCY NAME & ADDRESS(if different from Controlling Office)
EW-3-74

15. SECURITY CLASS. (of this report)
Unclassified

15a. DECLASSIFICATION/DOWNGRADING SCHEDULE
N/A

16 DISTRIBUTION STATEMENT (of this Report)

Distribution Unlimited

17 DISTRIBUTION STATEMENT (of the abstract entered in Block 20, if different from Report)

18. SUPPLEMENTARY NOTES

Available in DDC

19. KEY WORDS (Continue on reverse side if necessary and identify by block number)

Water Vapor	Supersaturated	Equilibrium
Clusters	Metastable	
Nucleation	Undersaturated	
Condensation	Expansion	
Nonequilibrium	Supersonic	

20. ABSTRACT (Continue on reverse side if necessary and identify by block number)

The kinetic theory of cluster formation in a condensing gas proposed by Buckle[1] attempts to calculate the course of homogeneous condensation from molecular rather than thermodynamic precepts. Here it is applied to the rapid nonequilibrium expansion of atmospheric water vapor in air. A methcd is established for demonstrating the validity of this theory, originally proposed for a mono-molecular gas, in the case of a complicated species such as water vapor. Cluster conditions in the temperature range 210-

DD FORM 1473 EDITION OF 1 NOV 65 IS OBSOLETE

UNCLASSIFIED 406 993

20. Abstract (continued

295°K and the vapor pressure are calculated throughout the collapse of a supersaturated metastable vapor.

An effective molecular pair interaction energy and nearest neighbor coordination number is found based on the classical zero-point enthalpy of sublimation and by iteration to satisfy initial equilibrium limiting constraints at 273°k. The internal energy redistribution frequency results from close matching of the experimental pressure distribution. A method of determining the cluster size at which macroscopic properties become relevant is described; the size is found to be a cluster of about 122 molecules at 273°K based on a hard sphere model collision cross section. For the water vapor dimer an equilibrium constant of 4.0×10^{-21} (cm^{-3}) is found at 273°K compared to 3.1×10^{-21} (cm^{-3}) obtained from Keyes[3] data. Two models for water vapor clusters result (from satisfying all constraints imposed on the theory) which are given in terms of number of nearest neighbors, pair interaction energy per molecule (2.9kcal/mol at 273°K) and possible structure on a cluster by cluster basis for a classical hard sphere model and for a model approximating a Pauling type clathrate.

4 x 10 to the -21 power/cc

3.1 x 10 to the -21 power/cc

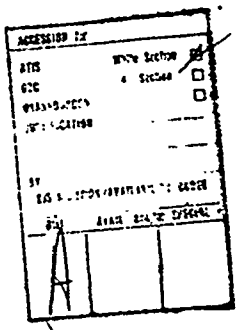

TABLE OF CONTENTS

I. ABSTRACT

The kinetic theory of cluster formation in a condensing gas proposed by Buckle[1] attempts to calculate the course of homogeneous condensation from molecular rather than thermodynamic precepts. Here it is applied to the rapid non-equilibrium expansion of atmospheric water vapor in air. A method is established for demonstrating the validity of this theory, originally proposed for a mono-molecular gas, in the case of a complicated species such as water vapor. Cluster conditions in the temperature range 210-295°K and the vapor pressure are calculated throughout the collapse of a supersaturated metastable vapor.

An effective molecular pair interaction energy and nearest neighbor coordination number is found based on the classical zero-point enthalpy of sublimation and by iteration to satisfy initial equilibrium limiting constraints at 273°K. The internal energy redistribution frequency results from close matching of the experimental pressure distribution. A method of determining the cluster size at which macroscopic properties become relevant is described; the size is found to be a cluster of about 122 molecules at 273°K based on a hard sphere model collision cross section. For the water vapor dimer an equilibrium constant of $4.0 \times 10^{-21} (cm^{-3})$ is found at 273°K compared to $3.1 \times 10^{-21} (cm^{-3})$ obtained[2] from Keyes[3] data.

Two models for water vapor clusters result (from satisfying all constraints imposed on the theory) which

are given in terms of number of nearest neighbors, pair interaction energy per molecule (2.9kcal/$_{mol}$ at 273°K) and possible structure on a cluster by cluster basis for a classical hard sphere model and for a model approximating a Pauling type clathrate.

II. FOREWARD

The work described here is an attempt at developing a method of applying the kinetic theory of cluster formation of E. R. Buckle[1] to experiments in supersonic nozzles. The patient support of the Power Branch and the Atmospheric Sciences Program, Office of Naval Research over many years and the recent support of the Naval Air Systems Command is acknowledged with many thanks. This effort has necessarily been an iterative one between theoretical development and numerical evaluation over more than ten years of investigation. Mathematical approximations were avoided from the start by relying on the digital computer from the start of development. Time-shared computer facilities were provided by the Naval Weapons Lab, Dahlgren, Virginia, as early as 1965 and since 1967 by the Naval Academy. The importance of interactive time-shared facilities which allow the investigator to treat the computer directly as a laboratory simulator is not to be underestimated, for without easy access to such a system this work could not have been completed.

The cluster theory[1] was developed for a binary mixture of monatomic gases and it seems a bit presumptuous to apply it to as complicated a system as water vapor in air. However, the best data and most clearly understood nozzle behavior was for such a mixture and at least a useful first approximation was hoped for. Moreover, the phenomenon of condensation is

universal and it was hoped that the solution could be worked out in terms of some such general manner, largely independent of the exact form of inter-molecular potentials. The end result is far better than expected and it appears that an average pair interaction energy can be used to describe as complicated a non-equilibrium interaction as that bonding a water molecule in a cluster.

The objective of this study is the development of a technique of applying the cluster theory[1] to the condensation of atmospheric water vapor in air while expanding in a supersonic nozzle (wind tunnel). Overall behavior of such flows is well understood[7,8,9] now and accurate measurement of experimental properties provides a means of comparison with theoretical results. It is attempted here to describe the course of the homogeneous condensation in a nozzle from molecular rather than thermodynamic parameters. Parametric studies of the influence of the adopted molecular parameters are given demonstrating the sensitivity of their influence on thermodynamic properties.

The general scheme is to establish a valid equilibrium initial value for the calculations, then by calculation follow the course of the expansion in a nozzle through the region of condensation[7,8,9]. Two models of water clusters evolve, one a hard sphere collision model and the other a clathrate type model more akin to water vapor. After establishing what

appears to be a valid initial equilibrium condition, the non-equilibrium expansion follows with a close matching of the experimental pressure to that calculated from the theory. One finds that the non-equilibrium cluster behavior is dominated by the behavior of the internal enerfy redistribution frequency.

The calculations described here were performed on a H-635 computer using the Dartmouth Time-Shared System (DTSS) with the long non-equilibrium calculations being performed on a Digital Equipment Corporation PDP-15/40 medium scale computer. The equilibrium solution requires about one minute while the non-equilibrium solution requires in excess of one hour.

The discussions over many years with Dr. W. Dunning, University of Bristol and with Dr. P. P. Wegener, Dr. B. T. Chu and other Yale University Researchers working on condensation, as well as Dr.'s B. N. Hale and P. L. M. Plummer at the University of Missouri-Rolla, were helpful and are acknowledged.

This work could not have been completed without the continuing advise and encouragement of E. R. Buckle, Sheffield University whose help was sincerely appreciated.

The author gives thanks to the Power above for allowing a glimpse into his very nature as seen in the dynamic beauty of these calculations.

III. CLUSTER DISTRIBUTIONS AT EQUILIBRIUM

1. Limiting Constraints

The cluster theory[1] is formulated such that non-stationary growth and decay rates of clusters of every size follow from phase integral specification of unimolecular and bimolecular reaction probabilities. Conceptually, each cluster was originally proposed as an assembly of atoms bound together by isotropic London forces. Consequently in extending this monomolecular theory to the polyatomic water molecule, one must accept an average value of the pair interaction energy complementing the isotropic London forces. As will be seen later this does yield meaningful results, even in the highly dynamic non-equilibrium situation considered later.

Furthermore, each molecule in a cluster can act as an oscillator with the number of vibrational degrees of freedom per cluster χ_g determined by

$$\chi_g = 3g - 5, \text{ for the dimer;}$$

$$\chi_g = 3g - 6, \text{ for all larger sizes;}$$

g, being the number of molecules in a cluster. The vibrational energy of these oscillators circulates within a cluster at frequency $\bar{\nu}$. As in any assembly of loosely coupled oscillators (with nearly similar vibrational characteristics), at any time a single oscillator may possess no energy or alternatively all of the energy. Before the latter condition could be realized, however, the unimolecular decay criterion[1] would cause the loss of that particular oscillator. That is, when

the energy of a single surface oscillator exceeds the "coupling" energy to its nearest neighbors it is lost from the cluster; this energy amounts to $\lambda_g u^\circ_{11}$ where λ_g is the nearest neighbor coordination number and u°_{11} is the pair interaction energy.

This decay energy or energy increment per loss (or gain) should not be confused with the cluster potential energy as in addition to the vibrational energy circulating from oscillator to oscillator, the cluster possesses energy binding it together; this is discussed further in III-8 and V-2.

Another parameter to be specified is $\{\alpha_g\}$* which apportions some fraction of the χ_g overall vibrational modes to be those of surface sites eligible for decay. The limiting constraints selected to obtain this parameter as well as those above are now considered.

The cluster theory independent parameters to be specified or determined are:

u°_{11} - pair interaction energy

$\bar{\nu}$ - cluster internal energy circulation frequency

$\{\alpha_g\}_{g>1}$ - surface site to internal site parameter

$\{\lambda_g\}_{g>1}$ - nearest neighbor coordination numbers

C_1 - monomer concentration

g_∞ - cluster size of effective numerical infinity

*{ } These brackets denote the set over all g.

where C_g is the stationary concentration (f_g is used for non-stationary states). It is the determination of these quantities from the limiting constraints that makes the solution unique to water. (In addition the collision cross sections, molecular masses involved, and some knowledge of the structure is required, see III-8). This is in marked contrast to a nucleation theory developed for a specific vapor[3] (water) where the vibrational characteristics of the particular molecule involved are included as parameters *within the theory*.

The limiting constraints to be satisfied here for saturated vapor equilibrium at any temperature far removed from the critical point are:

(1) Equilibrium constant; $\omega_\infty = \lim_{g \to g^\infty} \omega_g$

(2) Zero temperature sublimation enthalpy; $\Lambda_o = \lambda_\infty u^\circ_{11}$

(3) Saturated vapor pressure; $p_v = \sum_{g>o} C_g kT$

(4) Molecular number balance; $C_{10} = \sum_{g>o} g C_g$

(5) Incremental surface free energy change; $\delta\zeta = 0$ $\quad g \to g^\infty$

(6) *Static pressure profile; $\{p_k\}_{theor.} = \{p_k\}_{exp.}$

(calculated by starting from initial stationary $\{C_g\}$)

The computational procedure described next is iterative in nature; iterative within the equilibrium solution as well as between resulting equilibrium and non-equilibrium solutions. *Non-equilibrium condition satisfied later.

As will be seen later in V-2, even if satisfactory molecular descriptions of either the latent heat or surface tension were known, they would not be used instead of limiting constraint (6) to yield a complete evaluation of the theory because of the nature of $\bar{\nu}$. Approximate means of calculating these two parameters are proposed here but they are not used as limiting constraints.

The first of the variables discussed is α_g, the surface site to internal site parameter. Recall from the cluster theory[1] that this parameter apportions the fraction of total vibrational degrees of freedom that are decay vibrations, i.e., associated with surface sites. In the absence of a theoretical interpretation of this parameter in terms of the equations of molecular motion within the cluster, one must choose a model for the cluster structure. The very nature of the unimolecular decay mechanism in the theory obscures the precise effect of the internal structure of clusters, thus detail of this nature must come from other considerations.

The first approach is to envision a water vapor cluster as an assembly of hard spheres with collision cross sections defined in the classical sense[1]. For small size clusters all molecules would appear to be on the surface (See Figure VI-3.1) and paralleling the Pauling type clathrate cage where the first cage closes at size g = 20 we define

$$\alpha = 1, \qquad 2 \leq g \leq 20 \qquad \text{III-1.1}$$

The cluster theory[1] yields a limiting value of α_∞ for clusters having macroscopic properties in the equation preceding 8.14[1], i.e.

$$\alpha_\infty = \lim_{g\to\infty} \alpha_g = \left(\frac{36\pi}{g}\right)^{1/3} \qquad \text{III-1.2}$$

As will be seen later, the structure based on hard sphere collision diameters yields a value of g_∞ near 120. When $g_\infty \cong 120$, $\alpha_\infty \cong 0.98$ so the parameter α_g remains near unity. The behavior imposed here for what might be called the hard sphere collision (HSC) is:

$$\alpha_g = 1, \qquad 2 \leq g \leq 20$$

$$\alpha_g = 1\text{-}0.1\left(\frac{g}{g_\infty}\right), \qquad g > 20 \qquad \text{III-1.3}$$

The variation of α_g, $g > 20$ does not have a great overall effect on the cluster distribution. Calculations were performed with various forms of the expression for α_g and gave only minor differences in the final result, the same cannot be said for the parameter λ_g, however (see below).

In the interest of closer approximating the structure of water clusters a second structure was considered (see following discussion on collision diameters and Section V-2). Implicit in this second model is the departure from Van der Waal type forces but with a structure and bonding more akin to water. Calculations with the model now designated as the water clathrate model (WCM) show a shift of g_∞ to about $g = 200$ so α_∞ becomes about 0.83. For this case we have

$$\alpha_g = 1 - 0.2\,(\frac{g}{g_\infty}),\ 20 \leq g \leq 200 \qquad \text{III-1.4}$$

It will be seen that both models yield good results in predicting the dynamic behavior of non-stationary states (Section V-2).

For the hard sphere collision (HSC) corresponding to equation III-1.3, the hard sphere collision diameter is[1]

$$\sigma_{1,g} = r_1(1+g^{1/3}) \qquad \text{III-1.5}$$

A closer approximation to actual dimensions taken from a scale water clathrate model - WCM would be

$$\sigma_{1,g} = r_1(1+2(g)^{1/3}), \qquad \text{III-1.6}$$

which is used with α_g described by equation III-1.4. The value of r_1 used is $1.4.10^{-8}$cm for all calculations. A summary on all aspects of both models is given in Section V-3.

2. Iteration Scheme

Having specified the independent parameters of the theory and the limiting constraints which must be satisfied, it is now shown how these conditions are met. Referring to the iteration scheme of Table III-2.1, one initiates the problem by selecting values of temperature T, pair interaction energy u°_{11} and vibrational energy circulation frequency $\bar{\nu}$. A starting value of u°_{11} was obtained by subtracting 3kT (for rotation and translation modes and ignoring expansion work) from the latent heat *per molecule* at 273°K and equating the result to $\lambda_\infty u^\circ_{11}$. Selecting, arbitrarily, $\lambda_\infty = 3.0$ gives a starting value of $u^\circ_{11} = 2.98$ k cal/mole.

TABLE III-2.1

ITERATION SCHEME

	choose	T °K
	choose	u°_{11} (limiting constraint 2)
(A)	choose	$\bar{\nu}$
	calc.	C_1 (perfect gas at saturation pressure for $p \cong C_1 kT$)
(B)	choose	C_1 (since $p = \frac{\Sigma}{g>o} C_g kT$)
	calc.	λ_∞
	calc.	F_θ from ω_∞, (a), (Limiting case $g \to g^\infty$, $\omega(\nu, u^\circ_{11})$)
	calc.	$F(g,\theta)$ from ω_∞, (b), ($\omega_\infty = MLF(g,\theta) = \omega(u^\circ_{11}, \lambda_\infty)$
(go to A)	compare	$F(\theta)$ & $F(g,\theta)$ if $F(a) \neq F(b)$ within ε modify $\bar{\nu}$ (limiting constraint 1)
	choose	g_∞ (Section III-3)
(C)	choose	m_λ (slope of λ_g vs g)
	calc.	$\{C_g\}$
	calc.	P_v
(go to B)	calc.	C_{10}, if $p_v \neq p_v^{(4)}$ and $C_{10} \neq C_{1_{initial}}$, modify C_1 (limiting constraints 3 & 4)
(go to C)	plot	ζ, if $\Delta\zeta \neq o$ at $g = g_\infty$, modify m_λ (limiting constraint 5)
		Use $\{C_g\}$ as initial condition for non-equilibrium nozzle calculation. Follow expansion down to onset of condensation at pressure p_k, if $\{p_k\}_{theor.} \neq \{p_k\}_{exper.}$, modify $\bar{\nu}$ (limiting constraint 6)

Choice of the vibrational energy circulation frequency raises questions on its relation to that of vibration spectra of water observed experimentally. For water vapor[4] there are frequencies associated with shifts in mean molecular position as well as with individual molecular vibrational modes; the former range from about 10^{11} to 10^{12} sec^{-1} while the latter range upwards from 10^{12} sec^{-1} to well above 10^{13} sec^{-1}.

The cluster theory[1] assumes random distribution of the vibrational energy $\chi_g kT$ circulating at frequency $\bar{\nu}$ over χ_g vibrational modes. In the classical approximation

$$\bar{\nu} << kT/h \qquad \text{III-2.1}$$

(where h is Planks constant) such that the circulation frequency cannot exceed the frequency of any one vibration. It is assumed that the vibrational energy circulation frequency here is more closely related to water spectral frequencies associated with intermolecular vibrations (shifts in molecular position); this assumption is supported by later results (Section V-2). At the initial temperature of interest, 273°K, equality in equation III-2.1 gives

$$\bar{\nu} = 5.7 \times 10^{12} \text{ sec}^{-1}.$$

Next, the approximate manomer concentration C_1 is calculated from the perfect gas law ($p = CkT$) first taking $C \cong C_1$ and a linear least squares fit of vapor pressure data for the liquid state[5]. It is assumed then that

$$p \equiv \sum_{g>o} C_g kT, \qquad \text{III-2.2}$$

such that all clusters behave as a gas. The value of C_1 calculated above from the perfect gas law must be reduced to account for the partial pressure of the clusters and at the same time maintain conservation of mass by molecular number balance in limiting constraint (4); this latter condition requires that the number of molecules of water in any distribution does not exceed the number calculated originally from the vapor pressure and the ideal gas law.

Once the initial value of u°_{11} is chosen at the start of this iteration process, the value of λ_∞ is fixed by limiting constraint (2). The next step follows from the theory[1] as the equilibrium constant at saturation for the limiting case ($g \to g\infty$) is $\omega_\infty = 1/C_1$. This result comes from the definition of the parameter J,

$$J \equiv \ln C_1/\omega_\infty, \qquad \text{III-2.3}$$

which differs slightly from ln of the saturation ratio because equation III-2.2. At saturation J = 0 and $C_1 = 1/\omega_\infty = C_{1s}$ so an alternate expression for J is

$$J = \ln C_1/C_{1s}. \qquad \text{III-2.4}$$

Perhaps the most indirect of all the limiting constraints specified is condition (1) but this gives a means of selecting a value for the internal energy circulation frequency $\bar{\nu}$ that satisfies other conditions of the theory. Consider first the equilibrium constant which results from detailed balance for

each g size (see {8}, reference 1 for complete details)

$$\omega \equiv C_g/C_1C_{g-1} = ML_gF(g,\theta), \qquad \text{III-2.5}$$

where M, F, G are convenient groupings defined by

$$M = (8\pi u^\circ_{11}/m_1)^{1/2} r_1^2/\bar{\nu}, \qquad \text{III-2.6}$$

$$L(g>3,o) = (K_{g-1}/\alpha_g) \begin{pmatrix} \chi_g^{-1} \\ n_{g-1} \end{pmatrix} \Big/\!\Big/ \begin{pmatrix} \chi_{g-1} \\ n_{g-1} \end{pmatrix}, \qquad \text{III-2.7}$$

$$K \equiv (\sigma_{1,g}/r_1)^2/(\mu_{1,g}/m_1)^{1/2} \qquad \text{III-2.8}$$

$$F(g,\theta) = (e^\theta/\theta^{1/2})\ G(g,\theta), \qquad \text{III-2.9}$$

$$G(g>3,\theta) = \{\exp[\theta(\lambda_{g-1})]-\exp[\theta/(\lambda_g-\lambda_{g-1}-1)]\}$$

$$/(1+\lambda_g\theta + \lambda_g^2\ \theta^2/_2), \qquad \text{III-2.10}$$

where $\theta = u^\circ_{11}/kT$, m_1 is molecular mass of water, μ is the reduced mass and λ is the nearest neighbor coordination number.

In the thermodynamic limit of size[1] $(g\to\infty)$, $K_{g-1}=g^{2/3}$, $\alpha_g=(36\pi/g)^{1/3}$ and $\lambda_g=\lambda_\infty$ giving the asymptotic values independent of size g.

$$L_\infty = (1/36\pi)^{1/3}, \qquad \text{III-2.11}$$

$$F(g,\theta) = F(\theta) = [\exp(\lambda_\infty\theta)-1/$$

$$\theta^{1/2}(1+\lambda_\infty\theta+\lambda_\infty{}^2\theta^2/_2), \qquad \text{III-2.12}$$

$$\omega_\infty = ML_\infty F\theta \qquad \text{III-2.13}$$

Now, making use of the thermodynamic limit of size $(g\to\infty)$ at the condition of a saturated vapor (J=0) gives, by equation III-2.3, III-2.11 and III-2.13

$$F(\theta) = \omega_\infty/ML_\infty = \frac{1}{C_{1s}ML_\infty} \qquad \text{III-2.14}$$

allowing equality here with equation III-2.12. Having already defined values of u°_{11} and λ_{∞} in this iteration sequence some value of $\bar{\nu}$ will satisfy both III-2.12 and III-2.14.

At this point some implicit conditions of the theory[1] must be satisfied. The surface free energy in terms of the equilibrium constants is

$$\zeta = -kT \sum_{i=2}^{g} \ell n(\omega_i/\omega_{\infty}). \qquad \text{III-2.15}$$

As ω tends to ω_{∞} ($g \to \infty$) and the clusters take on bulk properties (at saturated equilibrium), by equation III-2.15 the increment of surface free energy $\Delta\zeta = \zeta_g - \zeta_{g-1}$ must approach zero; this requirement becomes limiting constraint (5). Also, by equation III-2.5 the value of $\Delta\zeta$ is positive when $G(\theta)/G(g,\theta) > L_g/L_{\infty}$.

This important condition begins to limit the range of u°_{11} and $\bar{\nu}$. In general, high values of u°_{11} require high values of $\bar{\nu}$ in order that $\Delta\zeta$ be positive over all g; too low a value of $\bar{\nu}$ causes a hump in the distribution $\{C_g\}$ with $\Delta\zeta < o$. At the upper bound on $\bar{\nu} \approx 5.7 \cdot 10^{12}$ sec^{-1}, u°_{11} must be reduced to about 2.91kcal/mole to satisfy the condition $\Delta\zeta > o$, $g \to \infty$ as well as equations III-2.12 and III-2.14.

3. Numerical Infinity

In any numerical iteration technique an upper bound on the calculations must be specified. Selecting the value of cluster size corresponding to numerical infinity is considered next although this in reality is a separate iteration and an independent method of determining the size at which clusters

take on bulk properties. A first approximation at the value g_∞ is arrived at by the method described next, further refinement is a result of iteration to satisfy limiting constraint (5).

We must borrow from the following section the description used for surface coordination number for nearest neighbors, λ_g. The simplest behavior of this parameter would be a linear variation with cluster size. The slope of such a variation is taken as m_λ, which is, in fact, the incremental change in surface coordination number per unit increase of cluster size (above the trimer). The equilibrium computer program (See VIII-2) is now run with all variables held constant except for m_λ. An arbitrary value of this parameter yields a minimum (artificial) in a plot of the resulting saturated equilibrium cluster concentration versus size g. Defining the cluster size at the minimum in concentration as $g=g^*$ and plotting this against the assumed value of m_λ gives the result in Figure III-3.1. The difference in the quantity $\lambda_\infty-\lambda_{g^*}$ is also plotted; λ_{g^*} being the value of λ_g corresponding to the minimum in $\{C_g\}$.

As the value of slope m_λ is decreased the cluster size g^* at the minimum in $\{C_g\}$ tends upward in size, the difference $\lambda_\infty-\lambda_{g^*}$ approaches zero and as is shown next the increment in $\Delta\zeta$ approaches zero. Below a slope of $m_\lambda \cong 0.01$, the minimum in g^* rapidly exceeds 10^3 (HSC). Once this approximate value of m_λ is determined it is further refined by iteration to satisfy limiting constraint (5).

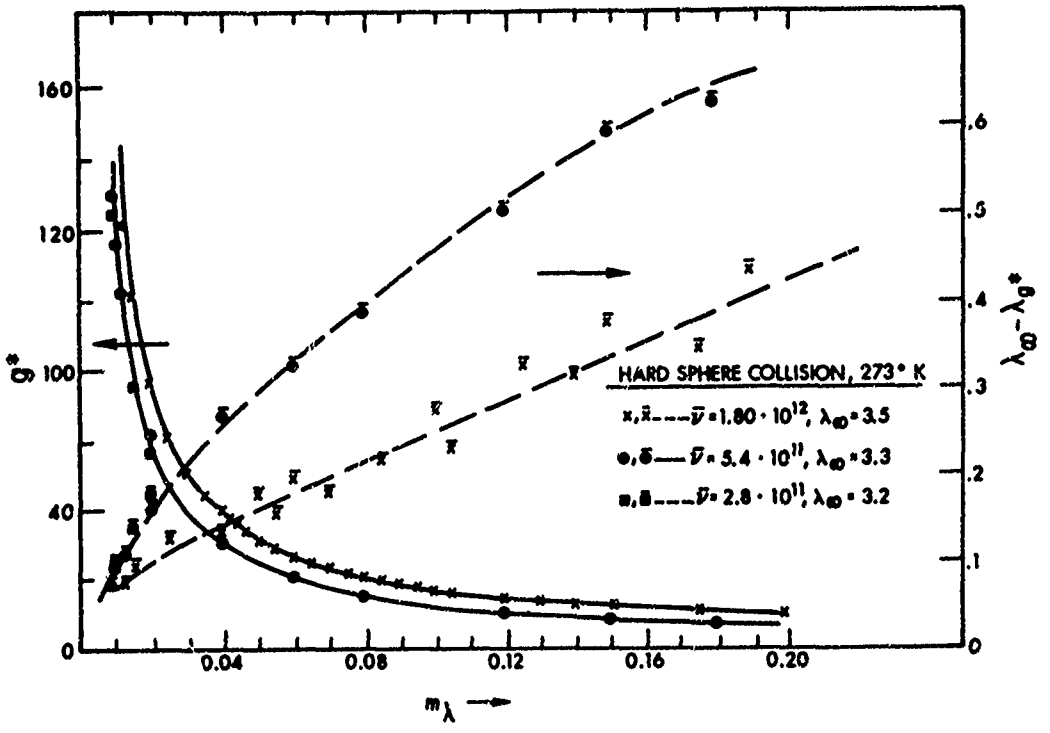

Figure III-3.1
Approximate Numerical Infinity

In Figure III-3.1 the effect of determining g* at several values of circulation frequency $\bar{\nu}$ and λ_∞ is evident with no great change occurring with small variations in either parameter. The effect of slight changes of slope m_λ on surface free energy are shown in Figure III-3.2 indicating its sensitivity to structural variation. At a cluster size of about g=123, $\Delta\zeta$ is effectively zero (to three figure accuracy) for the hard sphere collision for the conditions shown.

4. Nearest Neighbor Coordination Number

With regard to the variation of nearest neighbor coordination number λ_g, only the behavior with linear variation is present here; numerous other descriptions were attempted but satisfaction of the limiting constraints was not achieved. Considering the previous discussion on α_g we see that no matter what model is considered (HSC or WCM) the first 20 molecules are prescribed as surface molecules; the immediate consequence is that λ_g is a surface coordination number for $g \leq 20$. Since we use equation III-1.3 to describe α_g (HSC), g>20 nearly all of the other sites are surface sites and λ_g must be essentially a surface coordination number throughout. It will be seen later (V-2), that the principal contribution to the reaction dynamics is from small cluster sizes (g<10) so the distinction between surface and bulk coordination is unimportant for either the HSC or WCM case. In the absence of any further theoretical relation between λ_g and α_g we assume the following. The upper limit of the set $\{\lambda_g\}$ is λ_∞

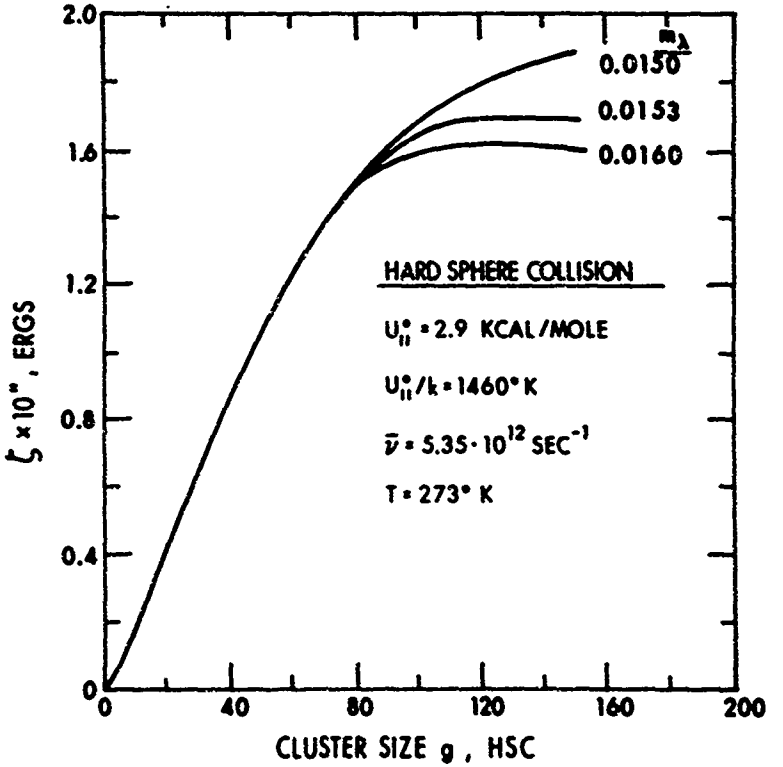

Figure III-3.2
Surface Free Energy

whose value is known from the asymptotic approximation discussed earlier (equation III-2.11 & III-2.13). A lower bound is also known since for the dimer, $\lambda_2 = 1$ and for the trimer $\lambda_3 = 2$. Thus for $g>3$ λ_g can vary only between the limits 2 and λ_∞. For water (or ice) it is reasonable to suppose λ_∞ cannot be far removed from a value of 4.0 representative of tetrahedral coordination[4].

Of the many variations of λ_g considered the following two linear models were most successful in satisfying the constraint:

$$\lambda_g = \lambda_3 + m_\lambda(g-3); \quad m_\lambda = \text{const.}, 3<g\bar{<}g_\infty,$$

$$\lambda_g = \lambda_\infty; \quad g>g_\infty, \qquad \text{III-4.1}$$

and

$$\lambda_g = \lambda_3 + \frac{g}{g_\infty}(\lambda_\infty-\lambda_3); \quad 3<g\bar{<}g_\infty$$

$$\lambda_g = \lambda_\infty; \quad g>g_\infty \qquad \text{III-4.2}$$

The second linear case, equation III-4.2, yields results quite similar to those of equation III-4.1 except that fine adjustment in m_λ allows attaining the zero change in incremental surface free energy required by limiting constraint (5), (See Figures III-3.2, and III-4.1 to 3) while adjusting g_∞ in equation III-4.2 does not. The behavior adopted henceforth is according to equation III-4.1.

The final limiting constraint, (6), which requires agreement between theoretical and experimental supersonic nozzle static pressure distribution is satisfied in section V-2.

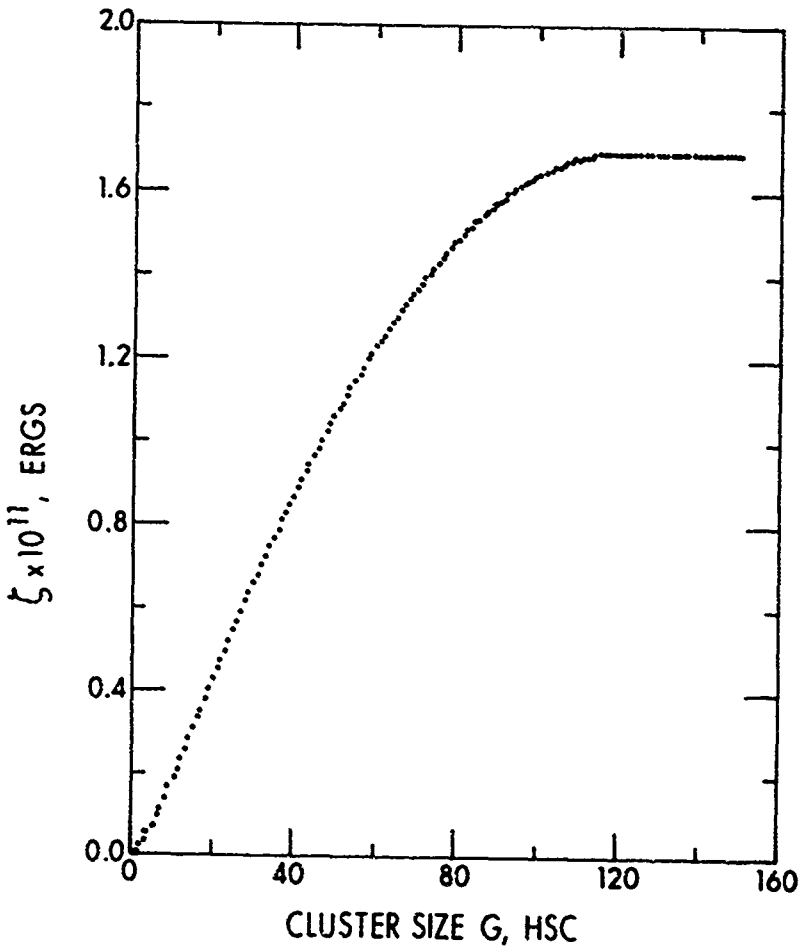

Figure III-4.1
Surface Free Energy at Saturation, 273° K

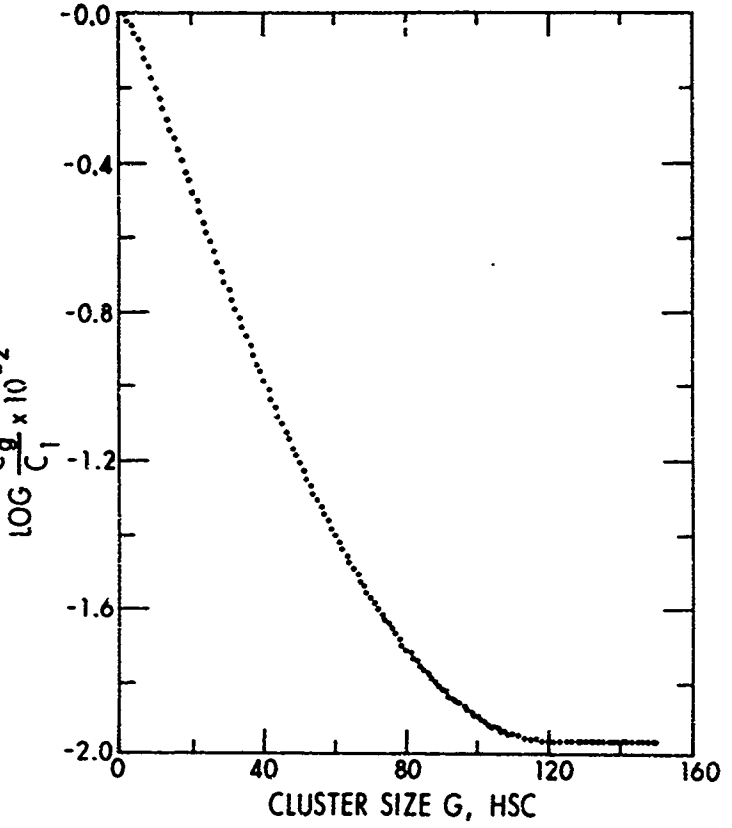

Figure III-4.2
Concentrations at Saturation, 273° K

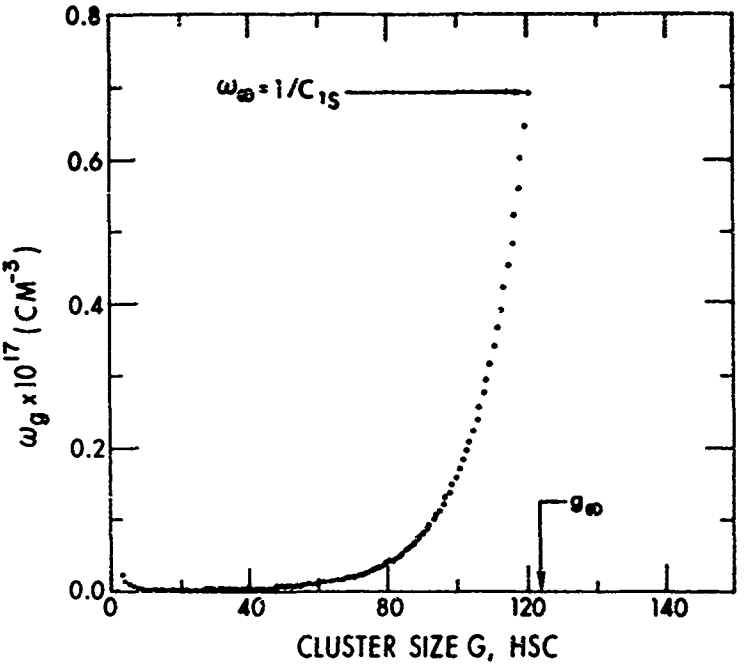

Figure III-4.3
Equilibrium Constant, 273° K

Solution of the equations for saturated equilibrium (8.1 to 8.16, ref. 1) for the case of water vapor in air is given in a FORTRAN interactive computer program in Appendix 2 with the nomenclature given in Appendix 1. Corrections to reference 1 are given in Appendix 4. A summary of HSC results for several values of pair interaction energy is given in Table III-5.1. Results are also given for the dimer equilibrium constant for comparison with that obtained[2] from Keyes [6] data.

5. Results at Saturated Equilibrium

When one succeeds in satisfying limiting constraints (1) through (5), the results appear (HSC) as in Figures III-4.1 to III-4.3. At conditions of saturated equilibrium, satisfying boundary condition (5) also implies that $\Delta C_g = 0$ as $g \to g_\infty$. This is evident from the equilibrium distribution[1]

$$C_g = C_1 \exp[(g-1)J - \zeta_g/kT], \qquad \text{III-5.1}$$

which at saturation (J=0) is

$$C_g = C_1 \exp[-\zeta_g/kT]. \qquad \text{III-5.2}$$

i.e., at a given temperature the variation in $\{C_g\}$ at saturation is entirely dependent on the incremental change in surface free energy $\Delta\zeta_g$ with cluster size. The use of the concept of an effective numerical infinity is tantamount to the assumption that clusters of size $g \cong g_\infty$ exhibit bulk properties.

In Figure III-3.2 it is evident that the distribution $\{C_g\}$ is quite sensitive to the variation in $\{\lambda_g\}$. A zero value of the slope m_λ in equation III-4.1 yields a nearly linear decreasing distribution $\{C_g\}$ with, of course, no minimum appearing. A finite value of m_λ causes a minimum in the distribution $\{C_g\}$ with limiting constraint (5) requiring that this minimum occur at effective numerical infinity. In the WCM case, Figure III-5.1 shows that the minimum in $\{C_g\}$ or alternatively $\Delta\zeta \to 0$ has shifted outward to the neighborhood of $g_\infty \cong 200$.

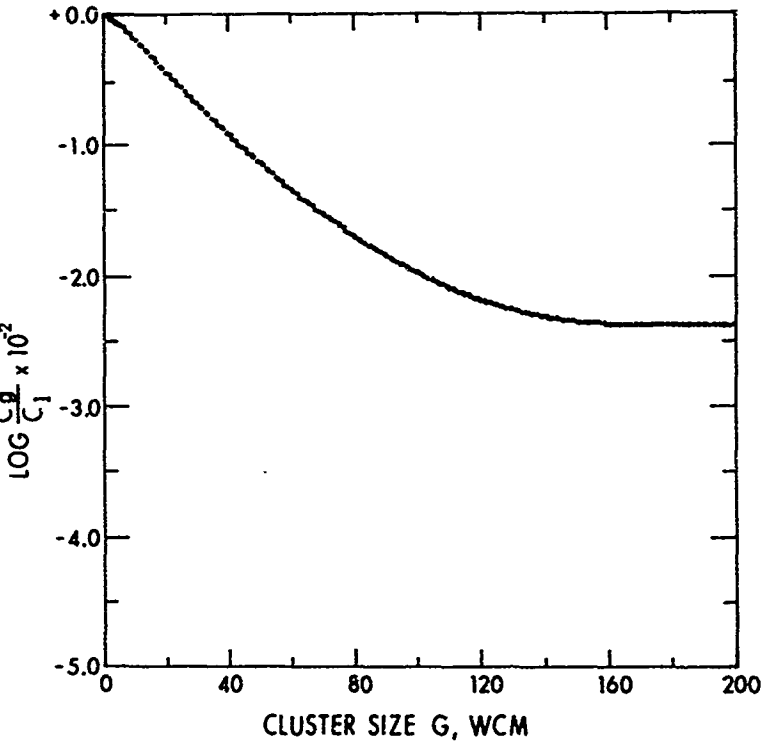

Figure III-5.1
Concentrations at Saturation, 273° K

TABLE III-5.1

EQUILIBRIUM RESULTS AT 273°K

1) HARD SPHERE COLLISION (HSC)

Case	u°_{11}/k(°K)	u°_{11}(Kcal/mole)	$\bar{\nu}$ (sec^{-1})	C_1 (cm^{-3})	λ_{∞}	g_{∞}	m_{λ}	pv(cmHg)	C_{10} (cm^{-3})	ω_2 (cm^{-3})
a	1387*	2.76	$5.30 \cdot 10^{12}$	$1.60 \cdot 10^{17}$	4.10	124	0.0169	0.452	$1.60 \cdot 10^{17}$	$3.11 \cdot 10^{-21}$
b	1421**	2.82	$5.35 \cdot 10^{12}$	$1.60 \cdot 10^{17}$	4.00	123	0.0162	0.452	$1.60 \cdot 10^{17}$	$3.50 \cdot 10^{-21}$
c	1460	2.90	$5.35 \cdot 10^{12}$	$1.60 \cdot 10^{17}$	3.90	124	0.0153	0.452	$1.60 \cdot 10^{17}$	$4.02 \cdot 10^{-21}$
d	1500	2.98	$5.31 \cdot 10^{12}$	$1.60 \cdot 10^{17}$	3.79	124	0.0144	0.452	$1.60 \cdot 10^{17}$	$4.69 \cdot 10^{-21}$
			2) WATER CLATHRATE MODEL (WCM)							
c	1460	2.90	$5.35 \cdot 10^{12}$	$1.60 \cdot 10^{17}$	3.90	195	0.0097	0.452	$1.60 \cdot 10^{17}$	$4.02 \cdot 10^{-21}$

*Iteration to satisfy dimer equilibrium constant $\omega_2 = 3.1 \cdot 10^{-21}$ obtained[2] from Keyes data[6]

**Iteration to give $\lambda_{\infty} = 4.0$

6. Variations with Temperature

The computer program of Appendix 2 gives results at saturated equilibrium at any temperature by varying the input temperature. Having satisfied boundary condition (1) through (5) at 273°K, the parameters listed in Table III-5.1(c) were used at the other temperatures given. The monomer concentration satisfying boundary conditions (3) and (4) was the only iteration performed with the end result that condition (3) was satisfied at the temperatures given. The HSC concentrations obtained are given in Figure III-6.1 with the net result that boundary condition (5) was satisfied over the range 290°K-230°k. (See later discussion on $\bar{v}$, however, in Section V-2 with regard to condition (1)).

7. Surface Tension of Clusters

Theory[1] gives for the small cluster property corresponding to the specific tension in the vapor-liquid interface

$$\Gamma = (\zeta_g/g\alpha)(\rho/m_1)^{2/3}, \qquad \text{III-7.1}$$

which differs from the classical result obtained by equating the product of surface area and surface tension equal to surface free energy, i.e.:

$$\Gamma = (\zeta_g/g^{2/3})(\rho/m_1)^{2/3} \;/\; (36\pi)^{1/3}, \qquad \text{III-7.2}$$

where in effect $\alpha = (36\pi/g)^{1/3}$, but note that this is α for a flat surface (cf. line 3, pg. 1280, Ref. 1). Early attempts at evaluating the theory included satisfying equation III-7.1 as a boundary condition. Examination of results in Figure

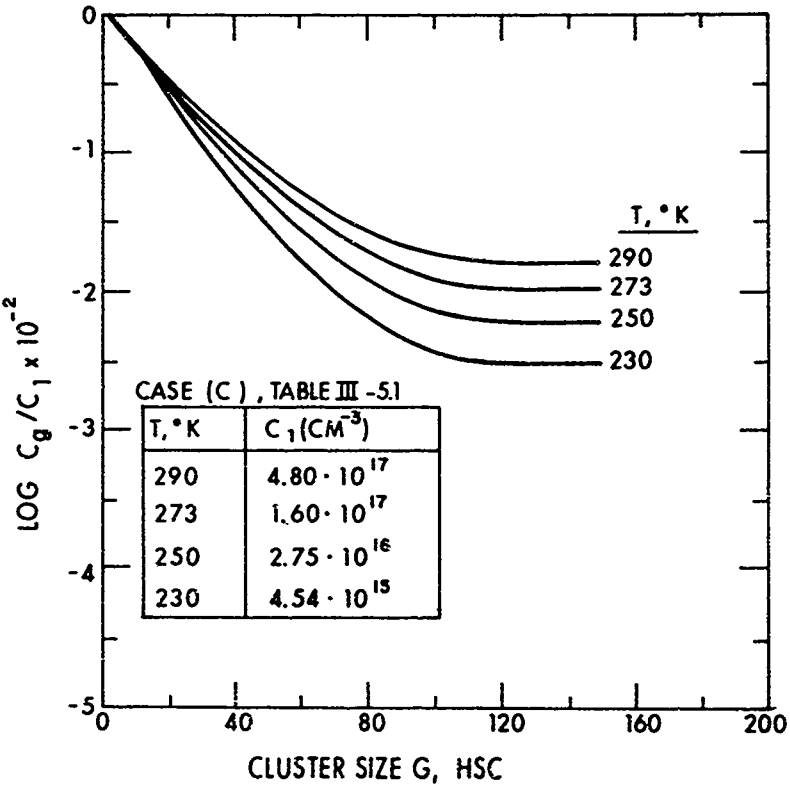

Figure III-6.1
Concentrations at Saturation, 290° to 230° K

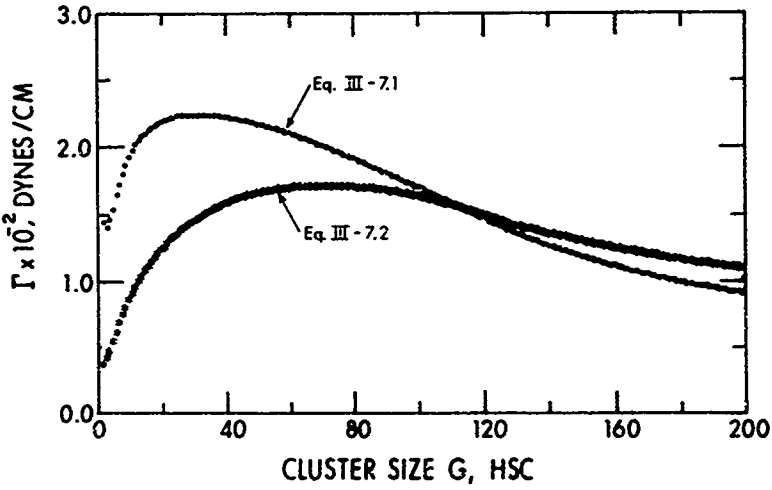

Figure III-7.1
Surface Tension Variation, Saturation 273° K

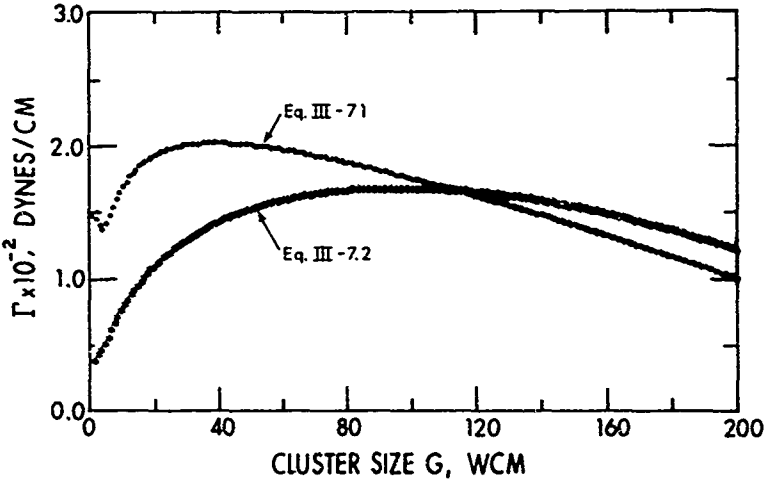

Figure III-7.2
Surface Tension Variation, Saturation 273° K

III-7.1, however, shows that for the Hard Sphere Collison, macroscopic levels (~ 75 dynes/cm at 273°K) are not reached until the cluster size approaches g = 200 using equation III-7.1, or much larger sizes by equation III-7.2. To conform with conditions specified thus far, for $g<g_\infty \cong 124$ equation III-7.1 is appropriate and for larger size, equation III-7.2 would seem more appropriate. Results in Figure III-7.2 for WCM indicate that macroscopic levels of surface tension would not be attained in either case until sizes in excess of about 250 were reached.

The net result is that the use of surface tension as a limiting constraint precludes the possibility of satisfying all other limiting conditions imposed. It appears that the simple molecular viewpoint used to interpret the equilibrium theory here requires that the property Γ corresponding to small clusters be considered higher than the macroscopic, even at the cluster size satisfying other limiting constraint for $g \to g_\infty$.

8. Latent Heat

As a possible alternative limiting constraint the thermodynamic property known as latent heat was considered. In the absence of a molecular description of this property the following crude model is proposed.

Consider the energy added to a system in going from the liquid to vapor state (at constant pressure, temperature) as the energy used in breaking bonds in the liquid to establish

and energize an equilibrium population of monomer, dimer, trimer, etc. in the vapor plus the work in moving the system boundaries. In the liquid state some of the nearest neighbors may be hydrogen bonded in tetrahydral coordination[4], others may not be involved in hydrogen bonds. The fraction not involved in such bonding may be as high as about 0.6 at 273°K with most results[4] predicting a value near 0.5. A crude attempt is made below to allow for the overall effect of such unbonded water molecules in the liquid state.

In proposing this crude model of latent heat some knowledge of the structure of water clusters is required. Cluster structure which evolved in the course of the iterations to satisfy limiting condition (6) is discussed in section V-4 and the resulting number of bonds η_g per cluster is given in Table III-8.1 for both the HSC and WCM. The bonding scheme is important because the energy stored in these bonds must be considered as cluster internal potential energy in addition to its vibrational energy.

TABLE III-8.1
BONDING ARRANGEMENT

Liquid	Vapor	η,HSC	η,WCM
$\eta = \lambda_\infty = 4$, bonded	monomer	0	0
	dimer	1	1
$\eta < 4$, unbonded	trimer	2	2
	g-mer	$g\lambda_g/2$	g-1

For hydrogen bonded molecules in the liquid state with tetrahydral coordination, removal of a single molecule is taken here as the breaking of $\lambda_\infty = 4$ bonds; in the non-hydrogen bonded case the number is lower and is discussed below.

Using these concepts, for each dimer formed two molecules have their bonding changed from $\eta=\lambda_\infty$(liquid) to η_2(vapor). Assuming pairwise additive interactions for nearest neighbors (at absolute zero in temperature) the energy required to separate infinitely a single molecule from the liquid is $\lambda_\infty u^\circ_{11}$. In forming the dimer, two such actions are required and the energy regained on bringing two infinitely separated molecules to form a dimer is $\eta_2 u^\circ_{11}$. Hence, the energy required to produce a dimer from the liquid (at T=0) is $(2\lambda_\infty-\eta_2)u^\circ_{11}$. By similar reasoning, we have a g-mer: $(g\lambda_\infty-\eta_g)u^\circ_{11}$. There does not appear to be any reliable method of predicting what fraction of the liquid state molecules are hydrogen bonded in tetrahydral coordination, so simple reduction of λ_∞(liquid) from 4.0 to a lower value determined by iteration is introduced to give an overall or effective λ_∞ in the liquid state. Thus a resulting value of λ_∞= 4.0 would imply 100% bonding in tetra-hydral coordination; a lesser value implies the presence of unbonded molecules in the liquid state. Next, to adjust for temperature above zero we must add an amount of energy equal to the difference in thermal energies of the g molecules in the gaseous and liquid states as well as the work of moving the system boundary

outward from the liquid state to that encompassing both liquid and vapor. This additional volume is that required to allow full thermal energy for each cluster in the vapor.

We can now express the T=0 energy difference from liquid to vapor, say for the dimer as (in ergs per cc of dimer):

$$(g\lambda_\infty - \eta_2)u^\circ_{11} \frac{\text{bonds broken (net)}}{\text{dimer formed}} \times C_2 \frac{\text{dimers formed}}{\text{cm}^3} \times u^\circ_{11} \frac{\text{ergs}}{\text{bond}} \qquad \text{III-8.1}$$

For any other size, including the monomer we have $(g\lambda_\infty - \eta_g)$ $C_g u^\circ_{11}$ or in establishing the entire equilibrium population:

$$L^\circ = \Sigma L^\circ_g = \sum_{g>o} (g\lambda_\infty - \eta_g) C_g u^\circ_{11}, \qquad \text{III-8.2}$$

where $\eta_g = g\lambda_g/2$ HSC, g-1 WCM.

In addition to this, energy added to a system to vaporize it must do work against its boundaries and increase the kinetic energy from that in the liquid state to that of the vapor; here the kinetic energy of the liquid state is neglected. As in the theory[1] the clusters have vibrational, rotational and translational energy with the rotational and translational degrees of freedom for the water taken as 6, the dimer as 5 and all others are taken as 6. The vibrational energy is described by[1]

$$\epsilon_v = \chi_g \, kT \qquad \text{III-8.3}$$

where $\chi_g = 3g-5$ for the dimer and $3g-6$ for $g>2$. At constant pressure and temperature, the expansion work per molecule is

pv or considering the clusters as a perfect gas pv=kT.

Thus:

$$L' = L^\circ + \text{Energy}\{\text{trans, rotat., vib.}\} + \text{Work}$$

$$L' = L^\circ + \frac{6}{2} kT(C_1) + \frac{5}{2} kT(C_2) + \frac{6}{2} kT \sum_{g=3}^{g_\infty} C_g + kT \sum_{g=2}^{g_\infty} \chi_g C_g + kT \sum_{g>o} C_g. \qquad \text{III-8.4}$$

To compare this result with accepted data in the literature, such as L = 595.5 cal/g at 273°K[5], the total mass μ_T in grams for the population $\{C_g\}$ is required. Here

$$\mu_T = m_1 V \sum_{g>o} g\, C_g \qquad \text{III-8.5}$$

where m_1 is the mass of a single molecule and V is the total volume occupied. Consequently the density is given by μ_T/V g/cm^3. Thus tabular values[5] of latent heat L are converted to cal/cm^3 by

$$L' = (L \text{ cal/gram})(m_1 \sum_{g>o} g\, C_g \text{ g/cm}^3). \qquad \text{III-8.6}$$

Now, equating the results in equations III-8.4 and III-8.6 gives

$$L = \frac{u^\circ_{11}}{m_1} \sum_{g>o} \frac{(g\lambda_\infty - \eta_g) C_g}{\sum_{g>o} g\, C_g} + \frac{6}{2} \frac{kT}{m_1} \frac{C_1}{\sum_{g>o} g\, C_g} + \frac{5}{2} \frac{kT}{m_1} \frac{C_2}{\sum_{g>o} g\, C_g} + \frac{6}{2} \frac{kT}{m_1} \frac{\sum_{g=3}^{g_\infty} C_g}{\sum_{g>o} g\, C_g} + \frac{kT}{m_1} \frac{\sum_{g=2}^{g_\infty} \chi_g C_g}{\sum_{g>o} g\, C_g} + \frac{kT}{m_1} \frac{\sum_{g>o} C_g}{\sum_{g>o} g\, C_g}, \qquad \text{III-8.7}$$

which allows direct comparison with known values of latent heat in units of cal/g.

Iteration for λ_∞(effective) in equation III-8.7 for the liquid state at 273°K yields a value of 3.04 with L = 595.7 cal/g (HSC) and the term by term contribution to ζ is given in Table III-6.2.

TABLE III-6.2

Results of equation III-8.7 at 273°K, L = 595.7 cal/g, HSC and WMC

Term	1	2	3	4	5	6
Magnitude, cal/g	478	88.2	0.004?	0.002	0.02	29.4
% contribution	80.2	14.8	nil	nil	nil	4.9

with the monomer accounting for nearly all the energy. The solution of case (c) Table III-5.1 was employed here with identical results for both WCM and HSC because of the dominance of the monomer.

It does not appear fruitful to speculate further on the possible fraction of unbonded molecules in the liquid state. Reduction of λ_∞ from 4.0 to 3.04 with the nearest neighbor concept employed here does imply unbonded molecules in the liquid but the fraction is still unknown. The majority still could be in tetrahydral coordination with an appreciable fraction involved in fewer bonds.

Due to the uncertainties involved, the latent heat was not used as a limiting constraint in this work.

IV. CLUSTER DISTRIBUTIONS FOR SUPERSATURATED AND UNDERSATURATED CONDITIONS

1. Experimental Realization

The system considered is that of a dilute solution of water vapor in a carrier gas of air. To examine the states traversed by this mixture while it expands adiabatically in a nozzle it is convenient to refer to Figure IV-1.1 in coordinates of log ρ and log T. For the adiabatic expansion of the mixture $p = c\rho^{\gamma_i}$ where $\gamma_i = c_p/c_v$ and is to a close approximation equal to the ratio of specific heats of air, and $p = \rho Rt$. The slope of the adiabat (ABC) is only a function of the specific heat ratio (γ_i) of the carrier gas

$$\frac{d\ (\log\ p)}{d\ (\log\ T)} = \frac{\gamma_i}{\gamma_i - 1} \qquad \text{IV-1.1}$$

while for the vapor the saturation line (A'C') is obtained from data[5] or the Clausis-Clapeyron relation and $p = \rho rt$:

$$\log p_s = 9.3286 - 2367.713/T,\ 300 < T < 250 \qquad \text{IV-1.2}$$

The vapor and carrier gas temperature are assumed identical at all times[1]. For a mixture initially at point A, the vapor state is undersaturated and $J<0$[1]. Adiabatic cooling of the mixture occurs on expansion, with saturation at point B. Beyond point (B) the vapor is supersaturated with apparent collapse of supersaturation beginning at, say, C. Cluster distributions corresponding to thermodynamic equilibrium from point A to C are now considered with those beyond examined later.

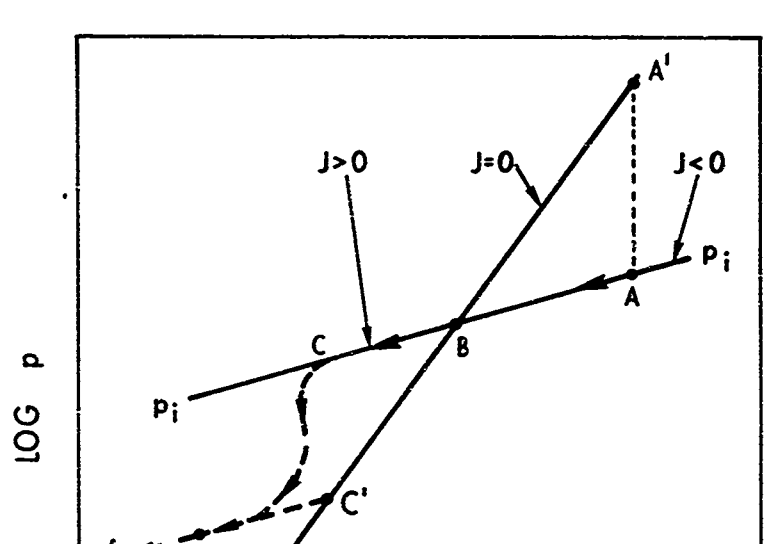

Figure IV-1.1
Hypothetical State Diagram for Adiabatic Expansion
of Water Vapor in Moist Air
A'BC' Saturation Line; ABC Adiabatic Line

Point A is typical of the initial condition encountered in the experiments described later. The undersaturated condition at point (A) where J<0 follows from equation III-5.1. Since $J=\ln C_1/\omega_\infty = \ln C_1/C_{1s}$, the monomer concentration C_{1s} at saturation (A') (at the temperature of point (A) must be calculated to define J_A. Conditions at (A') are known from the solution of Appendix (a) with iterations satisfying the saturation pressure equation IV-1.2, other parameters are retained from the results at 273°K. Once C_{1s} is known, the calculation is rerun yielding the stable undersaturated (J<0) distribution (a), (296°K), given in Figure IV-1.2.

For the supersaturated condition (J>0) again as in the undersaturated case the equilbrium equations must first be solved for C_{1s}. Once C_{1s} is known the solution proceeds as before with limiting constraints (3) replaced by the iteration for the isentropic pressure

$$p_i = 0.452 \left(\frac{T}{273}\right)^{\frac{\gamma_i}{\gamma_i - 1}} \qquad \text{IV-1.3}$$

Typical results for temperatures encountered in later experiments are given in Figure IV-1.2. As noted in the theory[1] the minimum present in $\{C_g\}$ when J>0 corresponds to Volmer's critical size at g=g*. For further discussion of this point see Section VII.

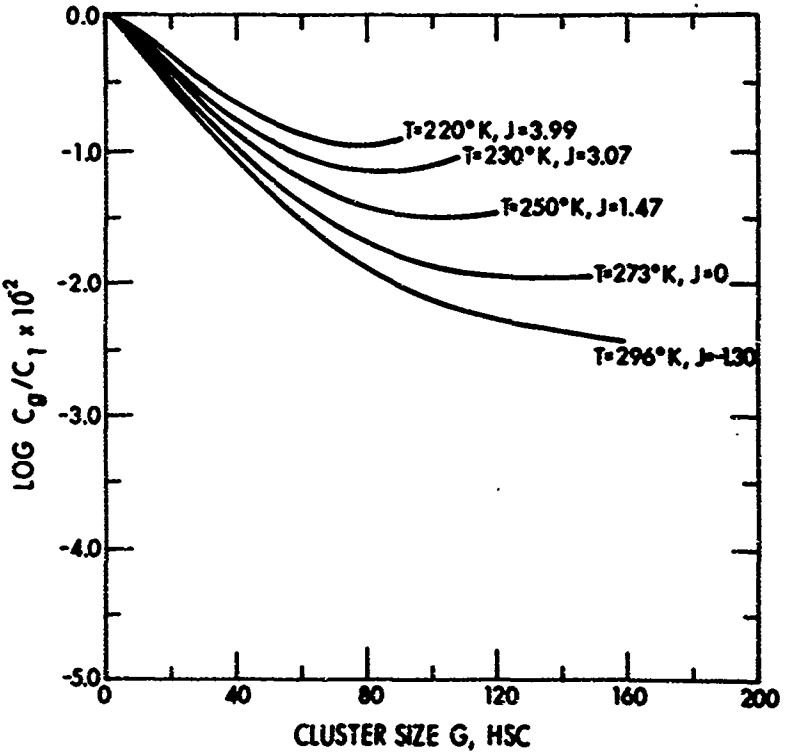

Figure IV-1.2
Equilibrium Under Saturated, Saturated and
Supersaturated Conditions

V. NON-EQUILIBRIUM AND RELAXATION CONSIDERATIONS

1. Constant Volume Quenching

In order to begin to compare the results of numerical analysis with experimental data, initial equilibrium conditions for the calculation must be known. Once the basic predictions of the theory of equilibrium are in hand it is possible to employ these results as initial conditions and begin the calculations involving a gradual departure from equilibrium; such is the case in the rapid expansion of a condensable vapor in an inert carrier gas. However, inasmuch as an adiabatic expansion is difficult to interpret on the molecular scale, it is useful to examine first the constant volume quenching process and then to proceed to the case of a steady expansion.

Consider a mixture of saturated vapor with a cluster population $\{C_g\}$ and inert gas initially in thermal equilibrium subjected to infinitely rapid cooling to a supersaturated state and maintained thereafter at constant volume. The clusters present initially at equilibrium are thus subjected to quenching with the rates of cluster growth exceeding the rates of cluster decay tending, in effect, towards condensation with an exothermal rate of heat production.

To calculate this heat production consider the gas phase reaction by collision of an A_{g-1} cluster and a A_1 monomer to give an A_g cluster

$$A_{g-1} + A_1 = A_g, \qquad \text{V-1.1}$$

in the interval during which the temperature T is constant and the total volume is unchanged. The kinetic theory of cluster formation[1] specifies the energy release associated with this reaction as $\lambda_g u^\circ_{11}$, the product of the nearest neighbor surface coordination number and the Van der Waals pair interaction energy. The objective here is to specify the net exothermal heat of reaction associated with all reactions, Eq. V-1.1 for a cluster population $\{C_g\}_{g>1}$ subjected to a rapid quench (or heat bath).

Several approaches to this problem were considered over the years with the most promising result given here. To describe the energy of reaction of V-1.1 an energy balance is first taken on the bimolecular mechanism

$$A_{g-1} + A_1 = A_g$$

and then followed with the unimolecular process

$$A_g = A_{g-1} + A_1$$

within a fluid element of constant volume, temperature and *concentration*.

Consider first the bimolecular reaction

$$A_{g-1} + A_1 \rightarrow A_g$$

proceeding forward at rate R_g^+. For every A_g cluster formed at rate R_g^+ from an A_{g-1} cluster, 1 monomer is 'consumed' and $\lambda_g u^\circ_{11}$ energy of reaction is involved per A_{mer} formed. A general energy balance on the element is (where $\dot{\xi} = d\xi/dt$)

$$\dot{\varepsilon}_{in} + \dot{\varepsilon}_{liberated} = \dot{\varepsilon}_{out} + \cancel{\dot{\varepsilon}}^{\,0}_{stored}$$

with bimolecular input equal to

$$\dot{\varepsilon}_{\substack{in,bi \\ lib,}} = \varepsilon^0_{g-1} R^+_g + \varepsilon^T_{g-1} R^+_g + \varepsilon^T_1 R^+_g + \varepsilon^R_g R^+_g \qquad \text{V-1.2}$$

per cluster. The reaction rate expressions from the theory are summarized in Table V-1.1. Energy ε^0 is the zero point cluster energy equal to the sum of all pair interaction energies within a cluster at zero temperature. This energy can be viewed as cluster internal or potential energy involving all molecules, both bulk and surface, of each cluster. Energy ε^T is the thermal energy corrections for temperatures above absolute zero contributed by the thermally-excited degrees of freedom previously defined (Section III-8). Thus, for the particles involved in this reaction we have:

Particle	Energy
A_g :	$\varepsilon^T_g = \varepsilon_{g\ \text{int.}} + \varepsilon_{g,\text{rot.}} + \varepsilon_{g\ \text{transl}} =$ $x_g\ kT + \frac{1}{2}\xi_g\ kT + \frac{1}{2} S_g\ kT$
A_{g-1}:	$\varepsilon^T_{g-1} = x_{g-1}\ kT + \frac{1}{2}\xi_{g-1}\ kT + \frac{1}{2} S_{g-1}\ kT$
A_1 :	$\varepsilon^T_1 = x_1\ kT + \frac{1}{2}\xi_1\ kT + \frac{1}{2} S_1\ kT$ V-1.3

Finally, we have $\varepsilon^R = \lambda_g u^\circ_{11}$ as the energy liberated in the bimolecular reaction[1]. It is important to focus attention on the individual particles involved as it is the (g-1) size cluster and the monomer which enter the fluid element while the reaction "within" the element is written for the (g) size

TABLE V-1.1

SUMMARY OF NON-EQUILIBRIUM RATE EQUATIONS

$$\frac{df_g}{dt} = R^+_g - R^+_{g+1} + R^-_{g+1} - R^-_g$$

where: $\theta = u^\circ_{11}/kT$, and $\gamma^2 = u^\circ_{00}/u^\circ_{11}$;

$$R^+_2 = Z''_{0,1}\, f_0\, \underline{\underline{f_1}}\, Z''_{1,01}\, \underline{\underline{f_1}}\, \gamma\theta(1-e^{-\theta})/\nu_{01}$$

$$R^-_2 = Z''_{0,1}\, f_0\, Z''_{1,01}\, f_2\, \bar{\nu}\gamma\theta e^{-\theta}(1-e^{-\theta})\, Z''_{1,1}\nu_{01}$$

$$R^+_3 = Z''_{1,2}\, \underline{\underline{f_1}}\, f_2\, (1-e^{-\theta})$$

$$R^-_3 = \bar{\nu}\, f_3\, e^{-2\theta}(1+2\theta)/2$$

$$R^+_4 = 2Z''_{1,3}\, f_1 f_3\, (1-e^{-\lambda_3\theta})/(\chi_3)(\chi_3-1)$$

$$R^+_{g>4} = 6\, Z''_{1,g-1}\, f_1\, f_{g-1}\, (1-e^{-\lambda_{g-1}\theta})/\chi_g(\chi_{g-1}-1)(\chi_{g-1}-2)$$

$$R^-_{g>3} = 2\, \alpha_g\, \bar{\nu}\, f_g\, e^{-\lambda_g\theta}\, (1+\lambda_g\theta + \tfrac{1}{2}\lambda_g^2\, \theta^2)/(\chi_g-1)(\chi_g-2)$$

cluster. In essence we make an energy balance (bimolecular part of reaction) only on the new particles $df_{g,bi} = R_g^+ dt$ entering the element as f_g remains constant with the element.

The energy out of the fluid element associated with the bimolecular reaction is

$$\dot{\varepsilon}_{out,bi} = \varepsilon_g^0 R_g^+ + \varepsilon_g^T R_g^+ - dq^b/dt, \qquad V\text{-}1.4$$

where a positive value of heat input is in accord with the first law of thermodynamics for the total energy of the gas:

$$\frac{de}{dt} = \frac{dq}{dt} - \frac{dw}{dt} \qquad V\text{-}1.5$$

Next we consider the unimolecular reaction

$$A_g \rightarrow A_{g-1} + A_1$$

within the element proceeding at rate R_g^- and involving the decay of $df_{g,u} = R_g^- dt$ g size clusters. The initial energy before reaction is

$$\dot{\varepsilon}_{in,u} = \varepsilon_g^0 R_g^+ + \varepsilon_g^T R_g^+ \qquad V\text{-}1.6$$

with reaction energy $\varepsilon_g^R = \lambda_g u^\circ_{11}$ we have

$$\dot{\varepsilon}_g^R = -\varepsilon_g^R R_g^- \ *$$

So

$$\dot{\varepsilon}_{\substack{in,u \\ lib.,}} = \varepsilon_g^0 R_g^+ + \varepsilon_g^T R_g^+ + \varepsilon_g^R R_g^-, \qquad V\text{-}1.7$$

The energy--after the unimolecular event--leaving the fluid element is

$$\dot{\varepsilon}_{final,u} = \varepsilon_{g-1}^0 R_g^- + \varepsilon_{g-1}^T R_g^- + \varepsilon_1^m R_g^- - dq^u/dt \qquad V\text{-}1.8$$

*having taken heat liberated within the element as positive for bimolecular reaction

Rewriting the general energy balance on the fluid element as

$$[\dot{\varepsilon}_{out,bi} - \dot{\varepsilon}_{in,bi}] + [\dot{\varepsilon}_{final,u} - \dot{\varepsilon}_{initial,u}] = 0 \quad \text{V-1.9}$$

and substituting Eqs. V-1.2, V-1.4, V-1.7 and V-1.8 gives

$$\left.\begin{aligned} &+ (\varepsilon^0_g R^+_g + \varepsilon^T_g R^+_g - dq^b/dt) \\ &- (\varepsilon^0_{g-1} R^+_g + \varepsilon^T_{g-1} R^+_g + \varepsilon^T_1 R^+_g + \varepsilon^R_g R^+_g) \end{aligned}\right] \underline{\text{bi.}}$$

$$\left.\begin{aligned} &+ (\varepsilon^0_{g-1} R^-_g + \varepsilon^T_{g-1} R^-_g + \varepsilon^T_1 R^-_g - dq^u/dt) \\ &- (\varepsilon^0_g R^+_g + \varepsilon^T_g R^+_g - \varepsilon^R_g R^-_g) = 0 \end{aligned}\right] \underline{\text{Uni.}}$$

So

$$- dq^b/dt - \varepsilon^0_{g-1} (R^+_g - R^-_g) - \varepsilon^T_{g-1} (R^+_g - R^-_g) - \varepsilon^T_1 (R^+_g - R^-_g)$$
$$- dq^u/dt - \varepsilon^R_g (R^+_g - R^-_g) = 0$$

Defining $dq = dq^b + dq^u$ gives

$$\frac{dq}{dt} = - \varepsilon^0_{g-1} (R^+_g - R^-_g) - \varepsilon^T_{g-1} (R^+_g - R^-_g) - \varepsilon^T_1 (R^+_g - R^-_g)$$
$$- \varepsilon^R_g (R^+_g - R^-_g) \qquad \text{V-1.10}$$

Further, if $(R^+_g - R^-_g) \equiv \dot{\phi}^n_g$, or net flux on the element, Eq. V-1.10 can be written as

$$\frac{dq}{dt} = - (\varepsilon^0_{g-1} + \varepsilon^T_{g-1} + \varepsilon^T_1 + \varepsilon^R_g) \dot{\phi}^n_g \qquad \text{V-1.11}$$

where $\varepsilon^0_{g-1} = \frac{g-1}{2} \lambda_{g-1} u^\circ_{11}$ (HSC) or $(g-2)u^\circ_{11}$ (WCM). Conceptually, the balance on the fluid element now appears as in Figure V-1.1.

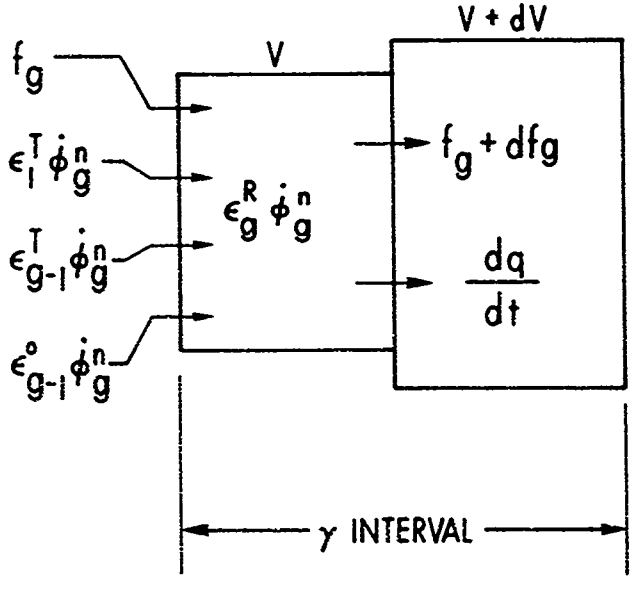

Figure V-1,1
Computation Model

This non-stationary result for dq/dt is not related to the latent heat, an equilibrium constant pressure, temperature concept. It does define the reaction energy on net growth or decay of clusters which behave as a perfect gas and is the heat addition term in the first law, Eq. V-1.5. In a binary system such as water vapor in air, care must be taken in precisely defining the overall system described by equation V-1.5 since the heat production described by equation V-1.5 is considered as originating in an external source.

If C_{vo} is the specific heat per cc of the carrier gas, the specific heat of the mixture is

$$c_v = C_{vo} + k \sum_{g=1}^{g_\infty} \{\chi_g + (S_g + \zeta_g)/2\} f_g, \qquad \text{V-1.12}$$

where f denotes a non-stationary concentration.

Combining Eqs. V-15 and V-1.11 for the constant volume cases gives for the mixture:

$$\frac{dT}{dt} = \frac{-1}{c_v} \{\varepsilon^0_{g-1} + \varepsilon^T_{g-1} + \varepsilon^T_1 + \varepsilon^R_g\} \dot{\varphi}^n_g \qquad \text{V-1.13}$$

If p° and T° are the pressure and temperature before quenching the perfect gas law is

$$\frac{dp}{dt} = \frac{p^\circ}{T^\circ} \frac{dT}{dT} \qquad \text{V-1.14}$$

$$\text{and } p = kT \left(f_o + \sum_{g=1}^{g_\infty} f_g\right) \qquad \text{V-1.15}$$

Equations V-1.13 and V-1.14 are non-integrable so that p and T must be solved for numerically from an initial equilibrium cluster distribution $\{C_g\}$ at p° and T°. The pressure may be arrived at either by V-1.14 or V-1.15 where[1] (see also Table V-1.1).

$$\frac{df_g}{dt} = R^+_g - R^-_{g+1} + R^-_{g+1} - R^-_g. \qquad \text{V-1.16}$$

With this set of equations one may evaluate in a step-wise manner the changes in state that occur in a constant volume containing moist air as it is quenched or heated. The temperature change produced by the entire population $\{f_g\}$ shift is applied after calculating equation V-1.16 for all g with the same instantaneous initial conditions.

The non-equilibrium behavior of the initial stationary cluster distribution $\{C_g\}$ described by case c, Table III-5.1 and subjected to an instantaneous temperature drop of 0.0001°K (the approximate average temperature drop per collision interval in later experiments) is given in Figure V-1.2. Details of performing this calculation are given in the following section and in Appendix (3); all expansion terms are simply nulled out for this constant volume case and the output is examined each calculating interval of 0.480 n sec. In order to gain some insight into the system behavior in the simplest case, the temperature changes indicated by equation V-1.13 (practically nil) are also suppressed after the initial quench of $^-$0.0001°K.

The ordinate of Figure V-1.2 is obtained by dividing each rate df_g by the final positive value calculated for that size g (defined df_τ) while the abscissa is the number n of time increments $\Delta t \cong 0.480$ n sec. The dimer behavior is not shown because of relative magnitude; at n=1, $df_2 = -1.22 \times 10^{8}$; at

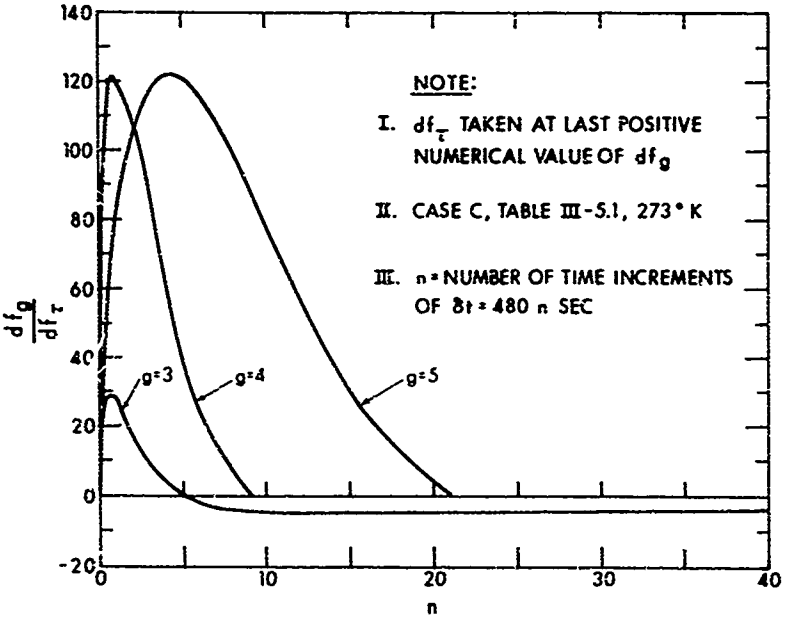

Figure V-1.2
Normalized Rates for Constant Volume Quench
$\Delta T = -0.0001°$ K

n=40, $df_2 = -0.708 \times 10^8$. The dimer, therefore, behaves here much like a monomer since its rate is negative throughout; larger size clusters all have rates which are first positive, then negative. It will be seen later that with expansion the dimer rate is positive until departure from the adiabat occurs.

On changing ΔT to a positive increment of +0.0001°K, or a heat bath, the opposite behavior is observed (though not symmetric) with the dimer increasing throughout. The dimer literally receives a "shower" of fractured trimer leading to positive rates. If ΔT is increased slightly to say 0.001 or 0.01, then a negative rate with the typical type of behavior for the larger cluster sizes shown in Figure V-1.2. The time to the first reversal of sign, i.e.. at df_τ, is given for each cluster size in Figure V-1.3 as a matter of reference.

The behavior of the cluster is evident in Figure V-1.2 with a wave-like disturbance oscillating in the medium until damped by the growth and decay processes. Interpreting the results of Figure V-1.3 as relaxation times (in attaining equilibrium) would be incorrect since gradients would still exist in the medium at the times shown.

A reassuring check on the theory and computer analysis is available at this point. Since the equilibrium solution was obtained by detailed balance involving non-equilibrium rates, the use of an equilibrium distribution $\{C_g\}$ at temperature T in a non-equilibrium calculation for $\{f_g\}$ at temperature T should yield stationary rates with $R^+_g = R^-_g$,

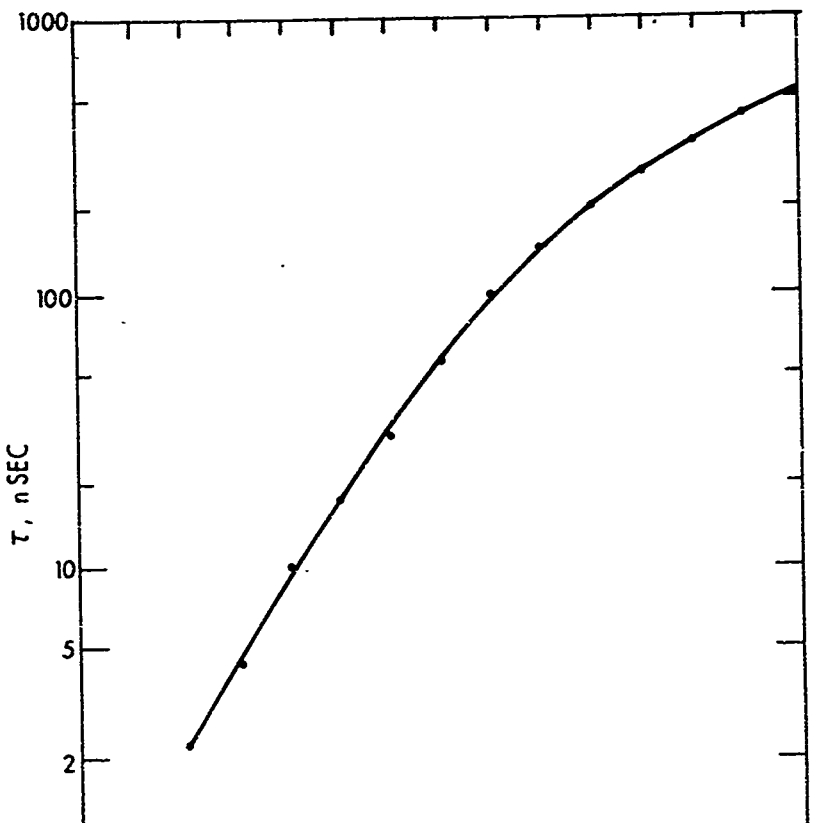

Figure V-1.3
Reversal Times for Quench of $\Delta T = -0.0001°$ K

all g. The use of hard sphere collision diameters gives a check to three digit accuracy. It was found, however, that a check to greater accuracy was possible by modifying the monomer, dimer collision cross sections, calculating the equilibrium distribution $\{C_g\}$, then checking for stationarity. For the hard sphere clathrate, the use of $\sigma_{1,2} = 1.95\ r_1$ (vice $2.0\ r_1$) and $\sigma_{1,1} = 2.05\ r_1$ (vice $2.0\ r_1$) gave equality in $R^+_g = R^-_g$ from three to five digits, all g, with the results at 273°K given in Table V-1.2.

For the constant volume quench (or heat bath) it would be possible to follow the behavior of individual clusters in attaining a new equilibrium by continuing the calculation of Figure V-1.2. If, however, a new temperature lower (or higher) by another increment of ΔT is imposed at time $t + \Delta t$, it becomes impossible to interpret what is happening on an individual cluster versus time basis. This is the process occurring in a rapid expansion where the rate processes of each time increment modify those of the succeeding one. It appears fruitless to try to relate such results to relaxation times, rather, investigation of the behavior of the cluster population on the whole is more rewarding.

TABLE V-1.2

STATIONARY GROWTH AND DECAY RATES AT 273°K

g	$R^+(cm^{-3}\ sec^{-1})$	$R^-(cm^{-3}sec^{-1})$
2	$0.40966 \cdot 10^{22}$	$0.40958 \cdot 10^{22}$
3	$0.26336 \cdot 10^{22}$	$0.26337 \cdot 10^{22}$
4	$0.47028 \cdot 10^{20}$	$0.47020 \cdot 10^{20}$
5	$0.12430 \cdot 10^{18}$	$0.12429 \cdot 10^{18}$
6	$0.25205 \cdot 10^{15}$	$0.25201 \cdot 10^{15}$
7	$0.43719 \cdot 10^{12}$	$0.43711 \cdot 10^{12}$
8	$0.68725 \cdot 10^{9}$	$0.68712 \cdot 10^{9}$
9	$0.10143 \cdot 10^{7}$	$0.10142 \cdot 10^{7}$
10	$0.14395 \cdot 10^{4}$	$0.14392 \cdot 10^{4}$

Adiabatic Expansion; Comparison with Experiment

The remaining limiting constraint, No. 6, is now considered. In the expansion of moist air in a supersonic nozzle pressure "humps" which are steady in time develop in the regions of condensation. The pressure distribution selected here for comparison is free of shock wave pressure disturbances which could be within a zone of condensation[7,8,9]. Consequently the entire difference in static pressure from that encountered in a moisture-free nozzle flow is due to the effects of heat addition from condensation. We know therefore that a matching

of calculated pressure with the experimentally measured pressure should be a meaningful test of the parameters involved in the theory. One further test (which is the subject of future investigation) is the prediction of other experimental results based on the parameters determined here.

Having gained some insight into possible modes of cluster behavior it is worthwhile referring to Figure IV-1.1 to define the approach used in comparing numerical calculations with experiment. For a given set of molecular parameters it is possible now to calculate conditions at saturation, $\{C_g\}_{J=0}$, point A', then calculate the undersaturated initial cluster distribution $\{C_g\}_{J<0}$, both at initial temperature T_{01}. Using $\{C_g\}_{J<0}$ as an initial distribution it will now be possible to calculate the change in cluster concentration df_g for all g, by rate expression V-1.16 modified to include the effects of expansion. The partial pressure of the entire population $\{f_g\}$ is then simply

$$p_v = \sum_{g>0} f_g \, kT \qquad \text{V-2.1}$$

The objective here, therefore, is to calculate this pressure, add to it the local pressure of the carrier gas and compare the result with the static pressure obtained from experiment along the equivalent path A-B-C, Figure IV-1.1. To do this we must add to the results of the previous section the effect of expansion occurring in the flow.

For the steady inviscid expansion experiencing no body

forces the net rate of internal energy change per cc is given by V-1.5 where

$$\frac{dw}{dt} = p \frac{d(\ln_v)}{dt}. \qquad \text{V-2.2}$$

Considering one dimensional steady flow at velocity u in a nozzle of cross sectional area A, density ρ, the mass flow rate obeys

$$\frac{d}{dt} (\rho A u) = 0, \qquad \text{V-2.3}$$

and the volumetric flow rate is simply Au. The quantity d(ln v)/dt is thus given by

$$\frac{d}{dt} (\ln v) = \frac{d}{dt} (\ln Au). \qquad \text{V-2.4}$$

Since d ln y/dt = 1/y dy/dt, hence

$$\frac{d}{dt} \ln Au - \frac{1}{Au} \left[A\frac{du}{dt} + u\frac{dA}{dt}\right] = \frac{d}{dt} [\ln u + \ln A] \qquad \text{V-2.5}$$

Now, rewriting equations V-1.5, V-2.2 and V-2.4 and defining $de = c_v\, dT$ gives

$$c_v \frac{dT}{dt} = \frac{dq}{dt} - p \frac{d(\ln Au)}{dt}, \qquad \text{V-2.6}$$

and having dq/dt by equation V-1.6, c_v by equation V-1.12 and p by equation V-1.15 allows expressing the temperature in equation V-2.6 by

$$\frac{dT}{dt} = \frac{1}{c_v} \left[- \sum_{g>1} (\epsilon^0_{g-1} + \epsilon^T_{g-1} + \epsilon^T_1 + \epsilon^R_g)\, \phi^n_g \right.$$

$$\left. - kT \left(f_o + \sum_{g>0} f_g\right) \frac{d(\ln Au)}{dt}\right]. \qquad \text{V-2.7}$$

The pressure follows from the ideal gas law since

$$\frac{dp}{dt} = p\,\frac{d(\ln T/v,}{dt} = p\frac{d}{dt}\,(\ln T - \ln v), \qquad \text{V-2.8}$$

so by equation V-2.4

$$\frac{dp}{dt} = p[\frac{d(\ln T)}{dt} - d\,\frac{('n\ Au)}{dt}], \qquad \text{V-2.9}$$

or combining equations V-2.9 and V-2.7 allows

$$\frac{d\ \ln\ p}{dt} = \frac{1}{C_v T}\,[-\sum_{g>1}\,(\varepsilon^0_{g-1} + \varepsilon^T_{g-1} + \varepsilon^T_1 + \varepsilon^R_g)\ \dot{\varphi}^n_g$$

$$- [1 + \frac{k}{C_v}\,(f_o + \sum_{g>o}\,f_g)\ \frac{d(\ln\ Au)}{dt}] \qquad \text{V-2.10}$$

Here again equation V-2.7 and V-2.10 are non-integrable and numerical solution is necessary. As in the constant volume case the pressure may be found from equation V-1.15 rather than from V-1.14.

One further consideration is needed to complete the description of the expanding medium. Since the volume of the system varies with time, a term

$$-\ f_g\ (d/dt)\ \ln\ V \qquad \text{V-2.11}$$

must be added to eq. V-1.16, while for the diluent gas we have

$$-\ f_o\ (d/dt)\ \ln\ V, \qquad \text{V-2.12}$$

noting that the volume change is already specified in terms of the area and local flow velocity in eq. V-2.5. The change in concentration of any cluster size during expansion is thus written as the sum of Eqs. V-1.16 and V-2.11

$$\frac{dt_g}{dt} = (R^+_g - R^-_{g+1} + R^-_{g+1} - R^-_g) - f_g\,\frac{d}{dt}\,(\ln\ V). \qquad \text{V-2.13}$$

For the monomer rate equation, we have (constant volume)

$$df_1 = - \sum_{g=2}^{\infty} g\left(\frac{df_g}{dt}\right) dt, \qquad \text{V-2.14}$$

or with expansion

$$df_1 = - \sum_{g=2}^{\infty} g\left(\frac{df_g}{dt}\right) dt - f_1 \frac{d}{dt} (\ln V). \qquad \text{V-2.15}$$

Adiabatic expansion of moist air in a supersonic nozzle can now be examined. The case considered here (Exp. 405, Ref. 8) is free of pressure discontinuities from shock waves so the only deviation of static pressure from that of a dry adiabatic expansion is that caused by the heat input of condensing vapor. The information required of the experimental conditions for input to the numerical calculations is the initial pressure, temperature, the nozzle profile, i.e., the area $A_{(x)}$ and slope dA/dx. In order to know the time per data interval the flow velocity $u_{(x)}$ in the nozzle is required; this follows from solution of the equations of motion[7,8]. Inputs from the equilibrium theory[1] are the initial cluster distribution $\{C_g\}$ and the accompanying parameters (Say case c, Table III-5.1). The objective is to match the pressure deviation in the nozzle observed at onset of condensation--thus satisfying limiting constraint (6):

The FORTRAN computer program for calculating the non-equilibrium rates of change of cluster concentration, the temperature, pressure and other parameters is described and given in Appendix 3; the general flow chart is also given.

In essence the program calculates the rates of growth and decay for each cluster size from the dimer upwards in each calculating interval thus giving the concentration of each species with respect to time (or location). The static pressure reported is thus the sum of the partial pressures of all species present, from the monomer upwards and the carrier gas.

The calculating interval used requires further consideration. The earlier discussion on cluster behavior under constant volume-quench conditions showed that time increments on the order of the collision interval were required in that case. With the complication of expansion the interval to be used was uncertain; the minimum was still the collision interval but perhaps a longer one could be used to conserve computer time.

Collision time corresponding to the mean free path is calculable from the collision numbers of the theory[1], i.e.:

$$\tau_g = (Z'_{og} + Z'_{1g})^{-1}, \quad \tau > (\bar{v})^{-1} \qquad \text{V-2.11}$$

where

$$Z'_{og} = Z''_{og}\, f_o$$

$$Z'_{1g} = Z''_{1g}\, f_1$$

and

$$Z_{x,g} = \left(\frac{8\pi kT}{\mu_{x,g}}\right)^{1/2} \sigma^2_{x,g}, \quad x = 0,1$$

Using concentrations from typical calculations we find, for example, that at 270°K, $\tau_{10} \sim$ 4nsec. This dictates a scheme of variable step size which is described further in Appendix 3.

There appears to be no significant difference in results, however, between a constant step size and a variable step size. It is possible by this method of variable step size, though, to reduce computer time from about 16 hours per solution to about 1.5 hours. A step size twice the largest collision interval will lead to an unstable numerical solution.

A further area requiring clarification is the experimental input data. For the case considered here data on Area, Velocity, etc. were for 0.1 cm intervals. This is too coarse and must be refined; simple linear relations were used between data intervals.

A final point of clarification concerns the initial cluster distribution. Referring back to Figure IV-1.1, moist atmospheric air entered the experimental apparatus in condition A. Some expansion already occurred at the point where experimental pressure was first measured. The temperature had already dropped to 273°K at this point from 295.8°k. To account for the change in cluster concentration from point A to B, two approaches were tried.

First, the undersaturated distribution at A was calculated and expanded adiabatically to 273°K considering the absolute number of each species to remain unchanged (frozen equilibrium). Second, the equilibrium distribution at 273°K was calculated. Inasmuch as the first method gave vapor pressures slightly lower than those on the adiabat, Figure IV-1.1, the second condition was used as the initial condition in the results

reported here. There was very little difference in the two distributions and both would give nearly similar final results except that the first case would follow a path just under the adiabat.

A bit of historical development is injected at this point to show how the final solution was attained. In evaluating numerical results, initially, the greatest confidence was placed in the results of the rate equation, V-1.12. The argument stemming from the fact that $\{C_g\}$ and $\{f_g\}$ are closely related through detailed balance at equilibrium; with most of the experience gained in the many variations of $\{C_g\}$. From this the mass fraction of "condensate" is defined by considering the evolution of all clusters from the dimer upwards. The mass fraction of water clusters per kg of air is obtained by

$$X = \frac{m_1}{m_o} \cdot 10^{-3} \sum_{g>1} \frac{g\, f_g}{f_o}, \qquad \text{V-2.12}$$

where m_1 and m_o are the mass per monomer and mass per air molecule (avg) respectively; the initial value of $X \cong 0.006$ being neglected. If this expression is summed to include the monomer, the mixing ratio (sometimes called the specific humidity) is obtained,

$$X_1 = \frac{m_1}{m_o} \cdot 10^{-3} \sum_{g>o} \frac{g\, f_g}{f_o} \qquad \text{V-2.13}$$

X_1 should remain constant throughout equal to the initial value, here equal to 4.86 g/kg. This is in effect another internal boundary condition to be satisfied.

The basis of comparison for X is the result of solution of the equations of motion for the flow and given elsewhere[7,8]. Although this earlier solution relies on the use of macroscopic latent heat and therefore has limited validity with respect to the condensate mass fraction, it does appear to be a useful first approximation and is plotted for experiment #405 in Figure V-2.1. Some early results for X are given in Figure V-2.1.

An interesting problem is encountered at this point, namely, the strong dependence of X on $\bar{\nu}$. If case c, HSC, Table III-5.1 is used, curve (c) results which is quite disappointing in that little or no condensate appears; the small amount appearing is late in time or downstream of experimentally observing results. If a temperature dependence is imposed on $\bar{\nu}$, say

$$\log \bar{\nu} = \frac{T}{T_o} \log 5.35 \cdot 10^{12}, \qquad \text{V-2.14}$$

with $T_o = 273$, still satisfying case (c) Table III-5.1, then curve (B) results which is premature or upstream of observed results.

At this point an intense investigation was made on the influence of other parameters in the theory as well as different initial condition (Table III-5.1). Referring to the rate expression in Table V-1.1 one finds that for curve (c) the decay rates are too large and the system evolution is incomplete by the time the nozzle exit at l = 9 cm is reached. Parametric

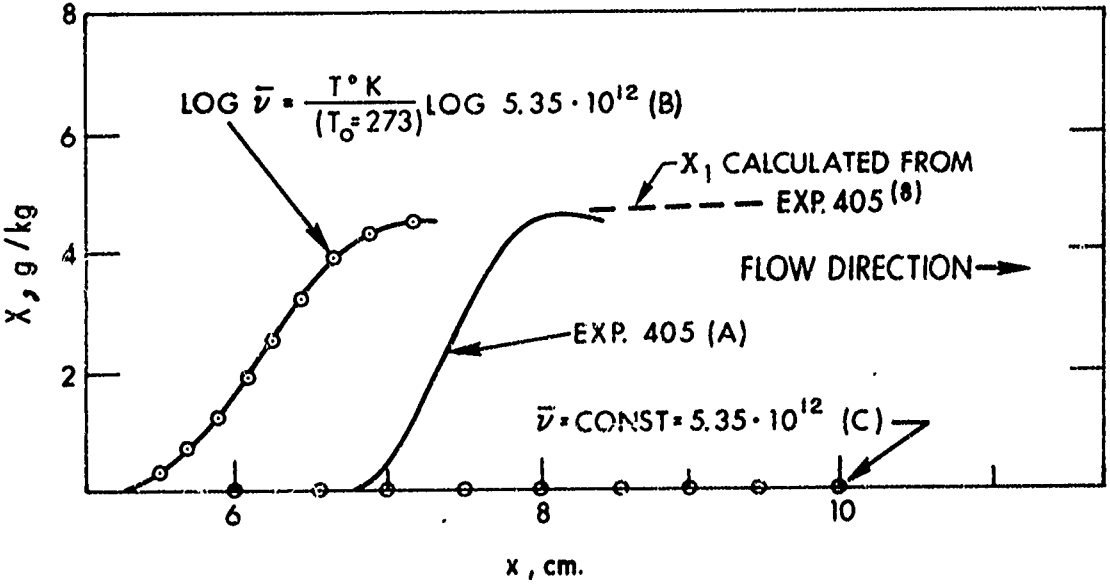

Figure V-2.1
Condensate Mass Fraction, HSC

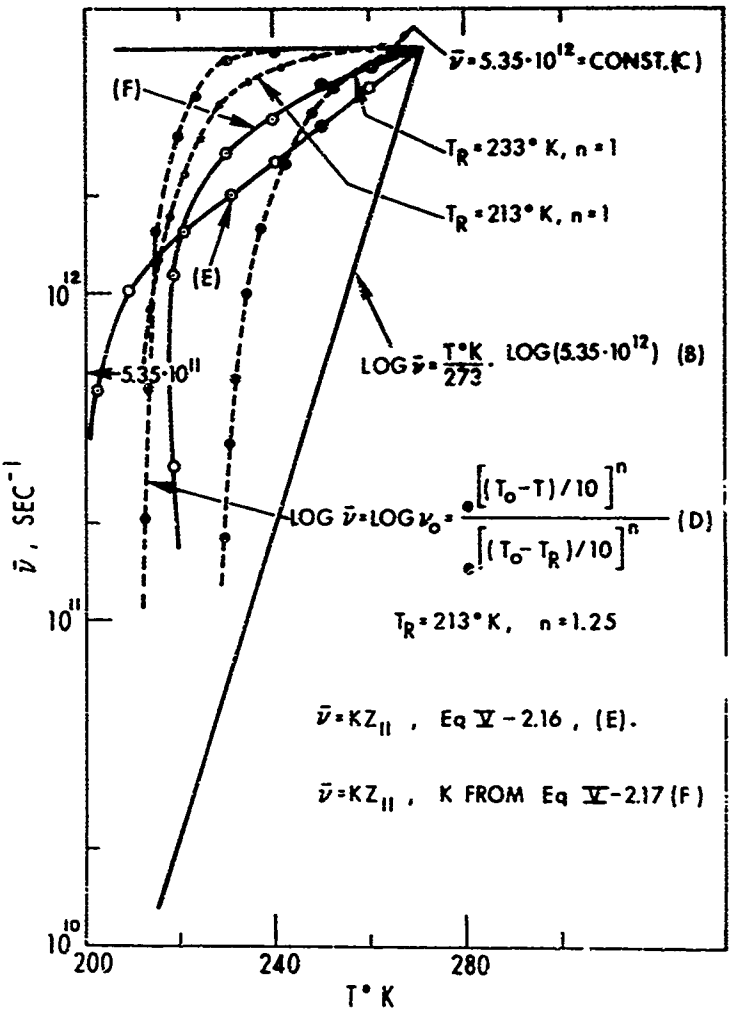

Figure V-2.2
Behavior of Internal Circulation Frequency

studies showed there was little possibility that variation of u°_{11}, γ, ν_{01}, etc. could substantially affect the system evolution so attention was turned to $\bar{\nu}$.

It appeared now that the frequency $\bar{\nu}$ was the dominant parameter involved. Examination of Figure V-2.2 shows some of the variations of $\bar{\nu}$ that were considered, with curve (c) and (b) corresponding to those in Figure V-2.1. Since the experimental results appeared to be bracketed by curves (C) and (B), intermediate variations for $\bar{\nu}$ were considered with the following yielding the most promising results (curve D)

$$\log \bar{\nu} = \log \nu_o - \frac{\exp[(T_o-T_i)/_{10}]^n}{\exp[(T_o-T_R)/_{10}]^n}. \qquad \text{V-2.15}$$

Having gained some insight into the nature of the behavior of the theory's parameters attention was shifted to comparison of numerical results with the actual experimental pressure distribution. Figure V-2.3 shows the degree of comparison in static pressure (dimensionless p/p_{01}) when n = 5/4 and T_R = 213°K, keeping in mind that the calculations were initiated at T = 273°K at X = 1.5 cm. The isentrope is followed numerically as is the experimentally observed pressure deviation. The result in Figure V-2.3 for X was expected to differ from the earlier result as pointed out previously because of the earlier use of latent heat.

Once the close match in pressure was achieved reexamination of parameters in the theory showed nearly direct proportionality

between $\bar{\nu}$ and collision number Z_{11} for the monomer-monomer interaction. If fact allowing

$$\bar{\nu} = k\, Z_{11} \qquad \text{V-2.16}$$

gave a match in static pressures within a few percent. A small variation in k (from 2.05×10^{-12} to 1.21×10^{-12}) with temperature and saturation according to

$$k = -7.431 - 0.0789\, s + 9.54\, \frac{T_o}{T}, \qquad \text{V-2.17}$$

yielded a pressure distribution nearly identical with experiment. (See Figure V2.3).

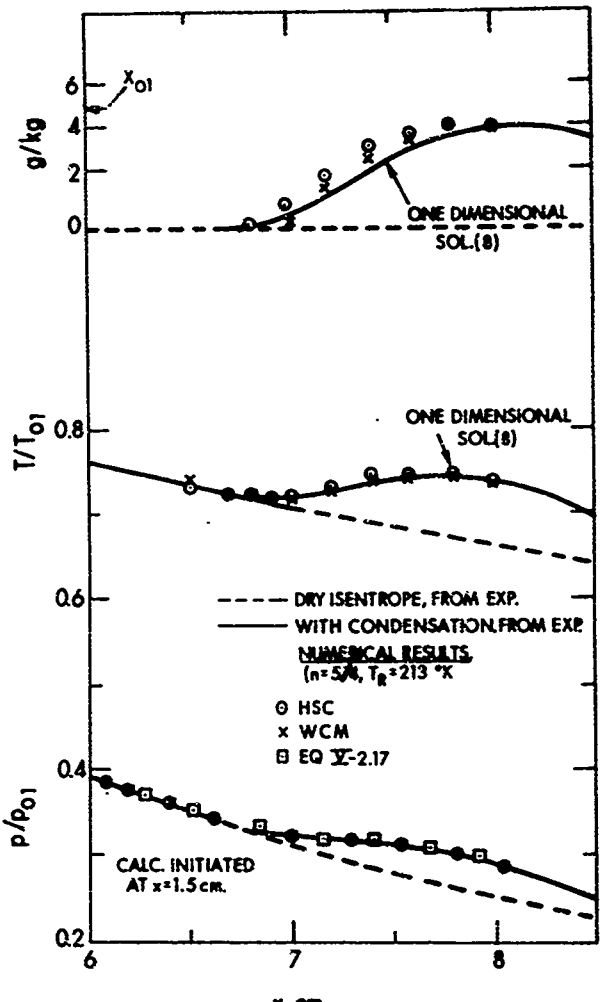

Figure V-2.3
Comparison of Present Results with Experimental Pressures and Earlier One-Dimensional Calculations

VI. COMPLETE EQUILIBRIUM AND NON-EQUILIBRIUM SOLUTIONS

1. Cluster Behavior

We summarize here the results obtained for both the HSC and WCM, case (C) and (e) Table III-5.1 as modified by $\bar{v}$ in equation V-2.15. A complete equilibrium iteration to satisfy all limiting constraints requires less than an hour at an interactive computer terminal (GE-H635) while a single non-equilibrium solution on a fixed collision interval basis requires about 15 hours of actual computer time (CPU) on a medium scale computer (PDP 15/40). This is reduced to about 1.5 hours by using variable collision interval basis described earlier and in more detail in Appendix 3. As any computed parameter is observable on an individual cluster size basis at any time, calculations were limited to size g=10 after observing virtually no numerical contribution to the results (i.e. p, T, X) above a cluster size of g=8.

Initial conditions for both the HSC and WCM case at 273°K (saturated equilibrium condition) are given in Table VI-1.1. The evolution of the cluster populations from the initial condition $\{C_g\}_o$ of Fig. IV-1.2 is given in Fig. VI-1.1 through VI-1.4. Recalling that the principal differences between both the classical HSC and the water model lie in the structure, η_g, the collision cross section $\sigma_{1,g}$ and the nearest neighbor parameter m_λ one finds identical results for static pressure and close agreement for temperature and condensate X. Also the larger WCM cross section tends to shift the hump in the

TABLE VI-1.1

INITIAL CONDITIONS, SATURATED EQUILIBRIUM, 273°K

Size g	HSC C_g	WCM C_g
1	0.16000000E+18	0.16000000E+18
2	0.10299099E+15	0.10299099E+15
3	0.37137217E+13	0.37137317E+13
4	0.60239349E+11	0.14863239E+12
5	0.47734832E+09	0.29168346E+10
6	0.20353456E+07	0.30693876E+08
7	0.62537311E+04	0.23091140E+06
8	0.15731362E+02	0.14066905E+04
9	0.34735999E-01	0.74236071E+01
10	0.70293203E-04	0.35375547E-01
11	0.13420118E-06	0.15648930E-03
12	0.24676055E-09	0.65534307E-06
13	0.44375285E-12	0.26360155E-08
14	0.78974221E-15	0.10297684E-10
15	0.14039987E-17	0.39412301E-13

distribution outward from g=4, HSC to g=6 WCM; the concentration of larger sizes being higher in the latter case. If, for example, n_{WCM} is used with σ_{HSC}, the static pressure and temperature calculated is about 5% lower than experimental. The disappearance of the smaller sizes, akin to Ostwald ripening is also accentuated in the WCM case. Once the zone of observed condensation (here $x \cong 7.0$ cm) is reached the smaller sizes (g=2,3, HSC) begin disappearing, i.e. $df_g<0$; for the WCM this applies to sizes through g=5.

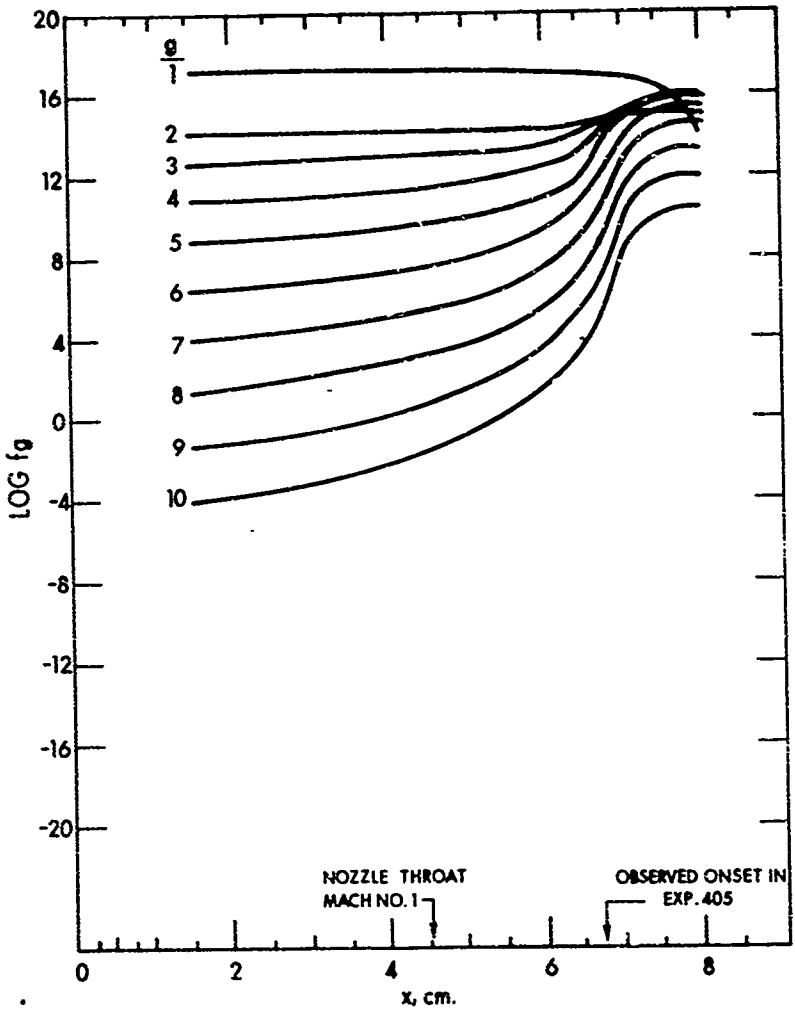

Figure VI-1.2
Variation of Cluster Concentration with
Nozzle Location, HSC

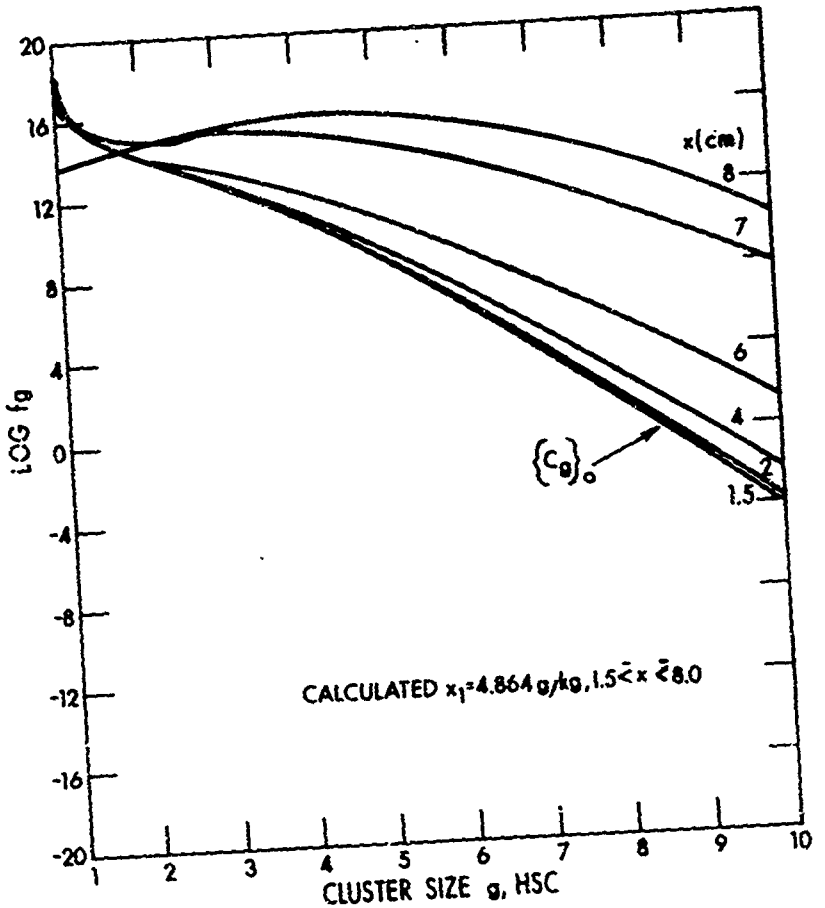

Figure VI-1.1
Variation of Cluster Concentration
with Size, HSC

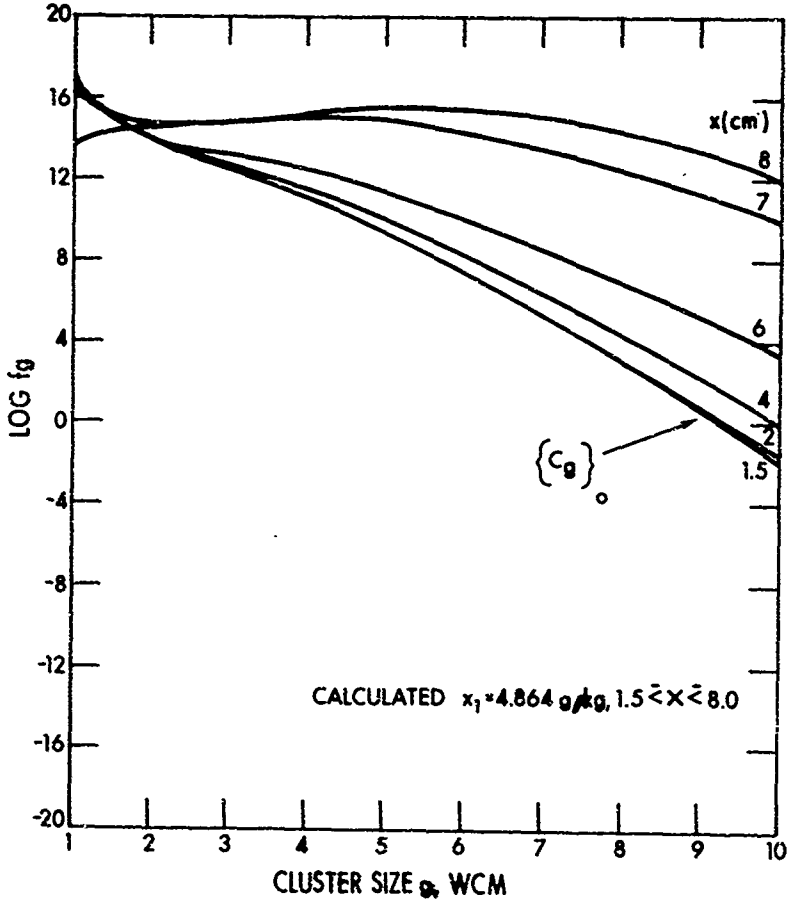

Figure VI-1.3
Variation of Cluster Concentration
with Size, WCM

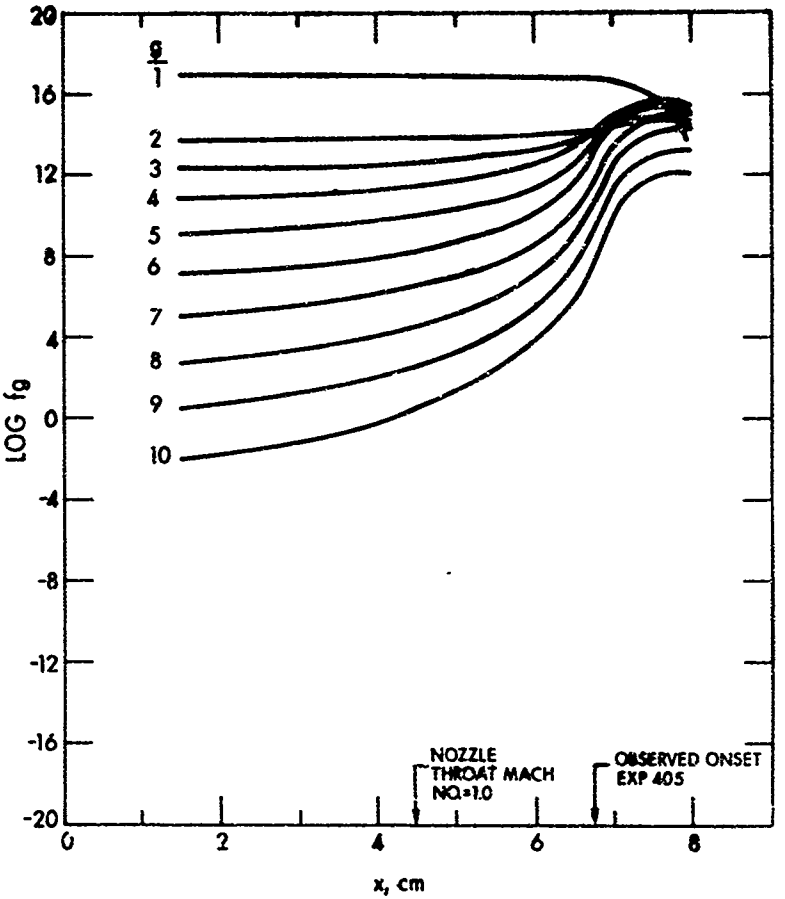

Figure VI-1.4
Variation of Cluster Concentration with Nozzle Location, WCM

2. Gas Phase Metastable Equilibrium

In Figure IV-1.1 the general expected path of the adiabatic expansion up to onset was described. Now, having satisfied all limiting constraints (1-6) a final check on the solution is to observe whether the adiabatic path up to onset is calculated and mass balance maintained.

Figure VI-2.1 gives the path calculated for both the HSC and WCM with calculated results falling on the adiabat for the carrier gas ($C_p/C_v = 1.4$); the flow Mach no. is also plotted. The vapor pressure given is calculated from

$$p_v = \sum_{g>0} kTf_g \qquad \text{VI-2.1}$$

Although the calculated pressure for $4.5<x<6.7$ indicates that equilibrium pressures are attained, the expanding mixture is not in true thermodynamic equilibrium since the gradients indicated, for example in Fig. VI-1.1, preclude equilibrium. Were sufficient time available for the system to evolve to equilibrium for $4.5<x<6.7$, metastable cluster distribution as in Fig. IV-1.2 would exist (or conversely, if the rates were sufficiently rapid).

The results of this calculation indicate that metastable equilibrium is not attained in the course of the moist air expansion considered here (exp. 405)[8] in spite of the presence of equilibrium vapor pressure. The vapor pressure up to onset is a result of the monomer partial pressure which follows the expansion hardly affected by cluster growth until onset as is evident in Figs. VI-1.2 and VI-1.4. Fig. VI-2.1

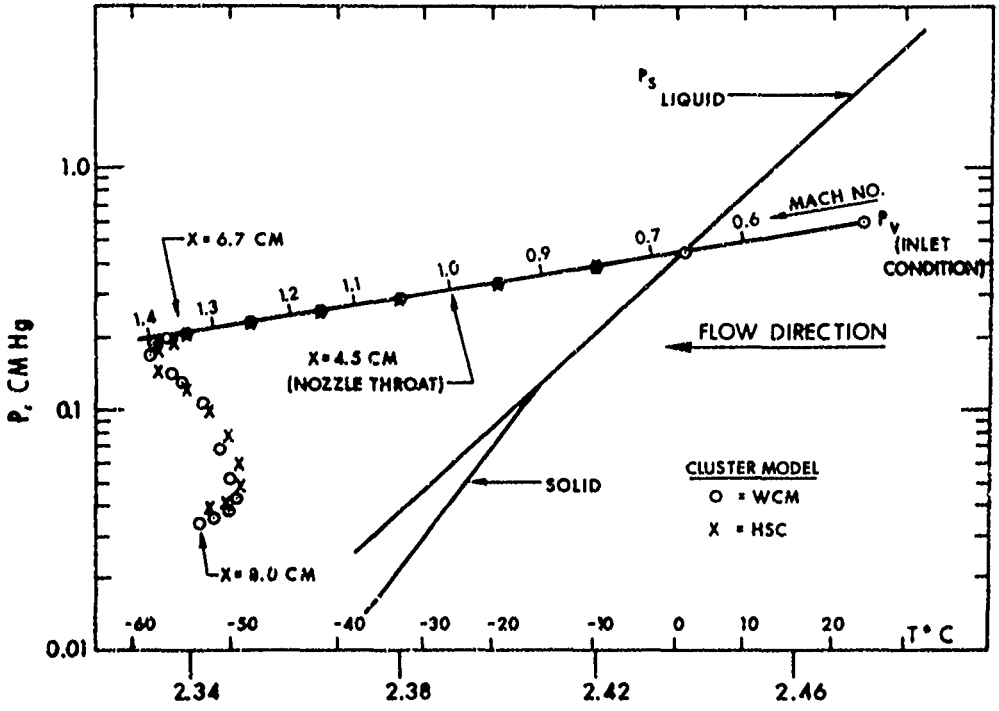

Figure VI-2.1
Calculated Vapor Pressure During Expansion

indicates the vapor pressure from experimental inlet condition to x = 8.0 cm. While interpreting the results after onset (x=6.7), it should be noted that the temperature increases due to the heat of reaction by about 24°K over the dry isentropic temperature. Over the course of the entire calculation the mixing ratio or specific humidity remains constant at x_1 = 4.864 g/kg indicating conservation of mass throughout. The path beyond x=8.0 is then again dominated by the continuing expansion of the carrier gas along another adiabat (GPE, Fig. IV-1.1; the process could be interpreted as an expansion with modified initial conditions. That other nozzle expansions behave in this manner is evident by the pressure curve envelope after onset [7,8].

It has generally been assumed in the past that onset of condensation is associated with collapse of metastable equilibrium; this would mean transition from a metastable supersaturated cluster distribution, Fig IV-1.2 to a saturated cluster distribution, III-6.1. The condensate would then be the difference in the quantity $m_{1\ g}\xi_{1g}C_g$ with the latter distribution falling below the former.

Were the reactions in our expansion sufficiently fast, the metastable supersaturated distributions of Fig. IV-1.2 would be obtained. It is seen, however, in the non-equilibrium evolution in Figures VI-1 through 4 that the metastable distribution of Fig. IV-1.2 are not attained - - - but since the calculated vapor pressure equals that predicted

by the equilibrium isentrope up to onset point in Fig. VI-2.1 the vapor would be assumed to be in metastable equilibrium. We see therefore that the metastable concept applies to vapor pressure and supersaturation but not to cluster distribution.

By the results of Figs. VI-1.2 and VI-1.4 we can interpret onset of condensation either in terms of monomer and associate departure from metastable vapor pressure with disappearance of the monomer or alternatively in terms of the entire cluster population upwards from the dimer. In terms of the monomer-onset is the 'collapse' of the metastable vapor pressure, in terms of the rest of the cluster population--onset is not collapse of the metastable cluster distribution (it never having been attained) but sudden growth caused by decrease in the cluster decay rates. This decrease is a direct result of the decrease in internal circulation frequency $\bar{\nu}$.

It appears from these calculations that the existance of the gas phase metastable vapor pressure, i.e. when $J>0$, is directly related to both the rates of growth and decay R^+, R^- on one hand, and to $\bar{\nu}$ on the other. It also appears that $\bar{\nu}$ may be related to the relative abundance of monomer by Equation V-2.16. When sufficient time has elapsed in an expansion for the cluster concentrations to have grown due to the continual 'quench' and consequently the increased rates R^+, R^- have begun to affect the monomer concentration, then the decrease in monomer concentration causes the frequency $\bar{\nu}$

to decrease which further accelerates the process as R^- is proportional to $\bar{\nu}$ and $R^- << R^+$. The net effect is the release of an enormous amount of energy in a short time with the temperature gradient of the flow changing to about 5×10^5 °K/sec. from about -5×10^5 °K/sec.

3. Possible Water Cluster Structures

The very nature of the cluster theory [1] originally developed for monomolecular vapors allows little detail or description of molecular structure. This attempt in applying the theory to a more complicated species like H_2O is encouraging especially since only an average or effective value of pair interaction energy u°_{11} is required but it raises the question of the behavior of the circulation frequency $\bar{\nu}$. Assuming that the $\bar{\nu}$ question is resolved then it appears that the limiting constraints developed here allow extension of the theory to other than monomolecular vapors.

A composite summary of both the hard sphere collision and the water clathrate model is given in Table VI-3.1 and Figs. VI-3.1 and VI-3.2. It should be recalled that $a_g = 1$ for $g \leq 20$ for both HSC and WCM which implies that all molecules in this size range of clusters are surface sites.

Inasmuch as the theory [1] is based on classical interpretation of intermolecular forces, the HSC case is in keeping with this concept. A conceptual view of HSC clusters, up to g=7 is given in Fig. VI-3.1 with an attempt to represent n_g, the number of bonds and λ_g, the number of nearest neighbors (taken here as the average).

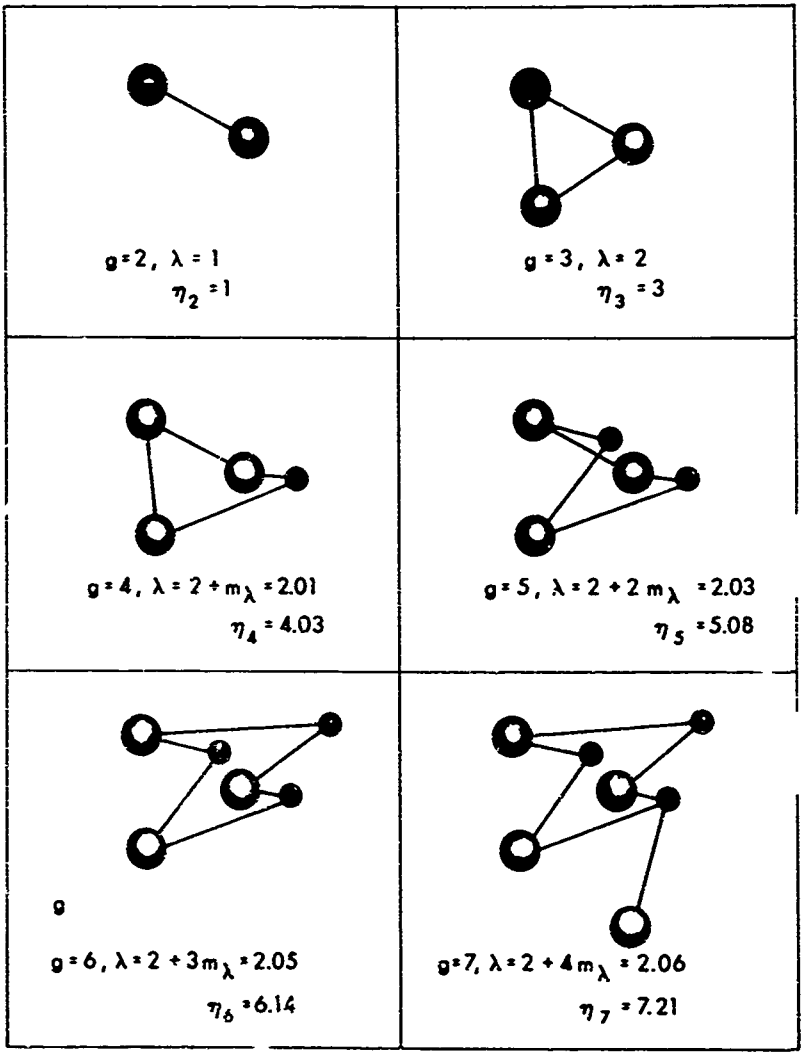

Figure VI-3.1
Interpretation of Structure, HSC

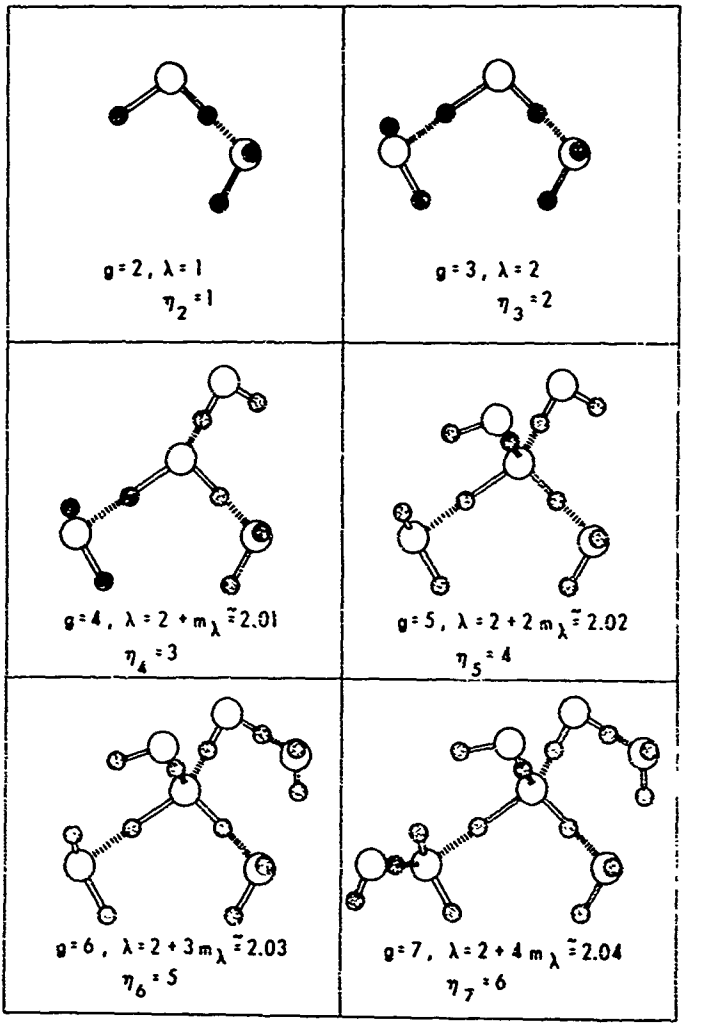

Figure VI-3.2
Interpretation of Structure, WCM

TABLE VI-3.1

HSC, WCM SUMMARY

Case	u°_{11}/k	u°_{11} (Kcal/mole)	$\bar{\nu}_{273^\circ K}$	λ_∞	g_∞	m_λ	n_g
HSC	1460	2.90	$5.35 \cdot 10^{12}$	3.9	124	0.0153	$g\lambda_g/2$
WCM	1460	2.90	$5.35 \cdot 10^{12}$	3.9	195	0.0097	g-1

The WCM requires some imagination as the linear variation of λ_g is still allowed but η_g is based on the structural model of Fig. VI-3.2. Recall that $\lambda_g \to \lambda_\infty$ as $g \to \infty (g_\infty)$; here $\lambda_\infty = 3.9$ at $g \cong 195$. Although, as pointed out earlier in III-4, numerous assumed variations of λ_g were allowed, none other than the present linear case of $\lambda = 2$ at $g = 3$ to λ_∞ satisfied limiting constraint (1-6). In the absence of theoretical prediction of λ, little more can be said.

Although η_g, WCM differs from η_g, HSC only by approximately unity, this difference is significant as appreciable energy is associated with the bonding (or potential energy) term in the reaction described by equation V-1.11.

It is gratifying to find that the parameters determined by the series of iterations required to satisfy limiting constraints (1-6) do, in fact, resemble those of water, especially since the value of pair interaction energy u°_{11}, HSC and WCM, agrees with recent results for an average value of 2.9 kcal/mol-bond.[10] This average result is deduced from molecular dynamics calculations where the detailed structure of H_2O was realistically defined. The point is also made in the molecular dynamics study[10] that it is legitimate, to use the concept of a pairwise additive potential in lieu of an 'exact' potential for water, *provided* the pair functions are *effective* pair potentials.

VII. COMPARISON WITH CLASSICAL THEORY

1. Nucleation Rates with Present Surface Tension

Earlier attempts[8] to compare the predictions of classical nucleation theory with rapid nozzle experimental results were partially successful with later studies reviewed more recently.[9] These studies have in common first, the application of isothermal equilibrium nucleation theory for 'birth' rates of critical size nuclei in highly dynamic supersonic expansions ($\Delta T/\Delta t = -10^5 °K sec^{-1}$, or more). Second, one is always faced with assigning the surface tensions of clusters of extremely small size of undetermined state (liquid, solid). And, thirdly, one must choose a growth law for clusters after their 'birth' together with an attendant condensation or 'sticking' coefficient.

As is evident[8,9] some degree of success is possible using the classical approach, however, little progress can be made in interpreting the dynamical aspects of phase change, in understanding the metastable state or, in fact, predicting a priori the outcome of a new physical situation.

Keeping in mind the earlier arguments of Sections V-2 and VI-2 with regard to attainment of metastable equilibrium, the earlier calculations[8] are repeated here using the surface tension corresponding to the minimum in $\{C_g\}$ found in Fig. IV-1.2. Plotting that value of $g \equiv g^*$ at the minimum in $\{C_g\}$ and the corresponding surface tension $\Gamma(g^*)$, gives the result in Fig. VII-1.1 with

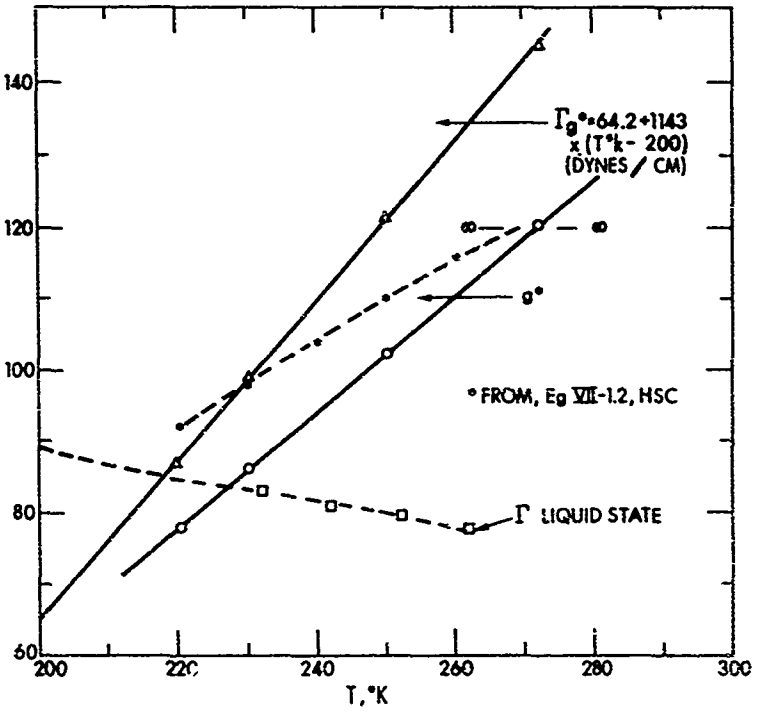

Figure VII-1.1
Surface Tension of Clusters if
Metastable Equilibrium were Attained

$$\Gamma_{g^*} = 64.2 + 1.143(T-200) \text{ (dynes/cm)} \qquad \text{VII-1.1}$$

An approximate relation for g* derivable from the theory [1] is

$$g^* = 3 + (\lambda_\infty - \lambda_3 - \frac{J}{\sigma}) \frac{1}{m_\lambda} \qquad \text{VII-1.2}$$

which is plotted in Fig. VII-1.1. The approximation diverges from exact values with increasing supersaturation or decreasing temperature. At saturation, however, the parameter $J = \ln c_1 / c_{1s} = 0$ and the approximation converges to the value required by limiting constraint (5), $\frac{\Delta\zeta}{g \to g_\infty} = 0$ this is true for both the HSC and WCM!

Again, recall that our present calculations indicate metastable cluster distributions are not attained during rapid expansion yet classical nucleation theories predict the rates for metastable equilibrium corresponding to the minimum at C_{g^*}. Thus it is not surprising that repeating the earlier calculations [7] with the value of surface tension given by equation VII-1.1 gives little if any improvement over previous results.

In Fig. VII-1.2 typical results are given for predictions of onset of earlier experiments. [7,8] It is possible to iterate and converge numerically on experimental onset by parametric variation for, say, experiment 405. Using the iterated parameters in predicting the location of onset for experiments 416 and 295 with considerably different supersaturation yields disappointing results.

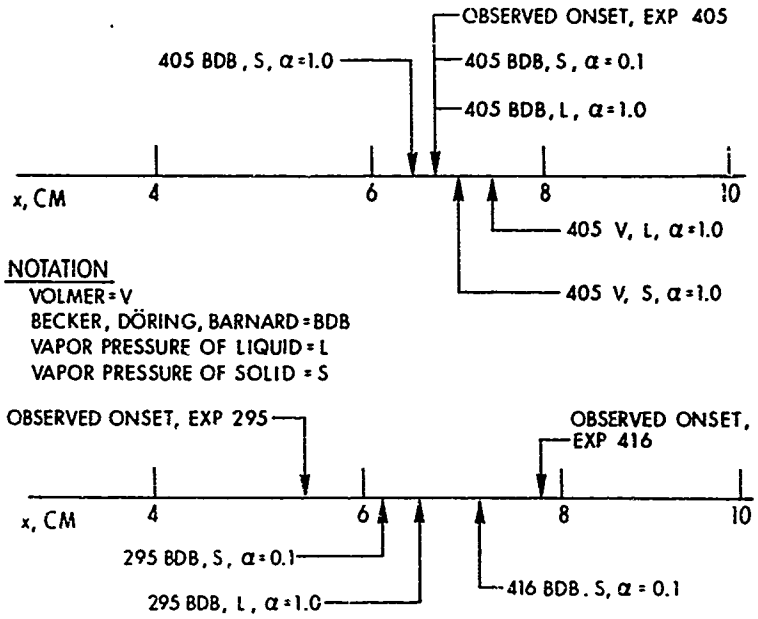

Figure VII-1.2
Location of Condensation Onset by Classical Nucleation Rates with Metastable Values of Surface Tension

The conclusion one can draw is that classical nucleation theory should not be invoked unless the time scale of the experimental situation is long with respect to time of evolution of the metastable state. Further investigation of relaxation aspect of the present theory[1] may yield criteria on the time of evolution of the metastable state.

2. Future Work

In order to apply the experience gained with water vapor to predicting other water vapor experiments, further investigation of the circulation frequency $\bar{\nu}$ is required. If, in fact, $\bar{\nu} = (Z_{11})$ then other experiments should be predictable from the parameters given here.

Reflection on the results presented raises a question needing further investigation of the net effect on the heat of reaction of the distinct approach used in Ref. (1) in arriving at the dimerization rate in contrast to that for larger sizes. The partition function is used in the first case, consequently accounting for the zero point energy while in the latter case it is not included. If the enthalpy change of reaction were calculated it would be complicated by this fact.

An obvious extension of this work should be to nozzle expansions of a monomolecular gas such as argon as well as to other species with molecular properties susceptible to forming clathrate structures, i.e. H_2S, H_2O, CO_2, SO_2, etc. although argon itself might form clathrates.

REFERENCES

1. E. R. Buckle, Trans. Far. Soc. 65, 1267 (1969)
2. R. W. Bolander, J. L. Kassner, Jr. and J. T. Zung, J. of Chem. Phys. 50, 4402 (1969)
3. M. Dace, L. H. Lund, P. L. M. Plummer, J. L. Kassner, Jr. and B. N. Hale, J. of Colloid and Interface Science, 39, 65 (1972)
4. D. Eisenberg and Kauzman, W., The Structure and Properties of Water, Oxford University Press (1969)
5. Handbook of Chemistry and Physics, Chemical Rubber Company (1966)
6. F. G. Keyes, J. Chem. Phys. 15, 602 (1947)
7. A. A. Pouring, Phys. Fluid 8, 1802 (1965)
8. P. P. Wegener, and A. A. Pouring, Phys. Fluids 7, 352 (1964)
9. P. P. Wegener, ed. Gas Dynamics, Part I, Vol I, Marcel Dekker (1969)
10. A.Rahman and F. H. Stillinger, J. of Chem. Phys. 55, 3336 (1971)

APPENDIX 1, NOMENCLATURE

SYMBOL	VARIABLE	REMARKS
A		*Eq. 8.8+1, Ref 1 2nd term
ALPHA	α_g	Surface to volume parameter
ALPHA G	"	*Surface to volume parameter
ALPP1	α_{g+1}	
AREA	A	Nozzle cross sectional area
AREA-MG	A	Sub-interval area
BIGG	G	*Eq.8.9, Ref 1, also Appendix 4
BIGM	M	*Eq. 8.4, Ref 1
BIGM2	"	"
BK	k	*Boltzman constant
BRCFG		$\Sigma(3g - (\xi_g+\xi_g))f_g$
C	C_g	*Equil. concentration
CF		*Conversion Factor
CHIG	χ_g	Vibrational degrees of freedom
CHI	χ_g	* "
CHIGM1	χ_{g-1}	
CHIGP1	χ_{g+1}	
CHI1	χ_1	

*Symbols for equilibrium solution that differ from nonequilibrium solution.

CKP		*Pressure conversion factor
COND	X	Condensate mass fraction in g/kg
CPØ	C_p	Specific heat
CUS	C_g	*Under-saturated equilibrium concentration
CVØ	C_v	Specific heat
C1INF	C_{ls}	Saturated equil. C_g
C1Ø		C_1 (frozen equil., see Appendix 2)
C1	C_1	*Equil. monomer conc.
C1Ø	C_1 (initial)	*Initial monomer conc.
C11	C_{11}	*Eq. 8.2, Ref (1)
C12	C_{i2}	*Eq. 8.4, Ref (1)
C1G	C_{lg}	*Eq. 8.4, Ref (1)
C1KE		*Eq. III-8.7, 2nd term
C2KE		*Eq. III-8.7, 3rd term
CGKE		*Eq. III-8.7, 4th term
CGVIB		*Eq. III-8.7, 5th term
CGWK		*Eq. III-8.8, 6th term
DADX	dA/dx	Slope, nozzle area
DADXMG		Sub-interval dA/dx
DAMG		Sub-interval dA
DDADX	d(Dadx)	

DDU	d^2u	
DELEP	$\Delta\varepsilon_g$	See Eq. V-1.4
DELEPØ	$\Delta\varepsilon°_g$	Eq. V-1.2
DELTAP		$P_{static} - P_{isentropic}$
DELTAT		$T_{static\ reaction} - T_{isentropic}$
DELTAX		Experimental data interval
DELZI	$\Delta\xi$	$\xi_g - \xi_{g-1}$
DELZET	"	" "
DENOM		Denominator, Eq. V-2.7
DENOM1		First term, DENOM
DENOM2		Second term, DENOM
DENIS		DENOM, no reaction (isentropic case)
DFG	df_g	Eq. V-1.13 (total)
DFGA	df_g	Eq. V-1.12 (reaction)
DFGEX		Eq. V-2.11 (expansion)
DFGM1	df_{g-1}	Eq. V-1.13
DFGP1	df_{g+1}	Eq. V-1.13
DFØ	df_o	Eq. V-2.12
DF1ØD	df_1 Initial	Initial value, no reaction
DFG12	df_1	Eq. V-2.15
DFG1EX	df_1	Eq. V-2.11
DFG2	df_2	Eq. V-2.13, g=2

DFG2M1		DFG2, previous time increment
DLDG	m_λ	Eq. III-4.1
DPISEN	dp_i	Eq. V-2.10, no reaction
DPSTAT	dp	Eq. V-2.10 or V-2.9
DQ	dq	(dq/dt)dt
DQDT	dq/dt	Eq VIII-3
DQDX	dq/dx	(dq/dt)/u
DTISEN	dt_i	Eq. V-2.7, no reaction term
DTM	dt	in seconds
DTSTAT	dT	Eq. V-2.7
DU	du	Experimental velocity increment
DUDXMG		du, calculating
DXCM	dx	Increment of length along nozzle axis
D1		Eq. VIII-3
D2		"
D3		"
EPSIF		*Iteration limit, statement 240
ETAG	η_g	Eq. III-8.2
FGTM	f_g	Non-stationary concentration (cm^{-3})
FI		*Eq. (8.8)+1, Ref (1), 3rd term
FIRST		Eq. VI-2.1, 1st term
FIRST		*Eq. III-8.7, 1st term

FØTM	f_o	Carrier gas concentration (cm^{-3})
FØTMØ		f_o, initial
PTHETA	F(θ)	*From Eq. 8.6, Ref (1)
FRT	F(θ)	*Eq. 8.15, Ref (1)
FTHETG	F(g,θ)	*Eq. 8.6, Ref (1)
F1ØD		f_1, no reaction, initial
F1TM	f_1	Non-stationary monomer concentration
F1TMØ		f_1, initial
F1C1R		f_1/C_{1s}, same temp. Eq. VI-2.1
F1TERM		Eq. V-2.7, 2nd term
F2TM	f_2	Non-stationary dimer concentration (cm^{-3})
GAMA	γ	Numerical constant, see App 3
GAMAS	Γ	Surface tension, dyne/cm
GAMAD	γ_d	$(u^o_{00}/u^o_{11})^{1/2}$ for dimer
GBAR	$\bar{g}$	Average cluster size
GGPLG	X	Eq. V-2.12
GLMDA	λ_g	Coordination number
GMAX		* = MAXG, below
GINF	g_∞	numerical infinity for cluster size
GRATIO	G(θ)/G(g,θ)	*>L_g/L_∞, pg 1282, Ref 1.

GTHETA	G(g,θ)	*Eq. 8.9, Ref 1
LG	g-1	
M	g+1	
MAXG		Upper limit on actual calculation
MAXGP1		MAXG plus 1
MG		Subinterval index
NG		Calculating limit
NGAMA		Experimental interval divisor
NSTEP		Stepping index
NØ		Index locating start of calculation
PAIR		Initial partial of an Isentropic pressure, cm Hg
PCOEF		Conversion factor
PI	3.14159	
PINF	p_s	Equilibrium saturation vapor pressure
PISEN	p_i	Isentropic static pressure (no reaction)
PPAR	p_v	Partial pressure of vapor
PPARØ		(p_v)=initial
PRES		*Calc. pressure, cm. Hg.
PSTAT	p	Static pressure of carrier gas vapor
PVAP		Partial pressure at initiation of program, ref. only

PØ1		Static pressure at inlet conditions
QOFX	$Q_{(x)}$	$\Sigma_x dq$, See DQ
RDTM	dt	Time increment (corrected)
REF		Eq. V-2.15
RMATG2	df_g/dt	Eq. V-1.12
RMATØ		Eq. V-2.12
RMAT22		Eq. V-1.12, g=2
RMAT1D		Eq. V-2.11, F, isentropic
RMI1U	R_g^-	Table V-1.1
RMIUP1	R_{g+1}^-	Table V-1.1
RMI2BI	R_2^-	Table V-1.1
RMI3U	R_3^-	Table V-1.1
RMI4U	R_4^-	Table V-1.1
RPLUS	R_g^+	Table V-1.1
RPLGP1	R_{g+1}^+	Table V-1.1
RTAA		Eq. V-2.5 (see comment in program)
RTUU		Eq. V-2.5 (See comment in program)
RØ	r_o	Mean molecular radius carrier gas
R1	r_1	Mean molecular radius vapor
S	s	Saturation ratio
SIGMA1	$\sigma_{1,g}$	Eq. III-1.5, collision cross section

SIGØ1	$\sigma_{0,1}$	Collision cross-section, carrier gas - monomer
SIGØ2	$\sigma_{0,2}$	Collision cross-section, carrier gas - dimer
SIG11	$\sigma_{1,1}$	Collision cross-section, monomer-monomer
SIG12	$\sigma_{1,2}$	Collision cross-section, monomer - dimer
SIGIG	$\sigma_{1,g}$	*See SIGMA1
SIG1G1	$\sigma_{1,\ g-1}$	*See SIGMA1
SIG1Ø1	$\sigma_{1,01}$	Collision cross section, mixed pair[1]
SLDADX	d^2A/dx^2	Slope of DADX
SLDU	d^2u	
SLU	du	
SLUM		du at x-1
SMGDFG	$\Sigma g df_g$	Alternate expression for Eq. V-1.5
SMNGRG		Eq. V-1.6, 1st term
SRDTM	t	Σ dt
SUM	log $\bar{v}$	Eq. VI-2.1
SUMCHI	$\Sigma \chi_g C_g$	See Eq. III-8.7
SUMCG	ΣC_g	" " "
SUMGCG	$\Sigma g C_g$	Eq. 8.17, Ref (1)
SUMDAX	$\Sigma\Delta$(DADX)	See App 3, multipoint derivatives

SUMDDU	$\Sigma\Delta(DU)$	See App 3, multi-point derivatives
SUMDU	2DU	"
SUMBRC		Eq. V-1.8, $\Sigma\{\ \}$
SUMGPG	Σf_g	
SUMGG	$\Sigma g f_g$	
SUMLCG		See 1st term, Eq. III-8.7
SUMLNW	$\Sigma(\omega_i/\omega_\infty)$	See eq. 8.13, Ref (1)
SXER	d/dx (XER)	Appendix VIII-4
TDK	T	Temperature °K
TDKIS	T_i	Temperature, isentropic °K
TDKØ	T_0	Temperature at initiation of calculations
TDKØØ	T_{00}	Temperature at inlet conditions
THETA	θ	$\theta = u^\circ_{11}/kT$
U	u	Flow velocity
UFAC		u°_{11} = UFAC x u°_{11}
UMG		Flow velocity, sub-interval
WG	ω_g	Eq. 8.3, Ref 1
WG3	ω_3	" for g=3
WINF	ω_∞	" for g=∞
UØØØ	u°_{00}	Pair interaction energy carrier gas-carrier gas

UØØ1	u°_{01}	Pair interaction energy carrier gas - monomer
UØ11	u°_{11}	Pair interaction energy monomer - monomer
XCM		distance on nozzle centerline
XER		multiplier, see program
XERØ		Initial XER
XJ		Computer index (note XJ)
XKG	κ_g	*Eq. 8.5, Ref (1)
XKGL1	κ_{g-1}	*
XK2	κ_2	*
XLD1F	$\lambda_\infty - \lambda_g$	*$\overline{>}0$
XLCGC1		*See eq. 8.10, Ref (1)
XLG	L_g	*Eq. 8.9, Ref (1)
XLGTDK		Eq. V-2.14
XLHT	L	*Eq. III-8.7
XLOGCG		*See eq. 8.10, Ref (1)
XLOGC1		*See eq. 8.10, Ref (1)
XLOGC		* *
XLOGNU	$\log \bar{\nu}$	Eq. V-2.14
XLPINF	$\log p_\infty$	Eq. IV-1.2
XLRTIO	L_g/L_∞	*Pg. 1282, Ref (1)

XMABAL	X_1	Specific humidity
XMØ	m_o	Molecular mass, carrier gas
XM1	m_1	Molecular mass, vapor
XMUØ	$\mu_{o,g}$	Reduced mass, carriar gas - cluster
XMU1	$\mu_{1,g}$	Reduced mass, monomer - cluster
XMU1G	$\mu_{1,g}$	"
XMU1G1	$\mu_{1,g-1}$	"
XMU12	$\mu_{1,2}$	Reduced mass, monomer - dimer
XMUØ2	$\mu_{o,2}$	Reduced mass, carrier gas - dimer
XNOWDA	NONDAT	Input data file
XNOW2	NON2	Input data file
XNU	$\bar{\nu}$	Circulation frequency
XNUMER		Eq. V-2.7, numerator
XNUM1		Eq. V-2.7, 1st & 2nd terms of numerator
XNUM2		Eq. V-2.7, 3rd term of numerator
XNUMIS		Eq. V-2.7, no reaction
XOUTFI		Output file
ZETAG	ζ_g	*Eq. 8.13, Ref (1)
ZI1	ξ_1	Monomer rotational mode
ZIGDD	$Z''_{1,g}$	Eq. V-2.11, collision number

Z1M1DD	$Z^{*}_{1,g-1}$	Eq. V-2.11
ZØ1DD	$Z^{*}_{0,1}$	Eq. V-2.11
ZØ2DD	$Z^{*}_{0,2}$	Eq. V-2.11
Z11DD	$Z^{*}_{1,1}$	Eq. V-2.11
Z12DD	$Z^{*}_{1,2}$	Eq. V-2.11
ZØ11DD	$Z^{*}_{1,01}$	Eq. V-2.11

APPENDIX 2

FORTRAN PROGRAM FOR CLUSTER DISTRIBUTIONS AT SATURATED EQUILIBRIUM

The solution given is for water vapor in air but it can be applied to any mixture of a vapor and a carrier gas. Inputs required are: T, g_∞, ε, g_{max}, r_1, r_o, u^o_{11}, m_1, m_o, σ_{11}, p_v, C_1, λ_∞ and m_i, the nomenclature used being given in Appendix 1. The iteration involved is given in Table III-2.1 and Flow Chart VIII-2.1.

A term in the program but not yet described is UFAC. This is a multiplier which facilitates the alteration of u^o_{11} from the value of u^o_{11} = 1500K (erg/°K) (or 2.98 K cal/mole assumed initially).

A further remark concerns σ_{11}. According to the cluster theory[1], hard sphere collision diameters are to be used. The value used here, however, is not $\sigma_{11} = 2.00r_i$ but rather $\sigma_{11} = 2.05r_1$. This value was obtained by cross iteration between the present equilbrium solution and the non-equilibrium solution of Appendix 3. The value of σ_{11} was adjusted until the cluster reaction rates became stationary to about 5 digits when the equilibrium distribution of cluster sizes was fed into the non-equilibrium program. Vapor pressure data[5] for liquid water when fitted by least squares approximation yields p_∞ = 9.3286 - 2367./T while the expression for adiabatic expansion of moist air from an initial temperature of 295°K and specific humidity of about 5g/kg is $P = 0.425\ (T/273)^{3.5}$. The pressure conversion factor cm Hg to dynes/cm^2 is 1.33×10^3.

Once initial conditions have been selected, the iteration in Table III-2.1 may proceed with the objective of satisfying limiting constraints (1) through (5); condition (6) is dealt with later in Appendix 3. For each cluster size from g = 2 upwards to an arbitrary upper limit $g_{max} < g_{\infty}$ equation III-5.1 must be solved for the concentation $C_g (cm^{-3})$. Also calculated is ζ_g. The approach of $\Delta\zeta$ to zero as g approaches numerical infinity can be checked numerically in file F2 or plotted separately for inspection.

To calculate a super or undersaturated cluster distribution one must first calculate the saturated distribution at the same temperature to obtain the value of C_1 in statement 915 for ClINF. Statement 800, $P = P_v$ must be deleted and statement 1010 deleted. All other parameters remain the same as for the saturated solution at that temperature.

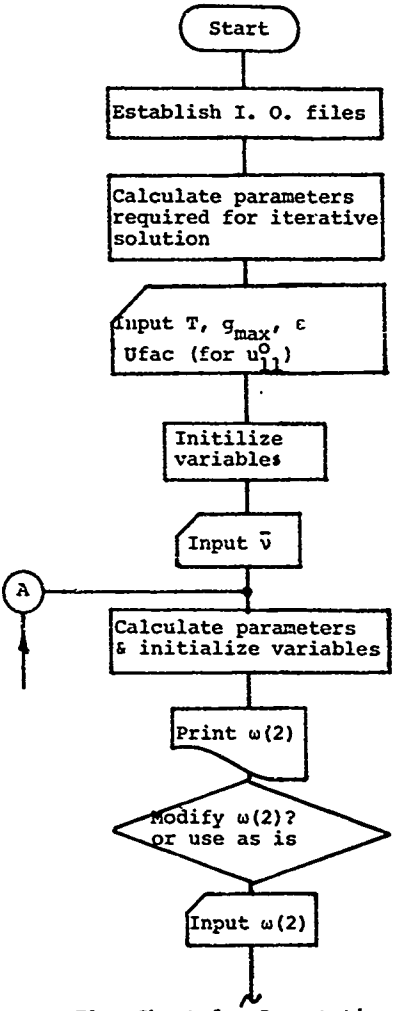

Flow Chart for Computation of Stationary Distributions

Figure VIII-2.1

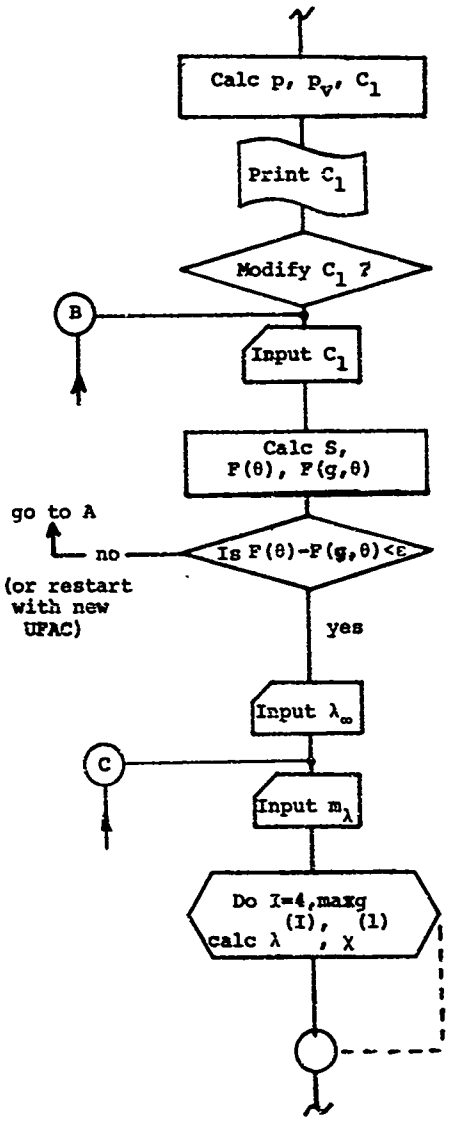
Calc p, p_v, C_l
Print C_l
Modify C_l ?
B
Input C_l
Calc S,
F(θ), F(g,θ)
go to A
no
Is F(θ)-F(g,θ)<ε
(or restart
with new
UFAC)
yes
Input λ_∞
C
Input m_λ
Do I=4,maxg
calc $\lambda_{(I)}$, $\chi_{(1)}$

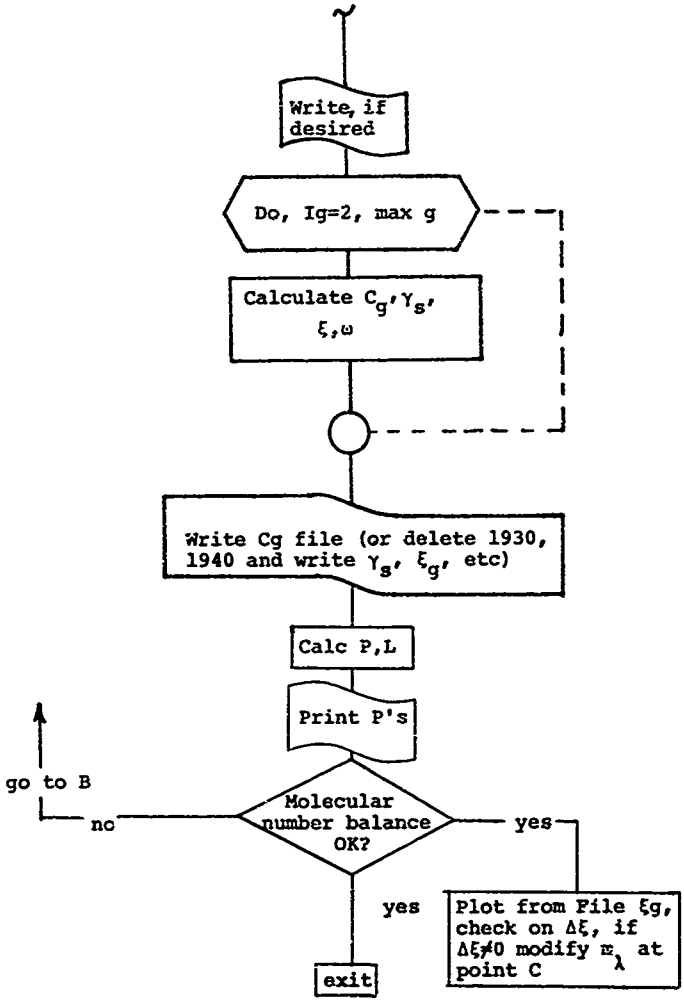
Write, if desired
Do, Ig=2, max g
Calculate C_g, γ_s, ξ, ω
Write Cg file (or delete 1930, 1940 and write γ_s, ξ_g, etc)
Calc P,L
Print P's
go to B
no
Molecular number balance OK?
yes
yes
Plot from File ξg, check on $\Delta\xi$, if $\Delta\xi \neq 0$ modify m_λ at point C
exit

```
110           DIMENSION C(300),GLADA(300),BIGG(300),CUS(300),AG(300)
120           DIMENSION ZETAG(300),XLOGC1(300),GAMAS(300),DELZET(300)
130           DIMENSION GRAT(300),XLRAT(300),CHI(300)
140C-              PROBLEM NAME IS HO40
160C-             CLUSTER DISTRIBUTIONS AT EQUILIBRIUM
170           FILENAME F2
180           F2="HOR2"
190           FILENAME F3
200           F3="HON3"
210           FILENAME IN
220           IN="       "
230           FILENAME OUT
240           OUT="      "
250           WRITE(OUT,150)
260           WRITE (OUT,90000)
270           INPUT,TDK
280           WRITE(OUT,200)
290           WRITE (OUT,90000)
300           INPUT,GMAX
310           WRITE (OUT,201)
320           WRITE (OUT,90000)
330           INPUT,EPSIF
340           GLADAI=6.0
350           BK=1.38E-16
360           JAP=1
370           PI=3.14159
380           XMAXG=GMAX
390           R1=1.4E-08
400           AG(1)=1.0
410           U011=1500.0*BK
420           WRITE (OUT,202)
430           WRITE (OUT,90000)
440           INPUT,UFAC
450           U011=U011*UFAC
460         U0C0=U000*FAC
470         U001=SQRT(U011*U000)
480           THETA=U011/(BK*TDK)
500           GLADA(1)=0.0
510           GLADA(2)=1.0
520           GLADA(3)=2.0
530           BIGG(1)=0.0
540           BIGG(2)=1.0
550           BIGG(3)=2.0*(EXP (THETA)-1.0)/(1.0+2.0*THETA)
552         CHI(2)=1.0
553         CHI(3)=3.0
560           X01=3.06E-23
570           X00=4.93E-23
580           X0U12=2.04E-23
590           WRITE (OUT,230)
600           WRITE (OUT,90000)
```

-2- **COPY AVAILABLE TO DDC DOES NOT PERMIT FULLY LEGIBLE PRODUCTION**

```
(continued)
610          INPUT,XMUBAR
612         TOKO=273.0
613         ZLOGU=ALOG(XMUBAR)/2.30258
614         XLGTDK=ZLOGU*TDK/TOKO
620          SIG11=2.05*RI
625           SIG12=1.95*RI
630          Z11 D=3.33E-05*SQRT(TDK/XMI)*SIG11**2
635          Z11 D=Z11D/2.0
640            C11=Z11D*SQRT(THETA)
650          G(2)=C11*EXP(THETA)/(XMUBAR*SQRT(THETA))
655          G(2)=Z11D*EXP(THETA)/XMUBAR
670   221      WRITE(OUT,232)
680            WRITE(OUT,234)G(2)
690C-             PINF HERE IS FOR LIQUID
700          WRITE(OUT,235)
710          WRITE (OUT,90000)
720          INPUT,G(2)
730   222    XLPINF=9.3235-(2367.713/TDK)
740          PINF=10.0**(XLPINF)
750C-             PV IS THE SATURATION VAPOR PRESSURE IN CM HG
760C-             P IS ISENTROPIC PRESSURE IN CM HG
770          P=0.4525*(TDK/273.0)**3.5
780            CXP=1.33E+03
790          PV=PINF/10.0
800            P=PV
810C                    PINF HERE IS SAT. PRES. IN DYNES/CM**2
820            PINF=CXP*PINF
830          CI=0.9...+ ...*P/TDK
840         CIO=CI
850    225     WRITE(OUT,237)
860            WRITE(OUT,238)CI
870            WRITE(OUT,239)
880             WRITE(OUT,90000)
890          INPUT,CI
900           S=P/PV
910           ...=U011/(PINF*THETA)
915         C11NF=CI
920            ...F=1.0/C11NF
930C-              FTHETA NOW REFERS TO ASYM VALUE
940          ALINF=(1.0/(36.0*PI))**0.333
950           ...=5.0*RI**2*SQRT(U011/XMI)/XMUBAR
960          FTHETA=.1 NF/(SIGM*XLINF)
970    240   FRT=(EXP(GLAMDAI*THETA)-1.0)/(SQRT(THETA)*
980          1(1.0+GLAMDAI*THETA+0.5*(GLAMDAI*THETA)**2))
990           DELF=ABS(FTHETA-FRT)
1000         WRITE (OUT,998) FTHETA,FRT,DELF
1010          IF(DELF-EPSIF)260,260,245
1020   245    WRITE(OUT,250)
1030          WRITE (OUT,90000)
1040          INPUT,GLAMDAI
```

```
MAIN     (continued)

1050           GO TO 240
1060   200     WRITE (OUT,998) THETA,FRT,DELF
1062         GLAGLIQ=3.04
1065         XLATE=UFAC*2.98*GLADAI
1066         PRINT,XLATE
1070           XJ=ALOG(C1*FINF)
1080         IDF=122
1090         GINF=INF
1092         WRITE(OUT,210)
1094         WRITE(OUT,9700)
1096         INPUT,DLDG
1100         DGLLAD=GLADAI-GLADA(3)
1110         DO 280 I=4,MAXG
1120          J=I
1130         L=I-1
1140         IF(I-INF)265,275,275
1150   265   GLADA(I)=GLADA(L)+DLDG
1152         CHI(I)=CHI(L)+3.0
1160         GO TO 280
1170   275   GLADA(I)=GLADA(L)
1172         CHI(I)=CHI(L)+3.0
1180   280   CONTINUE
1190   290    CONTINUE
1200         SUMGCG=0.0
1210         SUMCG=0.0
1220         SUMLCG=0.0
1230           SUMLIN=0.0
1240           C(1)=C1
1250           GAMETA=FACTA*SQRT(THETA)/EXP(THETA)
1260           EXJ=EXP(-XJ)
1270             GO TO 400
1280   300     WRITE(OUT,310)
1290           WRITE (OUT,311)S,C1,PV
1300           WRITE(OUT,312)XJ,THETA,GLADAI
1310           WRITE(OUT,313) BIGM,FINF,GAMAS
1320           WRITE(OUT,314) GMAX,XNUBAR,XNU01
1330           WRITE(OUT,315)U011,U001,U000
1340           WRITE (OUT,9999) EXJ
1350   400     DO 690 IG=2,MAXG
1360           G=IG
1370           LG=IG-1
1380           GLI=G-1.0
1390           SIGIG=R1*(1.0+G**0.333)
1400           XNUG=XNU*(G/(1.0+G))
1410         IF(IG-20)410,410,415
1420   410   ALPHAG=1.0
1430         GO TO 420
1440   415   ALPHAG=1.0-0.1*(G/GINF)
1450   420   CONTINUE
1460           XXG=(SIGIG/R1)**2/SQRT(XNUG/XNI)
```

No. 21 (continued)

```
1470            IF(IG-2)999,495,43)
1480      43    CONTINUE
1490            IF(IG-3)999,460,450
1500      450   CONTINUE
1510            BIGG(IG)=(EXP(THETA*(GL.DA(IG)-1.0))
1520           &-EXP(-1.ETA*(GL.DA(IG)-GL.DA(LG)-1.0)))/
1521           &(1.0+GL.DA(IG)*THETA+).5*(GL.DA(IG)*THETA)**2)
1530            A=3.0*6-7.0
1540            FI=3.0+A*(A-1.0)/((A-2.0)*(A-3.0)*(A-4.0))
1550            SIGIG1=R1*(1.0+GL1**0.333)
1560            XMUIG1=X.1*(GL1/(1.0+GL1))
1570            XKGL1=(SIGIG1/R1)**2/SQRT(XMUIG1/X.1)
1580            XLG=(XKGL1/ALPHAG)*FI
1590            FTHETG=(EXP(T.IETA)/SQRT(T.IETA))*BIGG(IG)
1600            IF(IG-4)999,455,470
1610      455   FTHETG=FTHETG*(1.0/3.0)
1620            GO TO 475
1630      460   FTHETG=(EXP(THETA)/SQRT(THETA))*BIGG(IG)
1640           ZP2=5.89E-08*SQRT(TOK)
1646           XMU12=X.1*(GL1/(1.0+GL1))
1650           C12=(ZP2*(SIG12)**2/SQRT(XMU12))*SQRT(THETA)
1652           XG(IG)=C12*FTHETG/X.UBAR
1655            XK2=(SIG12/R1)**2/SQRT(XMU12/X.1)
1660            XG3=BIGG*XK2*FTHETG
1666           GO TO 495
1670      470   ZP2=5.89E-08*SQRT(TOK)
1680            C1G=(ZP2*(SIGIG)**2/SQRT(XMUIG))*SQRT(THETA)
1690            XIGR2=C1G/(XMUBAR*XKG)
1700            XG(IG)=BIGR2=XLG*FTHETG
1710      495   SUMLN=SUMLN+ALOG(XG(IG)/XINF)
1720            FIRST=(G-1.0)*XJ
1730            ZETAG(IG)=-XK*TOK*SUMLN
1740           XMACH(IG)=10.2216F14*(ZETAG(IG)/G)
1750            XLOGC1=XJ*(G-1.0)+SUMLN
1760              XLOGC1(IG)=XLOGC1/2.30258
1770                XLOGCG=XLOGC1(IG)+ALOG(C1)/2.30258
1780              C(IG)=10.0**(XLOGCG)
1785           ETAG=GL1
1790           ETAG=G+GL.DA(IG)/2.
1795            SLC=(G*GL.DIG-ETAG)*C(IG)
1800           SUMLCG=SUMLCG+SLC
1810            SUMCG=SUMCG+C(IG)
1820           SUMGCG=SUMGCG+G*C(IG)
1824           SUMCHI=SUMCHI+CHI(IG)*C(IG)
1830              XLRTIO=XLG/XLINF
1840              GRATIO=GTHETA/BIGG(IG)
1850              XLDIF=GL.DA1-GL.DA(IG)
1860              GRAT(IG)=GRATIO
1900              XLRAT(IG)=XLRTIO
1910              DELZET(IG)=ZETAG(IG)-ZETAG(IG-1)
```

```
10801     (continued)

1920      390    CONTINUE
1930             WRITE(F2,2121)(IG,C(IG),IG=1,MAXG)
1940             GO TO 840
1950      695    WRITE(F2,2120)(IG,GAMAS(IG),ZETAG(IG),WG(IG),GRAT(IG),XLRAT(IG)
1955             *,IG=1,MAXG)
1960      697  CONTINUE
1970             WRITE(F3,2121)(IG,XLOGC1(IG),IG=1,MAXG)
1980               GO TO 840
1990      700    WRITE(OUT,811)
2000               IF(MAP-2)820,830,830
2010      820    WRITE(OUT,812)(IG,C(IG),XLOGC1(IG),WG(IG),ZETAG(IG),IG=1,
2020             *MAXG)
2030             GO TO 840
2040      830    WRITE(OUT,812)(CUS(IG),GLAMDA(IG),BIGG(IG),IG=1,MAXG)
2050      840    CONTINUE
2052           RN1=SUMCG+C1
2053           RN2=SUMCG-C(2)
2054           RN3=SUMLIQ*C1+SUMLCG
2060      900    CF=7.5E-05
2065      UBF=0.85+(1.0/200.0)*(273.-TDK)
2070             PRES=(U011/THETA)*RN1*CF
2072           C1KE=(6./2.)*(3.2965E-24/XM1)*TDK*C1/C10
2074           C2KE=(5./2.)*(3.2965E-24/XM1)*TDK*C(2)/C10
2076           CGKE=3.0=(3.2965E-24/XM1)*TDK*RN2/C10
2077           CGVIB=(3.2965E-24/XM1)*TDK*SUMCHI/C10
2078           CGWK=(3.2965E-24/XM1)*TDK*RN1/C10
2080           FIRST=(2.388E-08*U011/XM1)*(RN3/C10)
2082           XLHT=FIRST+C1KE+C2KE+CGKE+CGVIB+CGWK
2085           PISEN=P
2086           PRINT,FIRST,C1KE
2087           PRINT,C2KE,CGKE
2088           PRINT,CGVIB,CGWK
2090      905    WRITE(OUT,317)PISEN,PV,PRES
2100               WRITE(OUT,320)GAMAS(123)
2110           WRITE(OUT,330)XLHT
2130      910      GO TO 225
2140      992    STOP
2150      90000 FORMAT(2F 2)
2160      150    FORMAT(29H TYPE IN INITIAL VALUE OF TDK)
2170      200    FORMAT(13H TYPE IN GMAX)
2180      201    FORMAT(14H TYPE IN EPSIF)
2190      202    FORMAT(13H TYPE IN UFAC)
2200      210      FORMAT(13H TYPE IN DLDG)
2210      230    FORMAT(24H TYPE IN VALUE OF XNUBAR)
2220      232    FORMAT(17H CALCULATED WG(2))
2230      234    FORMAT(7H WG(2)=E15.5)
2240      235    FORMAT(14H TYPE IN WG(2))
2250      237      FORMAT(14H CALCULATED C1)
2260      239      FORMAT(11H TYPE IN C1)
2270      238      FORMAT(4H C1=E15.6)
```

```
      (CONTINUED)
 300  FORMAT(24H TYPE I  VALUE OF GL GAI)
 31   FORMAT(23H DATA AND INITIAL VALUES )
 311  FORMAT(10H        S=E10.3,10H       CI=E10.3,
     110H       PV=E10.3)
 31   FORMAT(10H       XJ=E10.3,10H    THETA=F10.5,
     110H    GL GAI=E10.3)
 313  FORMAT (10H      SIG =E10.3,10H     ALHF=E10.3,
     110H    GAMMAS=E10.3)
 314  FORMAT(10H     GMAX=F10.5,10H    XMUBAR=E10.3,
     110H     GG01=E10.3)
 315  FORMAT(10H     U011=E10.3,10H     U001=E10.3,
     110H     U000=E10.3)
 316  FORMAT (10HSIGS(IG)=E10.3,10H       GR=E10.3,
     110H    DELGR=E10.3)
 31   FORMAT(10H      P.R=E10.3,10H   RG(IG)=E10.3,
     110H   PTHETA=E10.3)
 317  FORMAT(10H   PISEN=E10.3,7H    PV=E13.6,
     110H      PRES=E13.6)
 32   FORMAT(12H GAMMAS(123)=E13.6)
 330  FORMAT(6H ALHF=E13.6)
 700  FORMAT(1X,I,5)
 211  FORMAT(31H   CONCENTRATIONS, G=1 TO GMAX)
 12   FORMAT(2X,I5,2X,E10.3,3X,E10.3,3X,E10.3,3X,E10.3)
 211  FORMAT(E10.3)
 2121 FORMAT(I5,2H ,E15.8)
 212  FORMAT(E15.8)
 18   FORMAT(I10,5X,3E10.5)
 2120 FORMAT(I5,2H ,E15.6,2H ,E15.6,2H ,E15.6,2H ,E15.6,
     12H ,E15.6)
 2130 FORMAT(I5,2H ,E15.6,2H ,E15.6,2H ,)
 99   FORMAT(3E15.5)
 9998 FORMAT(F10.5)
 9999 FORMAT(1X,3F10.5)
 9997 FORMAT(1X,2F10.5)
 9995 FORMAT(1X,F10.5)
 9993 FORMAT(1X,I5,3F10.5)
      END
```

APPENDIX 3

FORTRAN PROGRAM FOR NON-EQUILIBRIUM CLUSTER DISTRIBUTION DURING AN ADIABATIC EXPANSION

The calculation given here is for the expansion of water vapor in air in a supersonic nozzle of known geometric profile. Solution of the one dimensional equations of motion [7,8] yields the flow velocity u which is required as an input datum. The same solution gives the cross sectional area A and its rate of change along the flow axis dA/dx. Also required are the initial equilibrium cluster distribution from Appendix 2 and the cluster properties such as radius r, pair interaction energy u°_{11}.

The computational scheme or flow chart is given in Figure VIII-3.1 and the relation of the iteration time interval to data increments given in Figure VIII-3.2. The method is to divide the data interval (Δx = 1 mm) into sub intervals ($\Delta x/\gamma$) small enough to allow a non-oscillating solution by Eulerian numerical integration:

$$f(x + \Delta x/\gamma) = f(x) + d\ f/dx(\Delta x/\gamma) \qquad \text{VIII-3.1}$$

However, the fewer the subdivisions the shorter the computation time. The smallest value of γ giving stability was found to be about 5000 and this value already brings the calculation interval down to the order of the molecular collision time. An extensive effort was necessary to find a method to reduce the amount of computer time involved. Additional complications in that the collision time increases during the expansion process

and the numerical interval in Equation VIII-3.1 must be significantly longer than the collision interval to be consistant with equilibration of translational energies. An approximation technique yielding stable numerical results was developed after many trials. After dividing a data interval: $\Delta X' \equiv X/\gamma$, with a value of γ around 5000, a multiplier, XER for example, XER=2.0 is selected arbitrarily. This multiplier has the effect of lengthening the calculation interval because the second term in Equation VIII-3.1 becomes

$$\Delta x/\gamma \text{ (XER) } d F/dx \qquad \text{VIII-3.2}$$

To reduce the number of calculation intervals within the original data interval Δx, an end condition NSTOP is introduced where NSTOP = γ/XER. If XER is 2.0, the derivative d F/dx is thus applied over a length $\frac{2\Delta x}{\gamma}$ for each γ interval, but the calculation for a given data interval is terminated after $\gamma/2$ sub intervals. To take account of the increase in collision time due to expansion, the collision time for the g = 10 cluster is calculated at the beginning and end point of the overall calculation (an increase from about .5 nsec to 4nsec) and a linear fit to XER is determined. An increment SXER is added to XER and NSTOP recalculated before calculating over the next data interval. Thus, a crude correspondence between the collision interval and the calculation interval is maintained and the amount of computer time is reduced since NSTOP is decreasing continually.

In as much as the calculation proceeds at near the molecular

collision interval, interpolation of the experimental input data and the calculated flow velocity u is required. Multi-point (seven) derivatives are taken over the original numerical data and velocity then applied each γ subinterval. Thus, the original data for nozzle slope, DADX(J) (INDEX J increments each m.m.) becomes DADXMG for each γ interval. The expansion terms, Equation V-2.11 and V-2.12 are then corrected each γ interval.

Additionally, after calculating all rates up through g_{max} at any subinterval, the rates for cluster size (g_{max}+1) must be calculated to include the influence of f_{g+1} on f_g. In this calculation the influence of $f_{g_{max}+2}$ is ignored so that

$$\frac{df_{g_{max}+1}}{dt} = (R^{+}_{g+1} - R^{-}_{g+1}) - f_{g+1}\frac{d}{dt}(\ell n\ v)$$

rather than Equation V-2.13. This result is correct within a few percent as long as $f_{g+2} << f_{g+1}$. The calculation appears after statement 525 in the program.

An exact calculation over all γ subintervals and data intervals involves about 16 hours on the PDP 15/40. With XER=2.0, the time is reduced to about 4 hours while on using the SXER technique the time is about 1.5 hours. This is a valuable saving in computer time. No significant difference in the results is obtained between these three methods.

The initial debugging and program development of this program and the equilibrium program was done in an interactive mode over several years on a H-635 and DTSS (Dartmouth Time

Sharing System). The results described would have been impossible to achieve without this computer service where 50 or more short runs could be accomplished in one's own office in two hours. Once debugged the programs were shifted to the PDP 15/40 for the long runs. The accuracy could also be checked as 7-8 digits are significant on the H-635 while only 5-6 digits are significant on the PDP 15/40. Using double precision on certain quantities, closely similar results were obtained with the two computers.

Another feature that should be mentioned is the restart capability. If for some reason a run is terminated before completion, it can be restarted with loss of, at most, less than one data interval of computation. The restart is not precise since only average values of the nozzle geometry are used (see RESTART PATCH), however, if for some reason long runs become infeasible, the restart information could be fed into the initial file (OUTFIL SRC) each time NSTOP is reached (Statement 514 + 1).

When NSTOP is reached the value of all cluster reaction terms (R_g^+, R_g^-, R_{g+1}^+, R_{g+1}^-, df_g, etc.) and flow properties (p/p_{01}, T/T_{01}, T°K, etc.) are written out. Isentropic properties calculated by suppressing the reaction term of the expression for dT. (Equation V-2.7) are also reported. The partial pressure of the vapor obtained by summing the partial pressures of each cluster size is reported as PPAR.

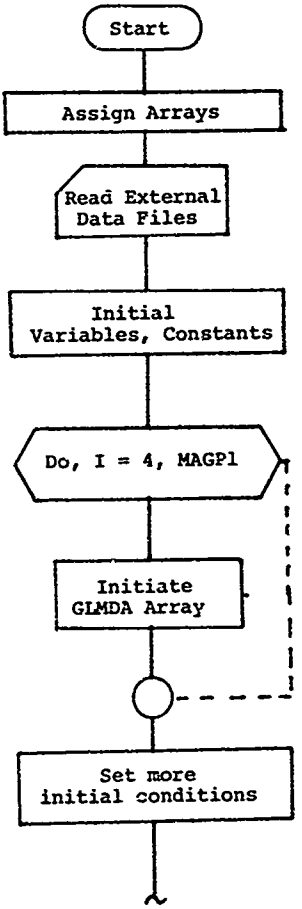

FLOW CHART FOR COMPUTATION OF EVOLVING DISTRIBUTIONS

Figure VIII-3.1

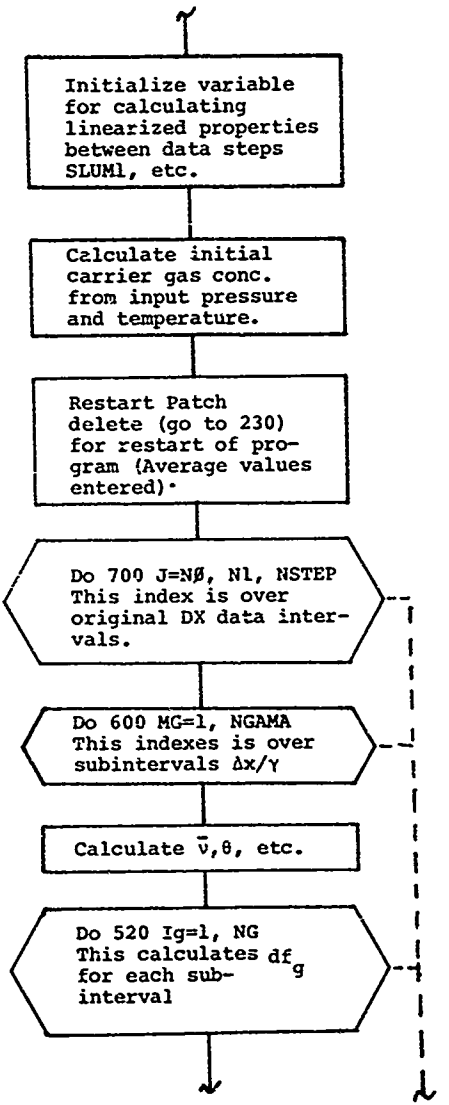
Initialize variable for calculating linearized properties between data steps SLUM1, etc.
Calculate initial carrier gas conc. from input pressure and temperature.
Restart Patch delete (go to 230) for restart of program (Average values entered).
Do 700 J=NØ, N1, NSTEP This index is over original DX data intervals.
Do 600 MG=1, NGAMA This indexes is over subintervals Δx/γ
Calculate $\bar{v}$,θ, etc.
Do 520 Ig=1, NG This calculates df_g for each subinterval

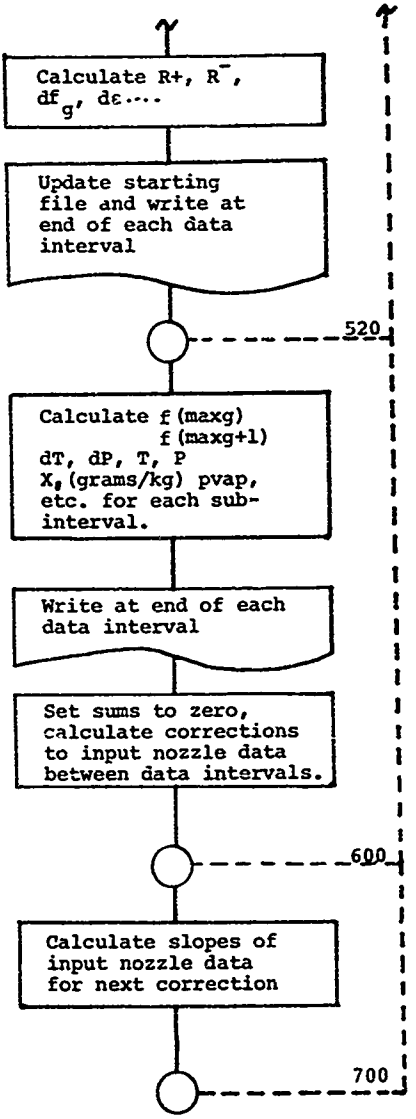
Calculate R+, R⁻, df_g, dε....
Update starting file and write at end of each data interval
520
Calculate f(maxg) f(maxg+1) dT, dP, T, P X_g(grams/kg) pvap, etc. for each sub-interval.
Write at end of each data interval
Set sums to zero, calculate corrections to input nozzle data between data intervals.
600
Calculate slopes of input nozzle data for next correction
700

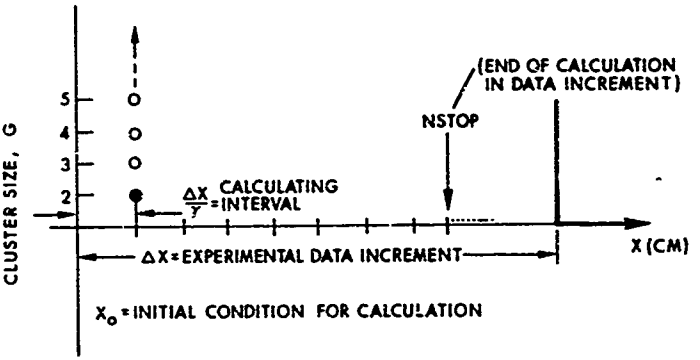

Figure VIII-3.2
Calculation Scheme for Each Data Interval

```
      DOUBLEPRECISION  RMAT2,RMAT22,DFGA,GDFG,SMGDFG,
     &RPL2BI,RMI2BI,RPL3BI,RMI3U,RPLUS,RMIINV,RPLGP1,PMIVP1,
     &SMNGRG,SUMGFG,DFG2,DFG,RMATG,DFG2M1,DFGM1,DFG1,DFG12,RMATG2,
     &SUMBRC,EXPT,DFGEX,DFG1EX,RMAT1,BRCFG,SUMGG,SMGRG,SUMGRG
      REAL A(2)
      DIMENSION GLMDA(20)
      DIMENSION U(100),XCM(100),AREA(100),DADX(100),FGTM(20)
     DIMENSION XNONE0(2),XNON2(2),XNONDA(2),XOUTFI(2)
     DATA XNONE0(1),XNONE0(2)/5HNONE0,4HSSRC/
     DATA XNON2(1),XNON2(2)/5HNON2 ,4H SRC/
     DATA XNONDA(1),XNONDA(2)/5HNONDA,4HTSRC/
     DATA XOUTFI(1),XOUTFI(2)/5HOUTFI,4HLSRC/
      DATA A/5HTAPE1,4H SRC/
      CALL ENTERC(7,A)
     CALL SEEK(2,XNONDA)
       E R BUCKLE,UNIV.  OF SHEFFIELD,ENGLAND , A A POURING, USNA,
            BUCKLE CONDENSATION XX REVISED 3 DEC 1975
        PREDICT EXPERIMENT 405 FROM INITIAL DIST., ALPHA,BETA,DELTA
        UNITS ARE CM,ERG,SEC,MOLECULE,MONOMER,CLUSTER,DEG.KELVIN
10    READ(2,100) N,XNU,DELTAX,T01,PVAP,PAIR
            DEFINE PVAP AS THE PARTIAL PRESSURE OF VAPOR AT XZERO
            TDK IS THE STATIC TEMP AT J=N0
      READ(2,200) (XCM(J),U(J),AREA(J),DADX(J),J=1,N)
      CALL CLOSE(2)
      CALL SEEK(2,XOUTFI)
      READ(2,205)MAXG,J,N0,PSTAT,PISEN,TDKIS
      READ(2,211)FGTM
      READ(2,211)F10D
      READ(2,211)TDK
      READ(2,211)QOFX
      MAXGP1=MAXG+1
      READ(2,211)(FGTM(IG),IG=1,MAXGP1)
     CALL CLOSE(2)
20    GLMDA(1)=0 0
      GLMDA(2)=1 0
      GLMDA(3)=2 0
      GAMA= 5000
      NGAMA=GAMA
            THIS IS HARD SPHERE CLATHRATE HSC MODEL
     DLDG=0 0153
     NSTOP=2500
     NWRITE=0
     UFAC=0 9732
     XNU=3 35E12
     TDK0=T01
      P01=76 2
      CP0=0 480E-15
      DO 220 I=4,MAXGP1
        L=I-1
     GLMDA(I)=GLMDA(L)+DLDG
220       CONTINUE
      N0=J
      IG=1
      NSTEP=1
      NBUC=1
      K1=J+NSTEP
        R1=1 4E-08
        R0=1 4E-08
      PI=3 14159
     XER=2 0
```

```
   PI=3 14159
   XER=2 0
   XJ=J
   GO TO 221
   SXER=0 085
   XER0=2 0
   XEP=XER0
   STOP=GAMA/XER
   NSTOP=STOP
21      CONTINUE
    BK=1 38E-16
    CU011=1500 0
    U011=BK*CU011
    U011=U011+UFAC
    U001=BK*400 0
    U000=BK*106 0
   GFAC=1 0
   XN=1 250
   REF=EXP(6 0*XN)
   REFU0=EXP(7 3)
   U0110=U011
   TDK00=273
   XMU0=5 35E12
   U000=U000+GFAC
    GAMAD=SQRT (U000/U011)
      XM1=3 06E-23
      XM0=4 93E-23
   XMU02=(2 0*XM0/(XM0+2.0*XM1))*XM1
    SIG02=R0+R1
   XMU12=2 0*XM1/3.0
   SIG12=1 55*R1
   SIG11=2 05809*R1
    SIG01=R1+R0
    SIG101=(SIG01+SIG11)/2 0
   SLUM1=2260 0
   DXCM=DELTAX
   D1=4 0*DXCM
   D2= 20 0*DXCM
   D3=60 0*DXCM
   DDADX=(DADX(N0)-DADX(N0-1))/GAMA
   DDU=12 0/GAMA
   SLU= (3 0*(U(N0+1)-U(N0-1))/D1)
&-(3 0*(U(N0+2)-U(N0-2))/D2)
&+((U(N0+3)-U(N0-3))/D3)
   DU=SLU*DXCM/GAMA
         DEFINE RTAA=(1/A)(DA/DX)(U(J)),RTUU=DU/DX
    RTAA=35 6*DADX(K1)*U(K1)/AREA(K1)
   RTUU=SLU
    DELTAX=DELTAX/GAMA
         DELTAX NOW CONTAINS GAMMA INTERVALS
         F1TM AND F0TM ARE THE INITIAL DISTRIBUTIONS OF MONOME
         AIK,THAT IS AT X ZERO.  PLEASE NOTE
   CF=7 3E-05/P01
    F1TM=FGTM(1)
    F2TM=FGTM(2)
    F0TM0=0 20E20
   F1TM0=0 1492E+18
    NG=MAXG
F IS CONVERSION FACTOR TO GIVE P/P01 DIMENSIONLESS,ONCE     0
         THE CONCENTRATIONS ARE KNOWN, IE P(G)/P01 = CF*(K*T*F
```

```
      WE TAKE INITIAL VALUE OF DTM TO START.THEN CORRECT EA
    DTM=DELTAX/V(K1)
    N1=N-5
   DFG12=-0 3E12
   SUM1=0 0
   XLGTDK=ALOG10(XNU0)/273.0
  FOTM=PSTAT (CF*BK*TDK)
   GO TO 230
         RESTART PATCH
   DTM=0 44607869E-09
   DDADX=0 19633276E-05
   SLU=2902 0582
   DU=0 29020581E-01
   DDU=0 31117370E-01
   SLUM1=2902 0582
   RTAA=-153! 0339
   RTUU=2867 7861
         THIS DO INDEXES OVER ORIGINAL DELTAX INTERVALS
230   DO 760 J=NO.N1,NSTEP
   MBUC=0
         THIS DO INDEXES OVER INTERVALS OF DELTAX/GAMA
   DO 400 MG=1,NGAMA
   DELTDK=(TDK00-TDKIS)/10.
   XLOGNU=ALOG10(XNU0)-EXP(DELTDK**XN)/REF
   IF( J-42)234,238,238
234   XLPINF=9 3286-(2367.713/TDKIS)
   GO TO 240
238   XLPINF=7 95039-(2022 003/TDKIS)
240    CONTINUE
   PINF=10 0**(XLPINF)/10.0
   C1INF=0 966E+20*PINF/TDKIS
   FIRST=XLGTDK*TDKIS
   SECND=1 590*ALOG10(F1TM/C1INF)
   THIRD=SUM1/DFG12
   SUM=FIRST+SECND+3.02*THIRD
242    CONTINUE
   XNU=10 0**(XLOGNU)
   XNU01=XNU
   NGM1=NG-1
   RT=SQRT(TDK)
   RT1=SQRT(TDK/XM1)
      RT1=SQRT(TDK/XM1)
      Z11DD=8 33E-08*RT1*SIG11**2
   Z11DD=Z11DD/2 0
   Z12DD=5 89E-08*SQRT(TDK)*SIG12**2/SQRT(XMU12)
    Z01DD=5 89E-08*SQRT(TDK/XM1*((XM0+XM1)/XM0))*
&SIG01**2
      Z02DD=5 89E-08*SQRT(TDK*XNU02)*SIG02**2
    Z011DD=5 89E-08*SQRT(TDK/XM1*(XM0+2 0*XM1)/
&(XM0+XM1))*SIG101**2
         RMATRIX ZERO = RMAT0
    RMAT0=-F0TM*(RTAA+RTUU)
    RMAT1D=-F10D*(RTAA+RTUU)
   THETA=U011/(BK*TDK)
         THIS DO INDEXES OVER ALL SIZE G
    DO 520 IG=1,NG
   N=IG
   MBUC=MBUC+1
    G=IG
 IF(IG 20)302,302,303
```

```
      ALPHA=1.0
      GO TO 304
    3 ALPHA=1.0-0.1*(G/GINF)
    4 CONTINUE
  305   IF(IG-2)370,310,320
            SECTION 310 TO 320 FOR SIZE G=2
           XNG DEFINED EQUAL TO LAMBDA
   10   CHIG=1.0
        CHIGP1=3.0
        CHIGM1=0.0
       XNG=1.0
       DELZI=-1.0
        GO TO 340
            SECTION 320 TO 330 FOR SIZE G=3
   20   CHIG=3.0
        CHIGM1=1.0
       XNG=2.0
       DELZI=0.0
        IF(IG-3)800,340,330
            SECTION 330 TO 340 FOR SIZE G=4 AND UP
   30   CHIG=3.0*(G-2.0)
        CHIGM1=       CHIG-3.0
       XNG=3.0
       DELZI=0.0
            FOLLOWING SECTION IS FOR SIZE G+1, DEFINE M=G+1
   40    M=IG+1
        G=M
            IF IG=NG, SKIP THES SECTION AND SCRUB PREVIOUW (G+1)
         VARIABLE NAMES ARE CHANGED INORDER TO SAVE THEM FOR PRINTI
   44   CHIGP1=3.0*(G-2.0)
  ZP1=5.89E-06*RT
            RETURN NOW TO REGULAR G
   46   G=IG
            ZP1 DEFINED ABOVE
          ZP2=ZP1
        SIGMA1=R1*(1.0+G**0.333)
        XMU1=XM1*(G/(1.0+G))
       XMU0=XM0*G/(XM0/XM1+G)
        Z1GDD=ZP2*SIGMA1**2/SQRT (XMU1)
        GO TO 400
            FOR MONOMER MONOMER COLLISION, Z1 MUST BE HALVED
            370 TO 372 ARE FOR G=1, ALL TIME
   70   XNG=0.0
        CHIG=0.0
        CHIGP1=1.0
        CHIGM1=0.0
       CHI1=0.0
       Z11=3.0
   80    GO TO 492
   90    LG=IG-1
        IF(IG-3)405,410,415
            FOLLOWING SECTION IS FOR SIZE G=2
  405  RPL2BI=(Z01DD*F0TM)*(F1TM/XNU01)
     &*(Z011DD*F1TM*GAMAD)
     &*THETA*(1.0-EXP(-THETA))
        RPL3BI=Z1ZDD*F1TM*F2TM*(1.0-EXP (-THETA))
        RMI3U=0.5*XNU*FGTM(3)*(1.0+2.0*THETA)*
     &EXP(-2.0*THETA)
      RM12BI=(Z01DD*F0TM)*(F2TM/XNU01)
     &*(Z011DD*XNU*GAMAD/Z11DD)
```

```
     &*EXP(-THETA)*THETA*(1 0-EXP(-THETA))
           VARIABLES HAVE BEEN REDEFINED HERE FOR PRINTING ONLY
       RPLUS=RPL2BI
       RMINU=RMI2BI
       RPLGP1=RPL3BI
       RMIUP1=RMI3U
         GO TO 460
               FOLLOWING SECTION IS FOR SIZE G=3
410      RPLUS=RPL3BI
         RPP1=Z1GDD*F1TM
         RPLGP1=RPP1*FGTM(IG)*2.00*(1.0-EXP (-GLMDA(IG)*THETA))/
     &(CHIG  *(CHIG  -1 0))
         RPL4BI=RPLGP1
412       GLMTA=GLMDA(M)*THETA
             DEFINE ALPP1=ALPHA(G+1)
         XM=M
       ALPP1=ALPHA
         RMIUP1=2 0*ALPP1*XINU*FGTM(M)*EXP (-GLMTA)*
     &(1 0+GLMTA+0 5*GLMTA**2)/
     &((CHIGP1-1 0)*(CHIGP1-2.0))
         RMI4U=RMIUP1
         RMINU=RMI3U
         SUMRPL=SUMRPL+RPL3BI
         SUMRMU=RMI3U
        DELEP0=-U011*GLMDA(IG)
        DELEP0=-(G+GLMDA(IG)/2.)*U011+DELEP0
        DELEP=DELEP0*BK*TDK*
     &(XNG+0 5*(DELZI))
        SMNGRG=SMNGRG-DELEP*(RPLUS-RMINU)
        DELTER=DELEP*(RPLUS-RMINU)
         GO TO 470
               FOLLOWING SECTION IS FOR SIZE G=4 AND UP
               RPLUS IS FOR GROWTH INTO SIZE G FROM SIZE BELOW
415      RPP1=Z1GDD*F1TM
                 RPLGP1 HERE COMPUTED BEFORE
417        RPLUS=RPLGP1
         RMINU=RMIUP1
420      RPLGP1=RPP1*FGTM(IG)*6 00*(1.0-EXP (-GLMDA(IG)*THETA))/
     &(CHIG*(CHIG-1 0)*(CHIG-2.0))
         XM=M
       ALPP1=ALPHA
         GLMTA=GLMDA(M)*THETA
         RMIUP1=2 0*ALPP1*XINU*FGTM(M)*EXP (-GLMTA)*
     &(1 0+GLMTA+0 5*GLMTA**2)/
     &((CHIGP1-1 0)*(CHIGP1-2.0))
         GLMTA=GLMDA(IG)*THETA
450      GO TO 465
               ENTER  G=2
460    RMAT22=(RPL2BI-RMI2BI)-(RPL3BI-RMI3U)
       DFGEX=FGTM(IG)*(RTAA+RTUU)*DTM*XER
      DFGA=RMAT22*DTM*XER
      GDFG=G*DFGA
       RMAT2=(RPL2BI-RMI2BI)*2.0
        SMGDFG=SMGDFG+GDFG
       DELEP0=-U01 *GLMDA(IG)
       DELEP0=-(G+GLMDA(IG)/2.)*U011+DELEP0
       DELEP=DELEP0*BK*TDK*
     &(XNG+0 5*(DELZI))
        SMNGRG=-DELEP*(RPL2BI-RMI2BI)
       DELTER=DELEP*(RPLUS-RMINU)
```

```
  DFG2=DFGA-DFGEX
 DFG=DFG2
   DFGZM1=DFG2
   GO TO 490
         ENTER G=4 & UP
55   CONTINUE
   DELEP0=-U011*GLMDA(IG)
   DELEP0=-(G+GLMDA(IG)/2.)*U011+DELEP0
   DELEP=DELEP0+DK*YDK*
&(XN*10.5*(DELZI))
   SMNGRG=SMNGRG-DELEP*(RPLUS-RMINU)
  DELTER=DELEP*(RPLUS-RMINU)
         ENTER G=3 & UP
70 RMATG2=(RPLUS-RMINU)-(RPLGP1-RMIUP1)
80  EXPT=FGTM(IG)*(RTAA+RTUU)
  DFGEX=EXPT*DTM*XER
 DFGA=RMATG2*DTM*XER
  DFG=DFGA-DFGEX
 GDFG=G*DFGA
   SMGDFG=SMGDFG+GDFG
  SUMDF1=SUMDF1+DFGA
         BRC IS (3*G-0.5*(SG+PSIG))*FGTM
         SUMBRC SUMS BRC FROM G=3 TO GMAX    F1TM,F2TM ADDED B
  BRC=((3 0*G)-3 0)*FGTM(IG)
  SUMBRC=SUMBRC+BRC
90 SUMGFG=SUMGFG+FGTM(IG)
         SUMGFG IS SUMMED FROM G=1,ALSO SUMGG,BUTF1TM IS ADDED
         DITTO FOR SUMGFG
  GFG=G*FGTM(IG)
  SUMGG=SUMGG+GFG
92  Z1M1DD=Z1GDD
         THIS COMPLEATS THE CALCULATIONS FOR CHANGES IN CONCEN
         IN THIS SUBINTERVAL OVER ALL CLUSTER SIZES PRESENT
         BELOW THIS POINT CONCENTRATIONS ARE FOR NEXT TIME INT
         NOTE THAT CONCENTRATIONS CANNOT BE CHANGED IMMEDIATEL
         THIS IS BECAUSE WE NOW REACH DOWN FOR F(G-1)WHILE COM
         THE CHANGE DF(G),WE NOW SAVE DFG BY CALLING IT DFGM1
         APPLY THE CHANGE AFTER COMPUTING THE NEXT HIGHER ONE
         F1TM MUST BE KEPT CONSTANT WHITHIN ONE TIME INTERVAL
         IT IS INVOLVED IN BIMOLECULAR PROCESS FOR ALL SIZE G
         IN THAT INTERVAL.  IT IS NOT CORRECTED UNTIL LEAVING
         INTERVAL
90   IF(IG-3)505,503,504
93   F2TM=F2TM+DFG2M1
   FGTM(2)=F2TM
   GO TO 508
94  FGTM(LG)=FGTM(LG)+DFGM1
96 CONTINUE
   DFGM1=DFG
85   CONTINUE
  Z1G=Z1GDD*F1TM*FGTM(IG)
   COMPARE IG WITH NG,IF SAME GO ON
         WHEN IG=NG,DFG(IG) MUST BE APPLIED BELOW
         SECTION BELOW IS USED TO STORE CONCENTRATIONS FOR
   CALC DERIVATIVES FOR REST OF INTERVAL
10 CONTINUE
  IF(MG-NSTOP)520,513,513
13   CONTINUE
   IF(IG-MAXG)515,514,514
4   CONTINUE
```

```
      CALL ENTER(2,XOUTFI)
      WRITE(2,2051)MAXG,K1,NO,PSTAT,PISEN,TDKIS
      WRITE(2,2111)F0TM
      WRITE(2,2111)F10D
      WRITE(2,2111)TDK
      WRITE(2,2111)CCFX
      WRITE(2,2111)(FGTM(IG2),IG2=1,MAXGP1)
      ENDFILE 2
  515 CONTINUE
      WRITE(7,576)
      IF(IG-1)516,516,517
  516 DFGEX=DFG1EX
      DFG=DFG12
      WRITE(7,570)IG,XCM(J+1),TDK,DTSTAT,DPSTAT
  517 WRITE(7,570)IG,PPLUS,RMINU,RPLGP1,RMIUP1
      WRITE(7,570)MEUC,FGTM(IG),DFG9,DFGEX,DFG
      CONTINUE
      FGTM(MAXG)=FGTM(MAXG)+DFG
        DFGP1=(RPLGP1-RMINP1-(FGTM(MAXGP1)*(RTAA+RTUU)))*DTM*XER
      FGTM(MAXGP1)=FGTM(MAXGP1)+DFGP1
      BRCFG=SUMDRC+3.0*F1TM+3.5*F2TM
      DFG1EX=F1TM*(RTAA+RTUU)*DTM*XER
    DFG12=-SMGDFG-DFG1EX
    DFGA=SMGDFG
    DFG=DFG12
      F1TM=F1TM*DFG12
      FGTM(1)=F1TM
  542 SUMGFG=SUMGFG+F1TM
     F1TERM=BK*TDK*(SMGDFG/(DTM*XER))*(CHI1+0.5*ZI1+3./2.)
     F12=UR11+2.1*SMGDFG/(DTM*XER)
     SMNGRG=SMNGRG+F1TERM
    XNUM1=SMNGRG
     XNUM2=BK*TDK*(F0TM+SUMGFG)*(RTAA+RTUU)
    XNUMER=XNUM1-XNUM2
      CV0=CP0-BK
      AZERO=CV0
    DENOM1=AZERO*F0TM
    DENOM2=BK*BRCFG
      DENOM=DENOM1+DENOM2
      DTSTAT=(XNUMER/DENOM)*XER*.DTM
     DPSTAT=PSTAT*(DTSTAT/TDK-(RTAA+RTUU)*XER*DTM)
      PPARO=BK*TDK*F0TM*CF
      PPAR=BK*TDK*CF*SUMGFG*P01
     S=PPAR/PINF
     F1C1R=F1TM/C1INF
      FCOEF=BK*TDK*CF
     TDK=     TDK+DTSTAT
      PSTAT=PSTAT+DPSTAT
            DEFINE T ISENTROPIC = TDKIS
            DEFINE P ISENTROPIC = PISEN
      XNUM1S=-BK*TDKIS*(F0TM+F10D)*(RTAA+RTUU)
     DENIS=AZERO+F0TM+BK*(3.0+F10D)
      DTISEN=(XNUM1S/DENIS)*XER*DTM
      DPISEN=PISEN*(DTISEN/TDKIS-(RTAA+RTUU)*XER*DTM)
      TDKIS=TDKIS+DTISEN
      PISEN=PISEN+DPISEN
      DELTAT=TDK-TDKIS
      DELTAP=PSTAT-PISEN
            NOTE Q IS DIMENSIONLESS
      DUDT=SMNGRG/(CP0*F0TM0*T01)
```

```
      DQDX=DQDT/U(J)
      DQ=DQDT*XER*DTM
      QQFX=QQFX+DQ
    COND=SUMGG
    GGPKG=(XM1/XM0)*(COND/F0TM)*1000
      SUMGG=SUMGG+F1TM
    GBAR=SUMGG/SUMGFG
    C10=(TDK0/TDK)**2.5*SUMGG
    SMGRG=SUMGRG
          XMABAL IS RATIO OF INITIAL MONOMER TO TOTAL NO OF
          MOLECULES OF H2O AT GIVEN LOCATION
    XMABAL=(XM1/XM0)*1E03*(SUMGG)/F0TM
    RMAT0=-F0TM*(RTAA+RTUU)
      DF0=RMAT0*XER* DTM
      F0TM=F0TM+DF0
      DF10D =RMAT1D*XER*DTM
      F10D=F10D+DF10D
    RDTM=DTM*XER
      SRDTM=SRDTM+RDTM
45  CONTINUE
    IF(MG-NSTOP)580,550,550
00  CONTINUE
      WRITE(7,579)
  WRITE(7,570)K1,XNUMER,XNUM1,XNUM2
  WRITE(7,570)MG,DENOM,DENOM1,DENOM2
  WRITE(7,570)MG,DELTAT,DELTAP,DQDT
    WRITE(7,570)MG,PSTAT,PISEN,TDK1S
  WRITE(7,570)MG,DQDX,DQ,QQFX
  WRITE(7,570)MG,GBAR,GGPKG,F0TM
      WRITE(7,)J,F10D,DTM,SDTM,SMNGRG,SUMGG,PPAR,C10,XNU
    WRITE(7,570)J,XER,RDTM,SRDTM
    WRITE(7,570)J,ITERM,XMABAL,PPAR
    WRITE(7,570)J,C10,XNU,THIRD
    WRITE(7,570)K1,FIRST,SECND,SUM
    WRITE(7,570)K1,C1INF,S,F1C1R
    NWRITE=0
      WRITE(7,260)
    SUM1=SMGDFG
00  Z1M1DD=0.0
    RPLUS=0.0
    RMINU=0.0
      SMNGRG=0.0
      SUMGFG=0.0
    SUMDF1=0.0
      SUMGG=0.0
      BRC=0.0
      SUMBRC=0.0
  SMGDFG=0.0
      BRCFG=0.0
    SUMDAX=SUMDAX+DDADX
    SUMDDU=SUMDDU+DDU
    DADXMG=DADX(J)+SUMDAX
    SUMDU=SUMDU+DU
    UMG=U(J)+SUMDU
    DUDXMG=SLU+SUMDDU
    DAMG=35.6*DADXMG*DELTAX
    AREAMG=AREA(J)+DAMG
    RTAA=35.6*DADXMG*UMG/AREAMG
    RTUU=DUDXMG
    IF(MG-NSTOP)600,790,800
```

```
590   CONTINUE
      SUMDA**0 0
      DDADX=0 0
      SUMDDU=0 0
      DDU=0 0
      SUMDU=0 0
      DU=0 0
      GO TO 620
600   CONTINUE
620   CONTINUE
      GO TO 621
      XJ=K1
      XER=XER+3XER
      STOP=GAMA/XER
      NSTOP=STOP
621         CONTINUE
680    K1=K1+1
      NWRITE=NWRITE+1
       DTM=DELTAX/U(K1)
      SLDADX=(3 0*(DADX(J+2)-DADX(J))/D1)
     &-(3 0*(DADX(J+3)-DADX(J-1))/D2)
     &+((DADX(J+4)-DADX(J-2))/D3)
      DDADX=SLDADX*DELTAX
      SLU=(3 0*(U(J+2)-U(J))/D1)
     &-(3 0*(U(J+3)-U(J-1))/D2)
     &+((U(J+4)-U(J-2))/D3)
      DU=SLU*DELTAX
      SLDU=(SLU-SLUM1)/DXCM
      DDU=SLDU*DELTAX
      SLUM1=SLU
700    CONTINUE
       CALL CLOSE(7)
       STOP
166    FORMAT(I10,E10.3,4F10.5)
200    FORMAT(F10.5,F10.3,2F10 5)
205    FORMAT(3I10,3F10.5)
111     FORMAT(1H ,E16.8)
151     FORMAT(1H ,3I10,3F10 5)
211      FORMAT(E16.8)
250    FORMAT(1H1)
570   FORMAT(1H ,I5,4E15.7)
576    FORMAT(/)
579    FORMAT(///)
900      STOP
       END
```

91 535E+13 0 10 295 6 0 5 58 7

-0 00000	17660 009	45 95357	-0 12661
0 10000	17896 835	45 52396	-0 12303
0 20000	18136 243	45 09343	-0 12113
0 30000	18384 327	44 66332	-0 11977
0 40000	18638 470	44 24244	-0 11693
0 50000	18895 769	43 83192	-0 11314
0 60000	19153 893	43 43731	-0 10895
0 70000	19411 688	43 05576	-0 10514
0 80000	19669 601	42 68859	-0 10143
0 90000	19927 662	42 33349	-0 09785
1 00000	20185 829	41 99167	-0 09443
1 10000	20444 541	41 66379	-0 09244
1 20000	20709 253	41 33591	-0 09049
1 30000	20971 948	41 01529	-0 08962
1 40000	21246 673	40 69850	-0 08819
1 50000	21528 103	40 38848	-0 08585
1 60000	21813 633	40 08812	-0 08277
1 70000	22100 728	39 79933	-0 07957
1 80000	22389 754	39 52144	-0 07647
1 90000	22677 771	39 25345	-0 07456
2 00000	22972 379	38 98803	-0 07414
2 10000	23279 234	38 72560	-0 07374
2 20000	23599 986	38 46639	-0 07115
2 30000	23929 897	38 22164	-0 06673
2 40000	24246 338	37 99415	-0 06150
2 50000	24559 627	37 70202	-0 05911
2 60000	24872 067	37 57800	-0 05606
2 70000	25190 821	37 38763	-0 05417
2 80000	25517 658	37 19360	-0 05186
2 90000	25850 835	37 01401	-0 04901
3 00000	26187 286	36 84483	-0 04603
3 10000	26526 240	36 68623	-0 04308
3 20000	26867 907	36 53813	-0 04009
3 30000	27211 920	36 40088	-0 03703
3. 40000	27557. 737	36 27432	-0 03410
3 50000	27906 656	36 15796	-0 03127
3 60000	28260 151	36 05193	-0 02823
3 70000	28616 404	35 95713	-0 02505
3 80000	28973 832	35 87336	-0 02204
3 90000	29334 936	35 80009	-0 01914
4 00000	29703 629	35 [illegible]	-0 01594
4 10000	30076 401	35 68701	-0 01238
4 20000	30443 972	35 64919	-0 00890
4 30000	30801 208	35 62323	-0 00576
4 40000	31152 809	35 60796	-0 00281
4 50000	31508 415	35 60333	0 00025
4 60000	31873. 154	35 61008	0 00361
4 70000	32251 626	35 62954	0 00739
4 80000	32645 739	35 66305	0 01150
4 90000	33051 532	35 71107	0 01526
5. 00000	33453 733	35 77167	0 01899
5 10000	33852 501	35 84740	0 02368
5 20000	34265 271	35 94154	0 02952
5 30000	34700 455	36 05571	0 03377
5 40000	35131 165	36 17827	0 03486
5 50000	35523 776	36 30227	0 03455
5 60000	35875 947	36 42593	0 03567
5. 70000	36204 620	36 55902	0 .03917
5 80000	36540 429	36 70686	0 04391
5 90000	36899 919	36 87143	0 04892
6 00000	37264 457	37 05379	0 05354
6 10000	37635 623	37. 25202	0 05767
6 20000	38008 663	37 46373	0 06124
6 30000	38379 481	37. 68773	0 06456
6 40000	38746 602	37. 92325	0 06777
6 50000	39073 639	38 17031	0 07104
6 60000	39428 033	38 42903	0 07431
6 70000	39761. 939	38 69931	0 07752
6 80000	40062 162	38 98090	0 08064
6. 90000	40322 392	39. 27352	0 08379
7 00000	40523 805	39 57750	0 08699
7 10000	40681 762	39 89307	0 09037
7 20000	40786 961	40 22131	0 09404
7 30000	40863 299	40 56294	0 09799
7 40000	40934 530	40. 91843	0 10147
7 50000	41018. 903	41 28406	0 10380
7. 60000	41134. 769	41. 65643	0 10522
7 00000	41492 042	42 41974	0 10977
7 90000	41735 030	42. 81519	0 11240
8 00000	42018. 711	43 21894	0. 11412
8 10000	42340 954	43 62684	0 11311
8 20000	42695 285	44. 03875	0 11633
8. 30000	43082 778	44. 45603	0 11837
8 40000	43478 685	44. 88269	0 12139
8. 50000	43893 332	45 32056	0 12457
8 60000	44300 003	45 76878	0 12704
8. 70000	44650 146	46 22388	0. 12850
8. 80000	45000. 814	46 68319	0 12954
8. 90000	45350. 426	47 14653	0. 13087
9. 00000	45750 853	47 61593	0 13301

NONDAT SRC

```
      19          15          15   0 75000   0 75000 272 99999
0.20000000E+20
0.16000000E+18
0.27299330E+03
0
0.16000000E+18
0.10299099E+15
0.37137217E+13
0.60239349E+11
0.47734832E+09
0.20333456E+07
0.62337311E+04
0.13731362E+02
0.34735999E-01
0.79293203E-04
0.13420110E-06
0.24676055E-09
0.44375285E-12
0.78974221E-15
0.14039987E-17
```

OUTFIL SRC

(HSC)

```
    10          15          15   0.75000   0 75000 272.99990
 2.00000000E+20
 1.60000000E+18
 2.27239990E+03

 1.60000000E+18
 2.10299999E+15
 2.37137217E+13
 1.14863239E+12
 2.91623456E+10
 3.30693876E+08
 2.23091140E+06
 1.14066905E+04
 7.4236071E+01
 2.33373547E-01
 2.15648930E-03
 2.65334307E-06
 2.63681155E-08
 1.10297684E-10
 2.34912301E-13
```

OUTFIL SRC

(WCM)

APPENDIX 4

CORRIGENDA TO REF. (1)

TRANS. FAR. SOC. 65, 1267, 1969

Equation 3.4 $\mu_{o,g} = g\, m_1\, m_o/(g\, m_1 + m_o)$

Equation 7.1+1 $(y_u)^{g^{2/3}} \quad (e/3g)^{3g}$

Equation 8.5 $K_g = (\sigma_{1,g}/r_1)^{2}/(\mu_{1g}/m_1)^{1/2}$

Equation 8.8 $G(3,\theta)=2.0(e^{\theta} - 1)/(1 + 2\theta)$

Equation 8.9 $G(g>3,\theta) = \{\exp[\theta(\lambda_g -1)]-\exp[\theta(\lambda_g -\lambda_{g-1}^{-1})]\}/$
$(1 + \lambda_g \theta + \frac{1}{2} \lambda_g{}^2\theta^2)$

Equation 9.1 $R_1 = \sum_{g>2} (R_g^- - R_g^+) + 2\,(R_2^- - R^+{}_2)$